1995

The geology petrology and volcanic history of the Crater Mountain volcanic complex Lewis and Clark County Montana

David Bruce Parker
The University of Montana

David B. Parker

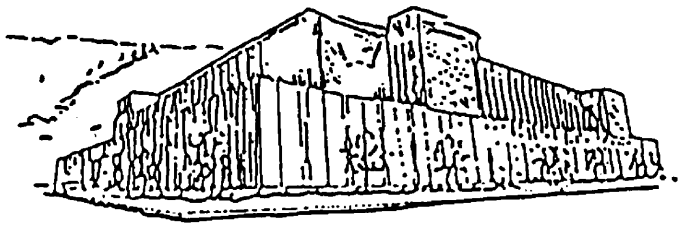

Maureen and Mike
MANSFIELD LIBRARY

The University of **MONTANA**

THE GEOLOGY, PETROLOGY AND VOLCANIC HISTORY OF THE CRATER MOUNTAIN VOLCANIC COMPLEX LEWIS AND CLARK COUNTY, MONTANA

By

David Bruce Parker

B.S. Humboldt State University, 1988

Presented in partial fulfillment of the requirements

for the degree of

Master of Science

University of Montana

1995

Approved by:

Donald W. Hyndman
Chairperson

Dean, Graduate School

September 18, 1995
Date

ProQuest LLC.
789 East Eisenhower Parkway
P.O. Box 1346
Ann Arbor, MI 48106 - 1346

ABSTRACT

Parker, David Bruce, M. S., August, 1995 Geology

The Geology, Petrology and Volcanic History of the Crater Mountain Volcanic Complex, Lewis and Clark County, Montana

Committee Chairman: Donald W. Hyndman

The Crater Mountain volcanic complex, located near Lincoln in western Montana, is part of the Eocene-Oligocene-age Helena volcanic field. The Crater Mountain complex consists of a lower intermediate-composition series of lava flows, and tuffs and an upper series of rhyolite ash-flow tuffs. The rocks of the lower series comprise, in stratigraphic sequence, porphyritic latite flows, flow breccias and associated intrusives, aphanitic trachyandesite flows, hornblende-phyric trachydacite flows, amygdaloidal trachyandesite flows and aphanitic dacite flows. The volcanic rocks of the lower series lie unconformably upon metasedimentary rocks of the Middle Proterozoic Belt Supergroup. The base of the upper volcanic series is marked by paleosols and, locally, by vitrophyre or laminated ground surge deposits. The upper volcanic series contains a 300-meter thick welded ash-flow tuff which is overlain in the northern portion of the study area by volcaniclastic rocks and locally by biotite-bearing ash-flow tuff. The volcaniclastic sediments were deposited in a variety of fluvial and lacustrine settings. Rocks of the upper series are overlain by up to 400 meters of volcaniclastic conglomerate and sandstone of probable Miocene age.

Major oxide and trace element plots show that rocks of the upper and lower series form two distinct suites. Both suites lie along a calc-alkaline trend, but the rocks of the lower series show higher Ba, Sr, Rb, Th, and Nb abundances consistent with subalkaline suites. Hornblende trachydacite of the lower series yielded a K-Ar age of 48.3 M.A while samples of rhyolite ash-flow tuff and biotite-bearing rhyolite tuff of the upper series gave ages of 38 M.Y. and. 36.5 M.Y., respectively.

The distribution of volcanic rocks in the Crater Mountain complex was controlled by northeast, northwest and north-striking normal faults which predate and postdate volcanic activity. A northeast-striking structure named herein the Blackfoot Valley fault displaces rhyolite of the upper series a minimum of 360 meters down to the north against aphanitic andesite of the upper series. Many structural elements in the area appear to have inherited their orientations from older fracture systems which were, in turn, influenced by the Montana Lineament and the Idaho-Montana porphyry belt.

ACKNOWLEDGEMENTS

I would like to thank Dr. Donald W. Hyndman (Committee Chairman), Dr. James W. Sears, and Dr. Ian Lange for their guidence, patience and encouragement during the preparation of this thesis.

Further thanks is extended to Greg C. Coffin, and Dr. William H. Wilkinson for their helpful advice during the field and research phases of the study.

Funding for whole-rock gechemistry and K-Ar dating was provided by Phelps Dodge Mining Company and M. Stephen Enders is thanked for his help in securing this support.

Thanks are extended to the Seven-Up Pete Joint Venture and Canyon Resources Corp. and to the Gehring and Chevalier Ranches for graciously allowing me access to their property.

Finally, I would like to dedicate this work to my wife and able field partner, Gloria whose loving support and encouragement made this study possible.

TABLE OF CONTENTS

LIST OF FIGURES

Figure Page

Figure Page

Figure Page

LIST OF PLATES

LIST OF TABLES

INTRODUCTION

Purpose and Scope of Study

The Crater Mountain volcanic complex of west-central Montana is part of the extensive Eocene-Oligocene-age Trans-Challis volcanic terrane which trends northeast across the northern Rocky Mountains. The Trans-Challis terrane includes includes the Challis, Absaroka-Gallatin, Garnet Range, Lowland Creek, and Helena volcanic fields (Figure 2). The Crater Mountain and Avon volcanic complexes are part of the greater Helena volcanic field, located along the margins of the Late Cretaceous Boulder Batholith and the coeval Elkhorn Mountain Volcanics (Chadwick, 1978; Watson, 1986). The Helena volcanic field consists of a series of lava flows, tuffs, intrusions, ash flow tuffs, and reworked pyroclastic rocks that range in composition from basalt to rhyolite.

Andesitic to rhyolitic-composition volcanic rocks comprise a significant portion of the geologic record from Late Cretaceous through Oligocene time. Eruptive centers may

be aligned along large-scale structures which have controlled magmatism in the region throughout the Eocene and Oligocene (Chadwick, 1981).

The Crater Mountain volcanic complex lies near the intersection of two major structural provinces. The Montana lineament is a broad zone of aligned fold axes and strike-slip faults that extends east-southeast from northern Idaho across western Montana (Weidman, 1965, Wallace and others, 1990). The Idaho-Montana porphyry belt is a poorly understood northeast-striking zone of aligned Late Cretaceous to Quaternary igneous centers, many of which are mineralized (Hyndman and others, 1977; Chadwick, 1981; Figure 1). The porphyry belt is colinear with the Great Falls tectonic zone, a belt of high-angle faults and shear zones which may have influenced igneous activity and tectonism from middle Proterozoic through Tertiary time (O'Neill and Lopez, 1985). Southwest of the Crater Mountain complex, all of the major volcanic centers are calc-alkaline whereas volcanic fields to the northeast, which lie along a similar trend, comprise the Central Montana Alkalic Province (Hyndman and others, 1977; Chadwick, 1981).

The Garnet Range volcanic field, 49 Km southwest of the study area, is alined along the Montana lineament. Andesitic to rhyolitic volcanic rocks in this field are primarily calc-

alkaline, but the presence of an eroded leucite basalt plug suggests an earlier episode of alkalic magmatism (Carter, 1982). These relationships suggest that the rocks of the Crater Mountain complex may have alkalic affinities and that volcanism and mineralization may have been influenced by a unique combination of regional structural features. Recent mineral exploration efforts in the region have led to a renewed interest in the timing and composition of rocks of the Crater Mountain volcanic complex.

The purpose of this study is to use the compositional and textural character of the rocks to explain the structural setting and volcanic history of the Crater Mountain volcanic complex. The timing and magmatic affinity of igneous activity is critical to the understanding of Cenozoic tectonism in western Montana.

Specific Goals of this study are to:

1. Determine the mineralogical composition and textural character of the rocks in order to define mappable lithologic units.

2. Delineate the geometry and volcanic stratigraphy of the complex to determine the mode of emplacement and eruptive chronology.

3. Fingerprint the geochemistry of the rocks to characterize their magmatic affinities and tectonic provenance.

4. Determine the absolute age of the lower andesitic and upper rhyolitic units.

5. Combine petrographic, geochemical, and radiometric age data to test for possible genetic relationships between the andesitic and rhyolitic rocks.

6. Compare the characteristics and evolution of the Crater Mountain complex with those of the Challis and Lowland Creek volcanic fields.

Location

The study area is located astride the Continental Divide in Lewis and Clark County, Montana, approximately 7 Km northeast of the town of Lincoln. The area lies between lat 46° 52'30" N and 47° 05' N and long 112° 47' W and 112° 22'30" W and is included in Townships 13 and 14 N., Ranges 7 and 8 W (Figure 2). Structurally, the area lies on the

northeast limb of a broad southeast-plunging syncline within the Sapphire plate of the Helena salient of the frontal Cordilleran fold and thrust belt (Bierwagen, 1964; Melson, 1964; Rutland and others, 1989; Figure 1).

Map Area

The map area is bounded on the southwest by Poorman Creek and on the north and northwest by State Highway 200 and Landers Fork of the Blackfoot River. On the northeast, it is bounded by Hardscrabble Creek and by Fleisher Pass. Virginia Creek and Stemple Pass delineate the southeastern boundary of the map area. Good access is provided by State Highways 200 and 279, U.S. Forest Service and logging roads and by the Continental Divide Trail as well as by numerous ranch roads and trails in the area.

Geomorphology

The study area ranges in elevation from 1387 meters in the Blackfoot Valley at the western edge to 2161 meters on the Continental divide. The area is characterized by northwest-trending ridges which are separated by narrow, steep drainages. The Continental Divide is expressed as a

steep-sided plateau along the southeastern portion of the area (Plate 1).

The area shows abundant evidence of glaciation. Glacial till covers the flanks of ridges. Broad valleys at the the mouths of the principal streams are floored with a thick veneer of glacially-derived gravel. Steep cliffs at the heads of major northwest-flowing drainages along the Continental Divide are probably the headwalls of former glaciers. The lunate scarp which forms the west slope of Crater Mountain is probably a cirque (Plate 1).

Landslide and debris flow features are common throughout the volcanic field. Several generations of debris flow lobes, the most recent of which exhibit fresh scarp morphology, can be recognized along the east flanks of Columbia Flat and Crater Mountain. Hogum Creek has incised a large debris flow lobe which must have once dammed its south branch. Hummocky landslide debris obscures much of the underlying stratigraphy south of Keep Cool Lakes and west of Lander's Fork. The ridge south of Krohn Lake exposes a spectacular series of landslide scarps.

North and east-facing slopes and many drainages support dense stands of lodgepole pine. In general, outcrop is restricted to ridge crests and stream channels. Several generations of logging roadcuts and clearcuts provide limited

exposures. Recent mineral exploration in the central portion of the area provides many new roadcut, drill pad, and trench exposures.

Regional Igneous History

From late Mesozoic through late Cenozoic time the geologic record in west-central Montana is punctuated by episodes of intense volcanism and plutonism. Igneous activity commenced in Late Cretaceous time and continued throughout Oligocene time. Volcanism and plutonism were most prolific from 80 to 60 Ma and from 54 to 45 Ma (Chadwick, 1981). Late Cretaceous-Eocene-age volcanism was primarily intermediate (andesitic-latitic) in composition whereas post-Eocene volcanic fields are characterized by bimodal basalt-rhyolite assemblages (Chadwick, 1978). To understand the regional significance of the volcanic sequence preserved in the Crater Mountain volcanic complex, I outline selected Late Cretaceous through Late Oligocene-age igneous centers in west-central Montana and south-central Idaho.

Late Cretaceous

The Elkhorn Mountain volcanic pile, which lies to the southeast of the study area, was emplaced 81-76 Ma (Figure 2; Robinson and others, 1968). A thick series of andesitic lava flows and volcaniclastic rocks is overlain by rhyodacitic-rhyolitic ash-flow tuffs, lava flows, and flow breccias (Klepper and others, 1957; Ruppel, 1963; Smedes, 1966). Although the volcanic rocks are deeply eroded, the presence of scattered vent-facies breccias indicates that the andesites were probably effused from numerous stratovolcanoes and the ash-flows may have erupted from poorly-defined cauldrons (Watson, 1986; Rutland and others, 1989). Andesitic-dacitic flows, tuffs and volcaniclastic rocks and rhyolitic welded tuffs of the Two Medicine Formation, which outcrops north of Helena, may also be related to the Elkhorn Mountain volcanic field (Schmidt, 1966).

The Cretaceous Boulder batholith is a composite epizonal plutonic complex which was emplaced about 80-70 Ma (Tilling and others, 1968). Satellite plutons of the batholith intrude and are considered cogenetic with the Elkhorn Mountain volcanic rocks (Robinson and others 1968; Klepper and others, 1971; Hamilton and Meyers, 1974; Tilling, 1974).

Paleocene-Eocene

Cenozoic alkalic magmatism in north-central Montana was focused in at least eight major centers, but extrusive rocks are present only in the Adel, Highwood, and Bearpaw Mountains (Figure 2). In the Adel Mountains, northeast of the Elkhorn Mountains field, trachybasalt, trachyandesite, and latite lava flows and breccias are associated with a complex of alkalic stocks, dikes and laccoliths. Although mafic-intermediate alkalic igneous activity has not been well dated, the Adel Mountain volcanic field is thought to be Late Cretaceous or Paleocene in age (Schmidt, 1972).

In the Highwood Mountains to the northeast, Eocene syenite, shonkinite and monzonite stocks, laccoliths, and dikes are thought to be the source for two successive volcanic sequences. Shonkinite lavas were deposited on eroded remnants of earlier quartz latite flows and pyroclastic rocks (Hearn, 1989a, b).

The Bearpaw Mountains expose a thick sequence of 54-50 Ma shonkinite and latite flows and intrusive rocks of equivalent composition. Alkalic shonkinite flows are interlayered with subalkalic latite flows and flow breccias. Associated dikes and stocks of similar composition show

mutual cross-cutting relations. A suite of rocks from the Bearpaw field shows both alkalic and subalkalic affinities and forms a complete mineralogical and chemical continuum between shonkinite and latite end-members. These relations suggest that mixing occurred between coexisting shonkinite and latite magmas. (Tureck-Schwartz and Hyndman, 1988, 1991).

The Garnet Range volcanic rocks, located 49 Km southwest of the study area, comprise a series of latitic-rhyolitic ash-flow tuffs lava flows, and contemporaneous lacustrine and laharic volcaniclastic rocks which are overlain by basalt and andesite lava flows. The presence of north-trending latite and andesite dike swarms suggest that the flows were extruded from numerous fissures. Radiometric ages (K-Ar) of 47.7-43.7 Ma have been reported for porphyritic quartz latite and rhyolite lava flows and associated dikes (Gwinn and Mutch, 1965; Callmeyer, 1984). An isolated leucite basalt plug intrudes metasedimentary rocks of the Belt Supergroup and is considered to be of "pre-Eocene age" (Carter, 1982).

The Eocene Lowland Creek volcanic field to the southwest of the Garnet Range constitute a thick pile of rhyodacitic-rhyolitic flows, tuffs, and volcaniclastic sandstones and conglomerates which lie along the western margin of the Boulder batholith (Smedes, 1962; Derkey and Bartholomew, 1988). The sequence was erupted 50-48 Ma from several small

caldrons as a series of localized, viscous flows (Smedes and Thomas, 1965). The volcanic section is uniformly tilted to the northwest, and is primarily preserved in a fault-bounded volcano-tectonic depression (Foster, 1987).

The Challis volcanic field, located southwest of the Lowland Creek volcanics in southern Idaho, is the most extensive Eocene-age volcanic field in the trans-Challis volcanic terrane. Volcanic activity began about 51 Ma with the effusion of a thick series of intermediate (andesitic-dacitic) flows from numerous composite cones (Moye and others, 1988, Hardyman, 1989).

Eruption of voluminous ash-flow-tuff sheets, which spanned a brief period from 49-45 Ma, followed cessation of intermediate volcanic activity. Explosive rhyodacitic-rhyolitic volcanism preceded and accompanied collapse of the Van Horn Peak cauldron complex, the Thunder Mountain caldera, and the Twin Peaks caldera (Hardyman, 1989; McIntyre and others, 1982; Leonard and Marvin, 1982; Ekren, 1982). During the waning stages of igneous activity, small rhyolite and alkali rhyolite dome complexes intruded the northern portion of the field. The 46.6 Ma granitic Casto pluton, emplaced near the eastern edge of the field, "intrudes its own ejecta" (McIntyre and others, 1982).

Eocene-Oligocene

The Helena volcanic field, defined by Chadwick (1978, 1981), includes a group of Eocene-Oligocene (40-36 Ma) primarily rhyolitic volcanic centers "scattered across a region which lies southeast, southwest, and west of Helena" (Figure 2). The Avon volcanic complex, located 20 Km southwest of the study area, is the western-most extension of the Helena field. It consists of a series of rhyolitic lava flows and ash-flow tuffs and isolated basalt lava flows deposited upon eroded remnants of aphanitic dacite interpreted as outliers of the Eocene Garnet Range volcanic pile (Peterson, 1985; Trombetta, 1987). Chadwick (1980) reported a radiometric age (K-Ar) of 39.4 +/- 1.6 Ma on sanidine from a rhyolite flow.

The Crater Mountain volcanic complex, which is the subject of this study, comprises the northern portion of the greater Helena volcanic field. The Crater Mountain volcanic complex contains a similar sequence of rhyolitic ash-flow tuffs which rest upon an older andesitic-latitic pile.

Previous Geologic Studies

A number of early geologic studies in the Lincoln area focused on definition of mineral deposits in the region. Barrell (1907) and Knopf (1913, 1950) described mineralization hosted by intrusive rocks in the Marysville Mining District. During their reconnaissance study of the mineral deposits of the greater Helena mining district, Pardee and Schrader (1933) mapped some of the important igneous contacts in the study area, but did not differentiate among volcanic units. Figure 3 shows areas which contain rocks of the Helena volcanic field that have been mapped during previous studies.

Melson (1964) first described geologic structures in the region and distinguished the formations of the Belt Supergroup. He recognized a lower volcanic series of undifferentiated andesitic-latitic flows, welded tuffs, and flow breccias overlain by an upper series of welded rhyolite ashflow tuffs. His work provided a general areal distribution of the volcanic rocks in the area.

Chadwick (1978) assigned the volcanic rocks in the Lincoln area to the Helena volcanic field. He obtained a K-Ar date of 27.8 Ma from rhyolite tuff collected from the

Crater Mountain volcanic complex (Chadwick, 1980, 1981). Data presented below indicate that this date is anomalously young in comparison to radiometric ages obtained from the Crater Mountain area during the course of this study and from those determined for other portions of the Helena volcanic field.

Carter (1982) and Callmeyer (1984) studied the Eocene-age volcanic rocks of the eastern Garnet Range, west of the study area, and Trombetta (1987) described the Eocene Avon volcanic complex to the southwest. McKee (1978) described rocks of the Crater Mountain complex in the vicinity of the Silver Bell stock.

In their regional investigation for the U. S. Geological Survey of the geology of the Rogers Pass area, Whipple and others (1987) mapped the volcanic rocks in the area as the volcanics of Crater Mountain. The rocks are described as undifferentiated rhyodacitic tuff, ash-flow tuff, and lapilli tuff with minor amounts of rhyolite flow breccia and andesite, latite, and trachyte lava flows. Their work provided a general geologic map of the study area as well as good descriptions of Belt Supergroup units.

Methods

I completed geologic mapping of the 150 square kilometer study area in 170 field days during the summers of 1989 to 1991. I marked contacts and sample locations on a topographic base map compiled from 1:24,000 scale reproductions of portions of the Stonewall Mountain, Silver King Mountain, Cadotte Creek, Lincoln, Swede Gulch, and Stemple Pass 7.5-minute Quadrangles (Plate 1).

In areas of little bedrock exposure, I commonly used float to locate lithologic contacts. I inferred subcrops where a particular map unit comprised 90 percent or more of float. The map shows indicated approximate contacts where vegetation and soil cover or talus precluded tracing them exactly.

I collected one hundred-eighty-four lithologic samples and analyzed sixty-nine of the samples by transmitted-light petrography. I etched eighteen samples and stained them with sodium cobaltnitrate solution to facilitate determination of potassium feldspar content.

I submitted thirty samples collected from nine of the map units for whole rock and trace element geochemistry. I also submitted seven samples for radiometric age determination. Collection and analysis methods are discussed

in the Geochemistry and Geochronology chapters. Sample locations are described in detail in Appendix I.

I measured attitudes of planar structural elements such as bedding, joints and foliations and recorded them on the base map. Where present, I also measured flow direction indicators such as flow banding, mineral lineations and foliations and minor intraformational folds were also measured.

Contact relations suggest that the volcanics of Crater Mountain were deposited upon a paleosurface with considerable relief. Although a number of studies have shown that flow banding measurements can be used to delineate flow geometry and source areas (see for example, Williams, 1942 or Christiansen and Lipman, 1966), flow banding is often coplanar with depositional surfaces and reflects the slope of local paleotopographic features. Joints commonly develop perpendicular to the surface of flows and, therefore, also may reflect paleotopography. Melson (1964) noted that the platy structure in the rocks of the lower volcanic series is commonly developed 'perpendicular to or at high angles to flow contacts' and 'is thus, not a reliable indication of the orientation of flows'. Syn or post-depositional rheomorphism or tectonic tilting may also affect attitudes of joints and flow bands. I approached the interpretation of flow geometry

or source area location on the basis of attitudes of flow banding and joints with these complications in mind.

UNIT DESCRIPTIONS and FIELD RELATIONS

Criteria for Description and Classification

Tertiary volcanic and volcaniclastic rocks of the Crater Mountain volcanic complex are divided on the basis of lithologic and textural character and field relations into ten mappable units (Plate 1). To minimize identification errors, I reclassified igneous rock units that I defined in the field on the basis of phenocryst assemblages using the IUGS classification scheme (Streckeisen and LeMaitre, 1979) on the basis of available whole rock geochemical analyses according to the chemical classification of Le Bas and others (1986). Color designations are from the G. S. A. Rock Color Chart (Rock Color Chart Committee, 1979).

Field characteristics are not always reliable clues to identification of lithologic units in volcanic sequences. Color or grain size changes may be indicative of cooling breaks or coalescing lobes within a complex flow unit. Color index may give a general estimate of the percentage of ferromagnesian minerals in the rock (Hyndman, 1985).

Phenocryst content may also vary within a rock unit. In their description of rock units of the Challis volcanic

field, McIntyre and others (1982, p. 4) noted that "Comparisons of phenocryst contents with whole-rock chemical analyses show that rock classification based solely on phenocryst mineralogy are misleading and generate considerable confusion when applied to these rocks." Classification of the rocks of the Crater Mountain complex presented similar problems. I discuss below the Tertiary volcanic rocks and underlying units, from oldest to youngest. Figure 43 depicts stratigraphic relations.

Rocks of the Proterozoic Belt Supergroup (Yg, Ys, Ye, Yh,Ysn, Zd)

Field Relations

Rocks of the Crater Mountain volcanic complex lie unconformably upon metasedimentary rocks of the Middle Proterozoic Belt Supergroup. In the east and southeast portions of the study area, ash-flow tuffs of the Crater Mountain complex rest upon rocks of the Grayson (Yg) and Spokane (Ys) formations carried by the Scapegoat Thrust plate. The tuffs locally lie upon Late Proterozoic diorite sills (Zd) which intrude the metasedimentary rocks. In the

northwestern portion of the area and in the central portion southeast of the Blackfoot River, latite and trachyandesite flows overlie metamorphosed calcareous mudstones of the Empire Formation (Ye) and dolomitic siltstones of the Helena Formation (Yh). Latite flows along the western margin of the area rest unconformably upon rocks of the Helena Formation and locally overlie a down-faulted block of argillite of the Snowslip Formation (Ysn). Although all of the rocks of the Belt Supergroup are well indurated and have undergone greenschist-grade metamorphism, they are discussed as sedimentary rock types in order to describe characteristics used to distinguish among them in the field.

Metasedimentary Rocks

Grayson Formation (Yg)

The Grayson Formation is the oldest unit which occurs in the field area. It consists of interlaminated or interbedded greenish-gray argillite and siltite. The base of the Grayson Formation is not exposed, but it reaches a maximum exposed thickness of 915 meters in the Eldorado thrust plate northeast of the study area (Whipple and others, 1987).

Spokane Formation (Ys)

The Spokane Formation overlies the Grayson Formation. It is composed of maroon, purple, or grayish-red non-calcareous siltite interlaminated with dark red argillite. Mudcrack partings and raindrop impressions are common. The base of the unit is not exposed, but its thickness is estimated to exceed 1525 meters (Melson, 1964).

Empire Formation (Ye)

The Empire formation overlies the Spokane Formation within the study area. It is characterized by interlaminated grayish-green dolomitic siltite and argillite. The base of the Empire Formation is placed at the stratigraphically lowest gray-green siltite beds which overlie dark red argillite. Melson (1964) and Bierwagen (1964) estimated the thickness of the unit in the map area to be 305 meters.

Helena Formation (Yh)

The Helena Formation overlies the Empire Formation and is in fault contact with the Spokane Formation in the southern portion of the map area. It is composed of green to gray calcareous to dolomitic siltstones mudstones and interstratified quartzite. "Molar tooth" dissolution structures are diagnostic of this unit and thin laminated siltstone beds which contain the stromatolite Collenia are common near the base. The Helena Formation was estimated by Melson (1964) to be 1524 to 2286 meters thick in the Lincoln area.

Snowslip Formation (Ysn)

The Snowslip Formation overlies and is locally in fault contact with the Helena Formation northeast of Poorman Creek in the southwestern portion of the area. It is 300 to 1800 meters thick (Melson, 1964) and consists of light gray laminated siltstone and light purple laminated sandstone and siltite (Whipple and others, 1987).

Igneous Rocks

Intrusive and extrusive igneous rocks of Late Proterozoic and Eocene ages crop out throughout the region. Eocene volcanic rocks, which are volumetrically prevalent in the map area, are the subject of this study. The relative age, chemical classification, mode of emplacement, and areal extent of major map units of the Crater Mountain volcanic complex are listed in Table 1. Table 2 lists modal mineralogical composition of the Eocene igneous map units.

Older Intrusive Rocks

Late Proterozoic Diorite (Zd)

Dark green to black, medium-grained diorite dikes and sills up to 150 meters thick locally intrude rocks of the Belt Supergroup. The diorite contains abundant equant, fresh plagioclase and dark green augite crystals with sparse apatite and quartz. The sills have been dated at 750 Ma by Mudge and others, (1968).

Andesite Porphyry (Tap)

Description: Intrusive andesite porphyry of the Silver Bell stock outcrops in the southern portion of the field area. This unit is texturally and compositionally similar to the andesite porphyry of McKee (1978) and was mapped as undifferentiated andesite by Whipple and others (1987). The porphyry is very coarse grained and is composed of one centimeter-long white euhedral plagioclase phenocrysts and subordinate two to three centimeter-long pink, equant orthoclase crystals with interstitial biotite books and lesser subhedral augite (?) crystals and anhedral quartz crystals in a greenish-gray aphanitic groundmass (Figure 4).

Petrography: Plagioclase and orthoclase phenocrysts are commonly twinned and show weak alignment (Figure 5). There are at least two distinct populations of plagioclase. Larger subhedral phenocrysts and glomerocrysts show oscillatory zoning and weak saussuritization along anastamosing microfractures. A second population of subhedral to anhedral laths are strongly resorbed and pervasively replaced by sericite, fine-grained epidote and carbonate. Orthoclase phenocrysts are poikilitic with inclusions of biotite and plagioclase and also exhibit oscillatory zoning. Crystal

edges are sharp and show no evidence of reaction or resorption. Biotite books are fresh and contain abundant inclusions of apatite and lesser sphene. · Quartz crystals are strongly resorbed and exhibit reaction rims composed of fine-grained carbonate and sericite. The groundmass is composed of directionless altered plagioclase microlites with interstitial felted masses of chlorite, epidote, and carbonate. Reaction rims and resorbed faces on quartz and altered plagioclase phenocrysts suggest that these phases were in disequilibrium with groundmass minerals. These relations may indicate mixing of coexisting felsic and mafic magmas or incorporation of xenocrysts from earlier phases of the Silver Bell stock.

Field Relations: Andesite Porphyry (Tap) forms two sill-like bodies which crop out near Stemple Pass. An irregular apophysis which extends north-northeast from the Silver Bell stock intrudes along the contact between the Helena and Empire Formations and is overlain by ash-flow tuff of the Crater Mountain volcanic complex. The other intrusion, which is well exposed at the head of Rooster Bill Creek, is locally concordant with bedding in the Spokane Formation and is also in contact with rhyolite ash-flow tuff.

Volcanic Rocks of the Crater Mountain Complex

The Tertiary volcanic rocks of the Crater Mountain volcanic complex dominate the map area. As noted by Melson (1964) the rocks can be conveniently divided into a lower series dominated by andesitic to latitic lava flows and an upper series of rhyolite ash-flow tuffs.

Lower Volcanic Series

The volcanic rocks of the lower series can be divided, on the basis of textural and petrographic characteristics, into five mappable units. The map units of the lower series are described from oldest to youngest below.

Porphyritic Latite

Porphyritic latite is exposed along the northwestern and southern margins of the volcanic field. Chemically, the rock is classified as trachydacite (see below), however, chemical classification schemes in current use do not discriminate between latite and trachydacite fields. To avoid confusion

with other trachydacites in the Crater Mountain complex, the rock is classified as porphyritic latite on the basis of modal phenocryst assemblages and textural similarity to well studied volcanic units classified as latite (see, for example Williams and others, 1982).

Porphyritic latite is the oldest unit in the Crater Mountain complex and rests unconformably upon metasedimentary rocks of the Belt Supergroup. The unit reaches a maximum thickness of 184 meters on a northwest-trending ridge west of Hogum Creek in the southwest quarter of Section 17, T 14 N, R 7 W.

Porphyritic latite can be divided into three mappable members: Porphyritic latite flow (Tpl), porphyritic latite intrusive (Tpl_i) and an ash-flow tuff facies (Tpl_t).

Porphyritic Latite Flows (Tpl)

Description: Porphyritic latite flow forms subdued outcrops and platy talus slopes along the flanks of ridges. Pale purple to grayish red purple latite weathers along hackly fractures into grayish blue irregular blocks. The distinctly porphyritic rock contains 20-30 percent white subhedral plagioclase laths, 3 to 10 percent biotite books, variable

amounts of broken, subhedral pyroxene and amphibole (hornblende ?), and rare olivine phenocrysts in a granular aphanitic groundmass (Figure 6). Plagioclase and biotite commonly form glomerocrysts.

Petrography: Plagioclase phenocrysts, which range from 5 millimeters to 1 centimeter in length, display polysynthetic twins and commonly exhibit oscillatory zoning (Figure 7). Plagioclase composition, determined optically and from CIPW normative mineral analyses, is oligoclase (An_{21}-An_{27}). Biotite books range from 1 to 3 millimeters in length and display golden brown-brown pleochroism. Euhedral, prismatic amphibole crystals are 3 to 5 millimeters long and show strong green-olive green-dark brown pleochroism. Stubby, prismatic, brown augite phenocrysts are commonly rimmed by blue-green amphibole. Sparse, subhedral olivine phenocrysts are completely replaced by reddish-brown "bowlingite" and may be rimmed by orange "iddingsite." The groundmass is composed of plagioclase and lesser K-feldspar and pyroxene microlites and interstitial dust. Accessory minerals include sphene, apatite, and leucoxene psuedomorphs after ilmenite. Phenocrysts and microlites show good subparallel arrangement (pilotaxitic texture). Rounded corners on oligoclase,

biotite, and pyroxene phenocrysts may reflect abrasion during effusion or partial resorption in the magma chamber.

Alteration: Throughout the Crater Mountain volcanic complex, porphyritic latite flows show evidence of deuteric alteration. Oligoclase phenocrysts are commonly deeply embayed by patches of fibrous epidote, sericite, opaque oxides and calcite, and may be altered to albite. Mafic minerals are rimmed or replaced by aggregates of chlorite, anhedral quartz, biotite, and white mica and are commonly pseudomorphed by reddish-black opaque oxide or clay minerals. Brown biotite books are generally fresh, but may contain thin chlorite lamellae.

Field Relationships: The basal contact of porphyritic latite is best exposed along Black Diamond Creek in the northwest quarter of Section 14, T 14 N, R 7 W where dark purple-red latite flow breccia contains abundant angular siltstone fragments from the underlying Spokane Formation. Along the Hogum Creek Road, in the southwest quarter of Section 20, T 14 N, R 7 W, a thin zone of hornfels delineates the contact between metadolomite of the Helena Formation and latite flow breccia which contains abundant angular fragments of metadolomite.

Porphyritic Latite Intrusion (Tpl_i)

Along the west fork of Humbug Creek (SE quarter Section 26, T 14 N, R 8 W) porphyritic latite forms a steep-sided conical knob (Figure 8). This feature is interpreted as an exogenous dome. The latite is texturally and mineralogically identical to the latite flows but it is unusually fresh and exhibits strong columnar jointing. Flow foliation dips steeply inward towards the center of the knob.

Porphyritic Latite Tuff (Tpl_t)

Porphyritic latite tuff outcrops northwest and south of the dome complex. Purple latite tuff weathers reddish purple and forms knobby ribs studded with subangular blocks. In outcrop, the tuff is a matrix to clast supported, poorly sorted tuff breccia. It contains abundant pumice lapilli with flattening ratios as high as 16:1 and locally, pumice fragments are streaked out into dark gray fiamme (Figure 9). According to the criteria established by Smith (1960a), the tuff is moderately to densely welded.

Petrography: In thin section, the tuff shows strong eutaxitic structure. Collapsed pumice lapilli wrap around subrounded lapilli-size fragments of porphyritic latite or are squeezed between plagioclase phenocrysts (Figure 10). Lithic clasts and are texturally and mineralogically similar to porphyritic latite flows. Pumice lapilli contain abundant plagioclase laths and fine-grained biotite. Broken plagioclase and altered mafic phenocrysts and shredded biotite books contain numerous inclusions of sericite, chlorite, and apatite. Phenocrysts and lapilli are set in clast-to-clast contact in a sparse matrix composed of broken plagioclase microlites and interstitial dust. The tuff is interpreted as a block-and-ash flow facies of porphyritic latite on the basis of mineralogical and textural similarities.

Field Relations: Field relations indicate that the porphyritic latite was deposited on an irregular surface incised into the underlying Proterozoic Belt rocks. The basal contact shows as least 200 meters of vertical relief (Plate 2). The alignment of phenocrysts and the paucity of pumice indicate that most of the porphyritic latite erupted as lava flows. Flow breccias, which occur throughout the section, may delineate the contacts between successive flows

or may reflect areas where a single viscous flow has repeatedly over-ridden its own flow-front debris. Porphyritic latite tuff is restricted to the Humbug Creek drainage and may represent a near vent facies associated with the collapse of the exogenous dome described above. Similar relations have been described for a number of historic lava dome eruptions (for examples, see Fisher and Schmincke, 1984 or Cas and Wright, 1988). The latite may have erupted from a number of such flow dome complexes.

Aphanitic Trachyandesite (Tat)

Aphanitic trachyandesite outcrops in the central and northern portions of the field area. The unit attains a maximum exposed thickness of 283 meters on a ridgetop in the northeastern quarter of Section 22, T 14 N, R 7 W. Chemically, the unit is classified as a trachyandesite on the basis of its high silica and potassium content.

Aphanitic trachyandesite forms prominent cliffs and hogback ridges with blocky talus slopes and reddish brown soils. The unit commonly exhibits polygonal columnar joints and platy fractures which develop along closely spaced flow bands (Figure 11). In outcrop, blackish red aphanitic

andesite weathers brownish gray and contains rare (less than 0.5 percent) green altered mafic phenocrysts. Sparse vesicles are filled with opal, calcite, or hematite. The unit is locally strongly ferromagnetic.

Petrography: Aphanitic trachyandesite is composed of plagioclase and subordinate augite microlites with intergranular altered augite (?) and interstitial magnetite dust. The microlites show strong trachytic alignment and flow bands are defined by subtle segregations of aligned microlites and reddish brown opaque oxides (Figure 12). Normative plagioclase composition is andesine to calcic oligoclase (An_{26}-An_{38}). Olivine microcrysts pseudomorphed by brown 'bowlingite' comprise 3 to 15 percent of the rock. Sparse 1 to 2 millimeter augite phenocrysts are commonly pseudomorphed by fine-grained aggregates of chlorite, sericite, epidote, and carbonate and rimmed with orange opaque oxide. Patches of chlorite with abundant apatite inclusions may replace biotite books.

Field Relations: Aphanitic trachyandesite nearly everywhere overlies porphyritic latite. Although the contact itself is not exposed, its position is often topographically expressed as a flat saddle or a prominent break in slope.

Flow breccias near the contact are commonly oxidized and contain abundant subrounded fragments of porphyritic latite and sparse fragments of Belt rocks. Excellent exposures of flow breccia occur in road cuts west of the Columbia Mine (SE quarter Section 20, T 14 N, R 7 W).

Abrupt changes in color, joint spacing and flow banding orientation within the unit indicate that the trachyandesite was erupted as a series of lava flows. The presence of abundant flow breccias, vesicular layers, and thin clay horizons suggests that individual flows are 6 to 30 feet thick. However, the lack of continous exposure and the scale of this project precluded the mapping of individual flow units.

Exploration drill holes in the McDonald Meadow area encountered a wide variety of sedimentary rock types at the same stratigraphic position as the aphanitic trachyandesite flows. Sedimentary rock types include oxidized paleosol horizons, volcaniclastic sandstones, thin airfall ash beds, and laminated black, pyritic mudstones. These sedimentary rocks apparently were deposited in a fluvial-lacustrine environment during periods of quiescence between successive trachyandesite eruptions.

Porphyritic Hornblende Trachydacite (Tpt)

This unit was originally mapped as hornblende andesite, but on the basis of total alkali vs silica content, it is classified as trachydacite. Hornblende trachydacite outcrops along the ridge top near the Columbia Mine known locally as Columbia Flat and along the west flank of Crater Mountain. Sporadic outcrops also occur along the east fork of Humbug Creek. The unit forms resistant knobs and ledges and displays pronounced columnar joints. In outcrop, the rock breaks along foliations into thin flaggy sheets. Freshly broken surfaces are studded with five to seven millimeter-long black amphibole phenocrysts which show strong trachytic alignment (Figure 13). Grayish black trachydacite weathers light purplish gray to light green. Phenocrysts in weathered exposures are commonly replaced by calcite or chlorite. The well developed trachytic texture and the absence of pumice or lithic fragments indicate that this unit was erupted as a lava flow or series of flows.

Petrography: Broken, subhedral hornblende phenocrysts, which comprise 7 to 20 percent of the rock, exhibit strong olive green-yellow-dark brown pleochroism and are rimmed by black opaque oxides (Figure 14). Hornblende crystals are

commonly partially resorbed, but show little evidence of alteration. Chlorite plates, with inclusions of apatite and wisps of sericite are probably altered biotite books. The trachytic groundmass is composed of plagioclase and subordinate K-feldspar microlites with interstitial chlorite, fine-grained carbonate, and brown opaque oxides. Domains of aligned feldspar microlites and opaque oxide define wavy, closely spaced flow bands.

Field Relations: Hornblende trachydacite is well exposed as a series of small knobs along the ridge top west of Columbia Flat and in a series of steep ledges east of the Rover Mine (NW quarter Section 29, T 14 N, R 7 W) where the unit reaches its exposed maximum thickness of 122 meters. Hornblende trachydacite overlies aphanitic trachyandesite. The contact is commonly marked by slope breaks or saddles which are covered by thin purplish-red clay-rich soils.

South of the Rover Mine, hornblende trachydacite flow breccia is exposed in a small east-facing bowl-shaped basin. Here,the rock is an unsorted, clast-supported monolithologic breccia composed of subangular block and lapilli-size clasts of hornblende trachydacite in a thin, crystal-poor matrix. In places, the flow banding orientation suggests that the matrix was extruded from a still-plastic core into cracks in

the solidified flow surface. According to Cas and Wright (1988) silicic lavas are extremely viscous and form short, steep-fronted flows with thick surface and flow-front breccias. The flows commonly override and are squeezed between blocks in their flow-foot breccias.

South of Crater Mountain, near the head of Humbug Creek, the trachydacite is lavender with light green altered hornblende phenocrysts. Here, it overlies both aphanitic andesite and porphyritic latite. Altered hornblende trachydacite also outcrops east of the latite dome complex along the North Fork of Humbug Creek. Outcrop patterns suggest that hornblende trachydacite lavas may have flowed down a paleovalley located along the axis of the Humbug Creek drainage. An isolated block of hornblende trachydacite near the mouth of the South Fork of Humbug Creek suggests that this unit may have been much more extensive than present exposures indicate.

Amygdaloidal Andesite (Taa)

Amygdaloidal andesite occurs in isolated patches near the Columbia Mine and north of Columbia Flat. (Section 20 , T 40 N, R 7 W). The unit is characterized by abundant

amygdules composed of calcite, hematite, and chalcedony in a dark gray, purple, or green aphanitic groundmass. The amygdules range from 5 millimeters to as much as 10 centimeters in diameter and comprise 5 to 30 percent of the rock. In some layers the amygdules are nearly spheroidal and of uniform size (Figure 15) whereas in other layers they are oblate or pipe-like and show no size preference. Calcite-dominated amygdules commonly contain cores of specular hematite or drusy or amethystine quartz. Samples of this unit were not submitted for geochemical analysis because of the ubiquitous presence of secondary minerals. The rock is classified as trachyandesite on the basis of color index, modal analysis of thin sections, and textural and mineralogical similarity to aphanitic trachyandesite.

Petrography: Under the microscope, many amygdules contain radiating fans of intergrown chalcedony and green chlorite. Others are filled with platy calcite or rimmed with polygonal quartz. Many exhibit colloform or banded textures indicative of open-space filling of primary vesicles (Figure 16). The amygdales are set in a trachytic groundmass composed of highly altered feldspar laths and interstitial black hematite. Rare 5 millimeter subhedral mafic phenocrysts are pseudomorphed by fibrous masses of chlorite and granular

quartz. Flakes of green biotite may be replaced by plates of chlorite with tiny inclusions of rutile and magnetite. Stubby prismatic grains replaced by granular serpentine with orange "iddingsite" fracture-coatings are probably altered olivine.

Field Relations: West of Columbia Flat, amygdaloidal andesite onlaps exposed knobs of hornblende dacite. The contact is locally baked, but no flow breccias were observed. To the north, amygdaloidal andesite is topographically above aphanitic andesite, but the contact is not exposed.

Aphanitic Dacite (Td)

Aphanitic dacite is exposed on the west flank of Crater Mountain and on the ridge top north of Crater Mountain. The unit overlies hornblende trachydacite and is overlain by rhyolite ash-flow tuff.

Description: Aphanitic dacite forms subdued ridge top outcrops with prominent flaggy talus slopes. Olive brown dacite weathers into thin, light gray plates which produce a distinctive porcelanous ring when struck. The rock is

characterized by curious wavy bands which show crude alignment in at least two orthogonal directions. The dark reddish brown bands exhibit finely granular light olive green cores and form arborescent patterns on freshly broken surfaces (Figure 17).

Petrography: In thin section, aphanitic dacite is composed of tiny feldspar and subordinate birefringent (augite ?) microlites with interstitial opaque oxides. There are two subequal populations of feldspar microlites. Feldspar microlites exhibit variable relief and some are lath-like with polysynthetic twins while others are platy and show simple twins characteristic of K-feldspar crystals. Although their size makes it difficult to accurately estimate relative percentages plagioclase appears to be the dominant type. Plagioclase composition, based on whole rock geochemistry, is oligoclase (An_{21} to An_{28}). Feldspar and augite microlites are strongly aligned in thin bands of alternating preferred orientation which define herringbone trachytic texture (Figure 18). Sparse subhedral mafic microcrysts are pseudomorphed by pale green chlorite. Rare quartz microcrysts are strongly resorbed and embayed.

Irregular bands of granular quartz cut across the trachytic flow bands. Flow bands adjacent to these

structures are disrupted and microlites are commonly entrained along them. Elongate cavities aligned along the quartz bands are lined with colloform chalcedony. These relations suggest that these structures are pipe-like gas escape structures which have been subsequently filled by secondary minerals. Quartz and chalcedony may have formed by vapor phase crystallization during cooling or may have precipitated as late open-space filling hydrothermal veins.

Field Relations: Aphanitic dacite is well exposed on the ridge top south of the Rover mine (NW quarter Section 29, T 14 N, R 7 W). The contact between the dacite and the underlying hornblende trachydacite flow breccia is delineated by a 2 meter-thick brick red, clay-rich soil layer. The paleosol contains abundant subrounded cobbles of weathered hornblende trachydacite.

Aphanitic dacite is also well exposed on the northwest slope of Crater Mountain (W half Section 32, T 14 N, R 7 W). Here, it forms a series of low serpentine frost-heave ridges with extensive platy talus aprons. The dacite is overlain and locally baked by rhyolite ash-flow tuff.

Upper Volcanic Series

The contact between the upper series and lower series is an erosional unconformity marked by thick paleosols and sparse gravel horizons. The upper series consists of volumetrically prevalent rhyolite ash-flow tuffs and lesser volcaniclastic sediments, and biotite-bearing rhyolite ash-flow tuffs. The map units of the upper series are described from oldest to youngest below.

Rhyolite Ash-flow Tuff (Trt)

Rhyolite ash-flow tuff is classified as crystal-lithic rhyolite lapilli tuff according to the IUGS classification scheme for pyroclastic rocks (Fisher, 1966b; Schmid, 1981). Rhyolite ash-flow tuff outcrops in the southeastern and northern portions of the field area. The unit reaches a maximum exposed thickness of 393 meters along a high plateau on the Continental Divide in Section 24, (T 14 N, R 7 W). Exploration drill holes in the north-central portion of the map area encountered over 450 meters of rhyolite ash-flow tuff.

Rhyolite ash-flow tuff forms flat-crested steep-sided plateaus which support stunted stands of lodgepole pine with very little undergrowth. The tuff commonly exhibits crude columnar and platy jointing (Figure 19). Light olive gray rhyolite ash-flow tuff weathers yellowish gray to pinkish gray.

In outcrop, the tuff typically contains 10 to 30 percent subangular lithic fragments, but isolated lithic-rich layers may contain greater than 80 percent lithic fragments in clast-to-clast contact. Lithic populations are dominated by metasedimentary formations of the Belt Supergroup, but also include porphyritic and aphanitic fragments from units of the lower volcanic series. Compacted pumice lapilli, which typically comprise 10-25 percent of the rock, exhibit flattening ratios which range from 3:1 to greater than 12:1. The tuff contains subequal amounts of subhedral 2 to 5 millimeter smokey-gray quartz phenocrysts and euhedral 3 to 7 millimeter sanidine phenocrysts. Quartz crystals are commonly broken and deeply embayed. Sanidine phenocrysts are chatoyant on freshly broken surfaces.

Petrography: Under the microscope, rhyolite ash-flow tuff shows strong eutaxitic texture characteristic of welded ignimbrites (Smith, 1960b). Flattened and elongated pumice

lapilli, lithic fragments, and quartz and sanidine phenocrysts are set in a groundmass composed of silt-size crystal and lithic fragments and shards of fresh dark brown glass (Figure 20). Deformed pumice lapilli define a strong foliation and are commonly draped around lithic fragments and phenocrysts. Pumice fragments contain tricuspate glass shards and rare quartz or sanidine crystals. Bipyramidal quartz phenocrysts are commonly broken and exhibit amoeboid shapes indicative of partial resorption. Sanidine phenocrysts are also deeply embayed and display Carlsbad twins, crude zoning, and strain lamellae and may locally exhibit microperthitic texture. Sparse plagioclase and augite xenocrysts show strong reaction rims. Twinned plagioclase crystals exhibit K-feldspar overgrowths in some samples. Rare euhedral books and skeletal or deeply embayed patches of pleochroic brown biotite (X = golden brown, Z = dark brown) comprise less than 1 percent of the rock.

Alteration: Devitrification varies from incipient to complete throughout the tuff unit. In most samples, glass shards in the groundmass and in pumice lapilli contain tiny tridymite and K-feldspar crystals.

Locally abundant lithophysae up to 60 centimeters in diameter occur near the base of the ash flow (Figure 21). On

the north slope of Crater Mountain the tuff contains discontinuous 1 to 2 meter thick light green layers composed of spherical 3 to 5 millimeter spherulites which show faint traces of both concentric and radiating growth lines.

Alteration petrography: In thin section, the spherulites exhibit strong orb texture defined by radiating sheaves of axiolitic fibers which appear to have nucleated on sanidine phenocrysts (Figure 22). The fibers have moderately low relief and are length-slow, but their small size prevents determination of any other definitive optical properties. R. L. Smith (1960a, p. 36) reviewed the results of many X-ray diffraction studies of welded tuffs and concluded that the most common devitrification products are cristobalite and feldspar in proportions similar to those of the unaltered glass. Fibrous axiolites of cristobalite intergrown with quartz and feldspar which comprise spherulites have been referred to microscopically as lussatite (Phillips and Griffin, 1981).

Ovoid to irregular amygdules contain granular patches and radiating fans of chalcedony. Sheaves of wedge-shaped tridymite crystals occur in some spherulites. According to Smith (1960A, B) and Ross and Smith (1961), tridymite forms during vapor phase crystallization of volatiles exsolved from

glassy fragments and heated ground water trapped in vesicles. Vapor phase crystallization occurs contemporaneously with or closely follows devitrification. Chalcedony may form during vapor-phase crystallization or may precipitate from later hydrothermal solutions percolating through the devitrified tuff.

Plagioclase phenocrysts in porphyritic volcanic fragments are commonly replaced by fine-grained aggregates of epidote, carbonate and sericite and plagioclase xenocrysts are albitized and exhibit reaction rims of sericite and chlorite. Sanidine and quartz phenocrysts contain few inclusions and show little evidence of alteration.

Field Relations: In the central portion of the study area, rhyolite ash-flow tuff lies unconformably upon units of the lower volcanic series, whereas along the western and southeastern portions the tuff rests upon formations of the Belt Supergroup. Although the ash-flow tuff exhibits considerable local variation in degree of welding, in general, the lower portion of the tuff is more densely welded than the upper portion. No unconformities, airfall or reworked bedded ash deposits, or interflow sediments were observed, thus, the ash-flow tuff conforms to Smith's (1960b) criteria for a simple cooling unit. The sequence is best

exposed on the west slope of Crater Mountain where it consists of a lower densely welded member overlain locally by unwelded volcaniclastic ash and pyroclastic breccia and an upper densely welded perlitic member.

The presence of opalescent or chatoyant sanidine crystals in the more densely welded sections of the ash-flow tuff also suggests that the ash-flow sequence cooled as a single unit. Chatoyancy in sanidine crystals is caused by cryptoperthitic exsolution lamellae and is most common in the slowly cooled portions of ash-flow tuffs (Smith, 1960a). Exsolution lamellae may develop in the magma chamber prior to eruption or within cooling ash-flows. However, because exsolution occurs in response to rapid changes in pressure, lamellae commonly form during cooling of thick lava or ash flows. Cooling of individual thin flow units would not provide the thermal insulation necessary for exsolution to occur.

Surge Deposit

Although poor exposure prevents recognition of individual ash flows within the cooling unit in most localities, the cirque wall on the west side of Crater Mountain provides excellent exposures of the basal portion of the ash-flow tuff sequence. Here, a 6 meter-thick sequence

of poorly consolidated bedded ash and lapilli tuff lies upon a 50 meter section of densely welded ash flow tuff and vitrophyre (Figure 23). The volcaniclastic section is comprised of unconsolidated fine to medium-grained ash with lapilli interbeds. The planar and low-angle cross-laminated beds dip gently to the south and show normal grading from fine ash beds upward to coarse lapilli-ash beds. The lapilli beds contain abundant rounded obsidian, vesiculated and unvesiculated cognate volcanic clasts and accidental metasedimentary and volcanic fragments which range from 5 millimeters to 5 centimeters in diameter.

This sequence has many features in common with pyroclastic surge deposits which have been described in association with many pyroclastic flow sequences worldwide. Surge deposits are characterized by planar or low-angle cross bed forms and graded bedding. The deposits are typically only a few meters thick and occur at the base of medium and large volume ash flows (Heiken, 1979; Fisher and Schmincke, 1984; Cas and Wright, 1988).

Origin of Surge Deposits

Sparks and others, (1973) proposed an idealized eruption unit for ignimbrite sequences (Figure 24). Ground surge deposits ("layer 1") are thought to form during the initial

stages of collapse of a column of gas-charged pyroclastic ejecta associated with a Plinian-type eruption or from the explosive collapse of a lava dome (Fisher, 1966a). As the eruption column continues to collapse, deposition the low density ground surge is closely followed by deposition of the main body of the pyroclastic flow ("layer 2"). Ground surges may also be produced by ingestion of air or volatization of vegetation at the head of a moving pyroclastic flow or by a directed blast such as the one that occurred at Mt. St. Helens in 1980 (Walker and McBroom, 1983; Cas and Wright, 1988). Ground surge deposits are commonly obliterated by deposition of the ensuing pyroclastic flows, but may be preserved in topographic depressions in the paleosurface (Sparks and Walker, 1973; Sparks and others, 1973; Fisher and Schmincke, 1984).

Ash-cloud surge deposits ("layer 3a") occur at the top of a pyroclastic flow and are thought to originate as turbulent, low density flows generated in the gas and ash cloud above the concentrated pyroclastic flow. The ash-flow surge is deposited by settling upon the denser underflow (Cas and Wright, 1988). Ash-cloud surge deposits may be closely followed by deposition of air-fall ash ("layer 3b") settling from the ash cloud during the waning stages of the pyroclastic eruption (Sparks and others, 1973; Sparks, 1976).

A third type of surge deposit, termed a base surge, is associated with phreatomagmatic eruptions such as those which accompany the formation of maars and tuff rings. These deposits generally show features such as accretionary lapilli or vesiculated tuff layers which indicate deposition as wet ash (Cas and Wright, 1988). Base surge deposits may show undulatory bed forms (Fisher and Schmincke, 1984). The section at Crater Mountain is classified as a ground surge deposit because it occurs at the base of an ash flow sequence and shows no features suggestive of a phreatomagmatic origin.

Block-and Ash Flow Deposit

Along the southwest slope of Crater Mountain, the ground surge deposit is overlain by a chaotic, dark green, well indurated volcaniclastic breccia (Figure 25). Angular volcanic and metasedimentary blocks which range from one centimeter to several meters in diameter are set in a sparse matrix of fine ash. In thin section, the matrix is composed almost entirely of isotropic brown glass and dust. Obsidian blocks contain many perlitic cracks which are commonly filled by fibrous hydration products. Spherulites and chalcedony amygdules are locally common. The blocky pyroclastic breccia forms a lensoidal body up to 40 meters thick which has fused

A third type of surge deposit, termed a base surge, is associated with phreatomagmatic eruptions such as those which accompany the formation of maars and tuff rings. These deposits generally show features such as accretionary lapilli or vesiculated tuff layers which indicate deposition as wet ash (Cas and Wright, 1988). Base surge deposits may show undulatory bed forms (Fisher and Schmincke, 1984). The section at Crater Mountain is classified as a ground surge deposit because it occurs at the base of an ash flow sequence and shows no features suggestive of a phreatomagmatic origin.

Block-and Ash Flow Deposit

Along the southwest slope of Crater Mountain, the ground surge deposit is overlain by a chaotic, dark green, well indurated volcaniclastic breccia (Figure 25). Angular volcanic and metasedimentary blocks which range from one centimeter to several meters in diameter are set in a sparse matrix of fine ash. In thin section, the matrix is composed almost entirely of isotropic brown glass and dust. Obsidian blocks contain many perlitic cracks which are commonly filled by fibrous hydration products. Spherulites and chalcedony amygdules are locally common. The blocky pyroclastic breccia forms a lensoidal body up to 40 meters thick which has fused

the upper 20 centimeters of the surge deposit into a dark green banded vitrophyre.

This breccia has may features in common with block-and-ash flow deposits. These deposits are generally unsorted breccias composed of cognate and lesser accidental lithic blocks within an ash matrix. Block-and-ash flows are commonly confined to topographic depressions and occur near the base of ash-flow sequences (Cas and Wright, 1988).

The pyroclastic breccia grades upward into dark red-brown densely welded perlitic rhyolite ash-flow tuff. Pumice lapilli in this portion of the section are compacted to the point that the pyroclastic nature of the rock is unrecognizable in outcrop. In welded ash-flow sequences, flattening of pumice is greatest near the base of the flow. In well preserved ash-flow sequences, length-to-width flattening ratios may be used to infer stratigraphic position (Peterson, 1979).

Origin of Foliation at Crater Mountain

The welded tuff exposed on the top of Crater Mountain was considered by Melson (1964) to be an exogenous dome or plug. However, contact relations show the rhyolite ash-flow tuff is a rootless body which lies unconformably on rocks of

the lower volcanic series. Baked, oxidized outcrops of aphanitic trachyandesite and hornblende trachydacite can be traced without interruption across the lower portion of the west flank of Crater Mountain. Plugs and domes are characterized by flow foliation which is vertical near the core and fans outward from the center of the intrusion (Williams and McBirney, 1979). Numerous foliation measurements show a consistent through-going flow foliation which dips to the northeast (Plate 1). The dip of the flow foliation appears to mirror the dip of the contact with the underlying trachyandesite (Figure 26). The dip steepens toward the southern end of Crater Mountain where it reaches a maximum of 45 degrees.

Thick sections of welded tuff may develop flow foliation by internal shearing produced by flowage or rheomorphism within the cooling and compacting flow unit (Wolff and Wright, 1981). Schmincke and Swanson (1967) showed that extreme flattening of pumice in the Gran Canaria welded tuffs in the Canary Islands resulted from laminar flow which occurred after transport had ceased. The foliation observed in the basal portion of the ash flow tuff at Crater Mountain may reflect shearing within the hot pyroclastic flow caused by slumping of the still-plastic tuff against the wall of a paleovalley incised into rocks of the lower volcanic series.

Similar relations were documented by Chapin and Lowell (1979) for the Wall Mountain tuff of central Colorado. The presence of block-and-ash and ground surge deposits which would be commonly preserved in a topographic depression supports the existence of a west-trending paleovalley on the west slope of Crater Mountain. Pleistocene glaciation and recent landslides have presumably stripped off much the overlying ash-flow tuff and exposed the volcaniclastic units which filled the paleovalley in the west-facing headwall.

Melson (1964) also considered an unnamed conical knob to the east in the center of section 34 (T 14 N, R 7 W) to be an intrusive plug. The presence of consistent flow foliation similar to that observed at Crater Mountain supports an ash-flow origin for this feature as well.

Local Textural Variations

Densely welded tuff exposed along the Continental Divide Trail on the west slope of the conical knob in section 34 exhibits pronounced eutaxitic texture defined by parallel black glassy collapsed pumice lapilli (fiamme). The lower portion of the densely welded zone contains abundant charred twigs (Figure 27).

(Figure 28). A dusky red 5 meter thick paleosol at the base of the ash flow on the northwest slope of Crater Mountain (Figure 29) contains abundant rounded obsidian pebbles which may have been winnowed from the ash cloud as the ground surge passed over the paleoridge.

Welded rhyolite ash-flow tuff is also exposed on a series of low ridges north of the Blackfoot River valley. Here, the upper forty meters of the tuff contains chatoyant sanidine and smokey quartz phenocrysts in similar proportion to that of outcrops of tuff south of the Blackfoot valley, but lithic fragments comprise less than five percent of the rock. Lithic fragments gradually decrease is size and abundance in the upper 100 meters of the section, but no interflow sediments or ash layers have been recognized between the crystal-rich and lithic-rich members.

Lithic-rich Member

Drill hole data obtained by The Seven-Up Pete Joint Venture during mineral exploration at the McDonald Project (T14N, R7W, sect.6) show that the lower lithic-rich portion of the ash-flow tuff is mineralogically and texturally indistinguishable from the section exposed near Crater Mountain. However, a number of lithic-dominated and pumice-dominated layers were observed. The lithic-dominated layers

range from beds the thickness of a single pebble or cobble to clast supported breccias up to ten meters thick. Breccia layers contain both angular and subrounded clasts and commonly show normal grading. Layers which are dominated by compacted pumice lapilli with flattening ratios as high as 16:1 commonly overlie the thick lithic-dominated layers. Pumice layers may exhibit reverse grading. Layers dominated by lithic fragments or pumice are extremely local and discontinuous and can only be traced for a few meters in any direction in outcrop.

Crystal-rich Member

The crystal rich member contains less than five percent lithic fragments. Quartz and feldspar crystals show little evidence of rounding and there are no sedimentary bedforms which would support an epiclastic origin. Crystal-rich tuff contains abundant flattened pumice and evidence of welding which indicates that it was deposited as a hot pyroclastic flow.

The crystal-rich member may result from the eruption of crystal-rich magma as progressively lower portions of the magma chamber were tapped during a single long-lived pyroclastic episode. The accompanying decrease in accidental lithic fragments may reflect sealing of the vent or conduit

walls and paleosurface by successive ash flow pulses during the earlier stages of the eruption.

Origins of Crystal and Lithic-rich Layers in Ash Flows

Hydraulic sorting processes in the vent and within the moving ash flow concentrate crystals and lithic fragments relative to the composition of the magma. Pumice concentrated buoyantly in the upper portion of the eruption column may be deposited from the ash cloud in the later stages of column collapse (Smith, 1960a; Fisher, 1966a). Crystal concentration may also be accomplished by epiclastic processes. Reworking and redeposition of ash-flow deposits may separate ash particles and concentrate crystals and lithic fragments (Fisher and Schmincke, 1984).

Concentrations of lump pumice or lithic fragments may indicate the boundaries between successive flow units within a simple cooling unit (Smith, 1960b). Lithic fragments may be derived from erosion of the magma chamber, conduit or walls of the vent or from erosion of the substrate at the base of a pyroclastic flow. Block or lapilli-size lithic fragments may be concentrated near the base of pyroclastic flows by sorting processes driven by density gradients

similar to those which produce lag deposits in epiclastic depositional systems. Lag-fall breccias have long been considered evidence of deposition proximal to a vent (see for example, Wright and Walker, 1977). However, in recent years, lithic breccias which are medial or distal to known vents have been recognized in many well-studied ash-flow sequences (Cas and Wright, 1988).

Lithic-rich layers at the base of a pyroclastic flow may form by gravitational sinking of lithic fragments within the main body of the flow, with fragment concentration enhanced by high shear gradients at the base (Sparks, 1976). They may also form "ground breccias" as pulses of the main flow temporarily accelerate ahead of the fluidized flow head, as proposed by Wilson (1985) for the Taupo ignimbrite in New Zealand. Roobol and others (1987) Described lithic rich breccias on St. Kitts, West Indies, which were segregated from finer-grained flows as small-volume pyroclastic flows were channeled down steep, vegetation covered gullies. Lithic-rich layers may show crude normal grading whereas pumice-rich layers commonly show inverse grading (Sparks and others, 1973; Buesch and Fisher, 1988; Cas and Wright, 1988).

Lithic populations in the lithic-rich layers appear to reflect the composition of the underlying substrate. This suggests that many of the fragments were locally derived

rather than transported from the vent area. Buesch (1992) described similar locally-derived lithic-rich layers within the lower Miocene Peach Springs Tuff in Arizona and California. The lithic-rich horizons form bodies which are continuous for hundreds of meters, have tabular or lenticular cross-sections, and occur at irregular intervals throughout the thick section of ash-flow tuffs. Paleotopographic reconstruction of the well-exposed ash-flow showed that lithic-rich layers were deposited at the heads of distributary paleochannels. As the pyroclastic flow moves over channels incised into the substrate, turbulence produced by shearing at the base of the flow may cause boundary layers composed primarily of fragments eroded from the substrate to become decoupled from the main body of the flow. Decoupled lithic-rich flows may either advance ahead of the ash-rich portion of the flow as flow-front lobes or "fall away" from the flow on the lee side of topographic ridges (Buesch, 1992; Figure 30).

Volcaniclastic Sediments, Lower Unit (Tvsl)

A complex series of volcaniclastic sediments, which seems to exhibit rapid lateral facies changes, rests disconformably upon the crystal-rich member of the ash-flow tuff. Although only the more resistant units outcrop, exploration drilling in the northeast corner of section 6 (T14N, R7W) has revealed that the volcaniclastic section ranges from 15 to over 80 meters in thickness and contains a wide variety of sedimentary rock types.

Laminated siliceous sinter outcrops sporadically on the low buttes south of Krohn Lake. The white sinter forms low, blocky exposures. It is composed of thinly banded or colloform chalcedony and exhibits planar to wavy, yellowish-brown iron oxide laminae which range in thickness from 2 to 10 millimeters (Figure 31).

Siliceous sinter grades into medium to fine-grained vitroclastic sandstone with pebbly interbeds. The massive, poorly indurated, yellowish-gray sandstone contains sparse (less than five percent) subrounded quartz and feldspar crystals in a matrix of reworked ash particles.

Vitroclastic sandstone is interfingered with moderately well indurated, thinly laminated siltstone, mudstone and claystone beds. The medium light-gray mudstones are locally

varved and contain black carbonaceous laminae and vitroclastic sandstone interbeds (Figure 32). The claystones are locally calcareous and may contain thin beds of gastropod or ostracod debris. Organic-rich carbonaceous beds up to two meters thick have also been observed (J. E. Volberding, pers. comm., 1990).

Rocks of the lower volcaniclastic sedimentary unit were derived by reworking of the crystal-lithic ash-flow tuff and deposition in a fluvio-lacustrine environment. Laminated siliceous sinter probably precipitated as terrace and flowstone deposits rimming hot spring pools. Vitroclastic sandstones with intercalated pebble conglomerates may represent stream channels or sheet flows fed by the hot springs. Varved, organic-rich mudstones and claystones with freshwater fossil debris must certainly have been deposited in lakes or ponds.

Biotite-bearing Rhyolite Tuff (Trb)

Biotite-bearing rhyolite tuff lies disconformably upon units of the lower volcaniclastic sedimentary package. Biotite rhyolite tuff is well exposed in isolated outcrops

along the west side of the Landers Fork valley and in an unnamed valley north of Fleisher Lakes.

The medium-gray tuff forms rounded, steep-sided knobs. The tuff is easily distinguished in the field by its characteristic reddish-brown weathering and by the presence of ubiquitous biotite books (Figure 33). Broken surfaces are studded with bipyramidal smokey quartz crystals and conspicuous chatoyant sanidine phenocrysts which range from 7 millimeters to 1 centimeter in length.

Biotite-bearing rhyolite displays a much wider range of compositional and textural variation than the crystal-lithic rhyolite tuff. In float, the tuff may be unwelded to densely welded with well developed fiamme. Pumice lapilli may be absent or may dominate the rock. Spherulitic zones may contain lithophysae up to ten centimeters in diameter (Figure 34).

Petrography: In thin section, Biotite rhyolite tuff typically contains 20 to 25 percent 2 to 5 millimeter quartz phenocrysts, 5 to 15 percent euhedral sanidine phenocrysts, 2 to 5 percent euhedral biotite crystals and 2 to 5 percent subhedral plagioclase laths set in a matrix of quartz and feldspar crystal fragments, glass shards, and red-brown dust (Figure 35). Subangular fragments of metasedimentary and

intermediate-composition volcanic units comprise less than 5 percent of the rock. Quartz crystals are fractured and embayed. Sanidine phenocrysts commonly show Carlsbad twinning and evidence of partial resorption. Twinned plagioclase laths, which commonly form parallel aggregates or glomerocrysts with sanidine crystals, are also partially resorbed and may exhibit sieve texture. Biotite books are commonly ragged or broken. Apatite occurs as sporadic inclusions in plagioclase, and biotite, zircon, and apatite appear as tiny euhedral microcrysts in the groundmass. Pumice lapilli are flattened and draped around lithic fragments and crystals.

Field Relations: Biotite-bearing rhyolite tuff is commonly removed from the section by erosion. However, the presence of biotite rhyolite as the dominant clast type throughout much of the conglomerate member of the upper volcaniclastic sedimentary package suggests that biotite rhyolite may have once covered a much more extensive area than present exposures indicate.

Volcaniclastic Rocks, Upper Unit (Tvsu)

Poorly consolidated conglomerates, sandstones, and mudstones of the upper volcaniclastic sedimentary unit disconformably overlie biotite-bearing rhyolite tuff or unconformably overlie members of the lower volcaniclastic unit where biotite rhyolite is missing. Rocks of the upper unit are exposed over an area of at least 8.5 square kilometers. In float, weathered conglomerate may be distinguished, with difficultly, from bouldery glacial till by the presence of iron oxide or clay coatings on clasts.

Southeast of Krohn Lake, east-west-trending ridge crests are strewn with boulders of biotite-bearing rhyolite up to 15 meters in length which have weathered out of the conglomerate. North-facing slopes of these ridges are scarred by numerous landslide blocks which exhibit fresh scarp morphology. These outcrops were mapped as biotite-bearing rhyolite during reconnaissance mapping of this area on the basis of the heterolithic nature of the float blocks

In outcrop, the upper volcaniclastic unit is composed of numerous sequences of boulder or cobble conglomerate which fine upward into coarse-grained sand and thin clay beds (Figure 36). The conglomerates commonly exhibit crude normal grading and are locally well imbricated. Well-rounded

boulders and cobbles are coated with iron oxide and lie in a sparse clay or sand matrix which may be partially cemented with ferrocrete. Boulder layers may be draped by thin clay beds. Clast populations are dominated by biotite-bearing rhyolite, but crystal-lithic rhyolite, porphyritic and aphanitic units of the lower volcanic series, sinter, and Precambrian quartzite are also represented. Near the tops of conglomerate sequences, channels armored with pebbles or cobbles are commonly truncated by coarse-grained, poorly sorted sandstone beds (Figure 37).

The upper volcaniclastic unit reaches a maximum exposed thickness of 90 meters in a scarp at the head of a landslide west of Landers Fork (west edge of Section 30, T 15 N, R 7 W). However, drilling near Sawmill Gulch (SW corner Section 32, T 14 N, R 7 W) intercepted up to 400 meters of poorly consolidated conglomerate and sandstone. Isolated lenses of bouldery gravel which occur on two northwest-trending ridges north of the Continental Divide Trail and at the mouth of Canyon Creek indicate that gravels of the upper sedimentary unit may have blanketed much of the volcanic field.

The upper volcaniclastic unit has sedimentary structures which suggest deposition in a braided stream or alluvial fan environment. The individual sedimentary sequences show a wide variety of grain sizes ranging from mud to boulders,

indicative of a wide range of hydraulic conditions. The great thickness and areal extent of the unit and the presence of abundant, pebble-armored cut-and-fill structures and clay-draped boulder layers favors an alluvial origin for this unit. The presence of iron oxide clast coatings and ferrocrete cement suggests deposition in an arid environment. Boulder and cobble sized clasts in alluvial fan sequences are characteristically subangular due to deposition as proximal debris flow lobes (Davis, 1983). However, the dominance of well rounded clasts in the upper volcaniclastic unit may be attributed to spherical weathering commonly observed in outcrops of biotite-bearing rhyolite.

Minor Intrusive Units

Aphanitic and porphyritic dikes which range in composition from mafic to felsic occur throughout the Crater Mountain volcanic complex. However, the volume of intrusive rocks is strikingly small compared to the volume of volcanic rocks in the complex. The intrusive latite dome complex in the Humbug Creek area is the only major vent source identified in the Crater Mountain complex. This may be due, in part, to the lack of continuous outcrop and the difficulty

in recognizing intrusive relationships among texturally and compositionally similar units, but may also be attributed to the northeastward decrease in abundance of dikes in the Eocene dike swarm which lies along the trend of the Idaho-Montana porphyry belt (D. W. Hyndman, pers. comm., 1991). Intrusive phases of the Crater Mountain volcanic complex are described below from oldest to youngest.

Porphyritic Trachyandesite Intrusions (Tpti)

Porphyritic trachyandesite dikes occur along the southern flanks of Crater Mountain and along the west slope of the steep, conical knob to the southeast. According to Melson (1964) similar dikes commonly fill en echelon high angle tension fractures in Belt rocks in the vicinity of the Silver Bell stock.

In outcrop, the dikes stand as vertical walls with prominent columnar joints. The dark brownish black trachyandesite weathers medium bluish gray and exhibits a crude flow foliation defined by alignment of euhedral 5 millimeter to 1 centimeter plagioclase laths (Figure 38). Tabular 1 to 2 millimeter pyroxene and biotite crystals show dusky red iron oxide rims.

Petrography: Under the microscope, the rock contains 25 to 35 percent plagioclase phenocrysts and glomerocrysts, with variable amounts of biotite, augite, and altered olivine phenocrysts and lesser amounts of hornblende crystals set in an aphanitic groundmass (Figure 39). Plagioclase commonly displays albite and Carlsbad twinning and oscillatory zoning. Plagioclase composition, determined using the Michel-Levy method, is andesine (An_{40}). Some plagioclase crystals have thin rims of albite. Rare, subhedral sanidine crystals occur in glomerocrysts with plagioclase. Subhedral augite phenocrysts are rimmed with opaque oxides and display pale-green-yellow pleochroism. Books of brown biotite show pale brown-dark brown pleochroism and contain abundant opaque oxide lamellae. Five to seven millimeter euhedral olivine crystals are skeletal or are pseudomorphed by 'bowlingite' and rimmed by 'iddingsite.' Accessory minerals include rutile and sphene. Prismatic brown hornblende crystals show rims of magnetite or earthy brown hematite.

The groundmass is composed primarily of aligned feldspar microlites with subordinate microcrysts of augite and lesser amounts of olivine. Opaque magnetite needles form scattered interstitial clots.

Field Relations: Along the south flank of Crater Mountain, porphyritic trachyandesite dikes intrude porphyritic latite flows. To the southeast, rhyolite ash-flow tuffs overlie porphyritic latite flows which are cut by porphyritic trachyandesite dikes. South of Swede Hollow (SE corner Section 23, T14N, R8W) a 30 meter-thick porphyritic trachyandesite dike intrudes a porphyritic latite flow and is truncated by aphanitic trachyandesite lava flows.

Aphanitic Mafic Intrusions (Tmi)

Aphanitic mafic dikes occur near the Precambrian-volcanic contact along the south side of the Blackfoot River Valley and on the top of Columbia Flat. Black aphanitic dikes form low, massive outcrops with hackly joint faces. Broken surfaces may show abundant equant 0.2 millimeter mafic microcrysts.

Petrography: In thin section, the rock exhibits intergranular texture defined by aligned plagioclase laths and interstitial prismatic augite crystals (Figure 40). Euhedral to subhedral olivine microcrysts, which comprise up to 15 percent of the rock, are pseudomorphed by yellow-brown

'iddingsite' and are rimmed with green augite. Pyroxene crystals commonly display rims of brown amphibole. Red-brown biotite forms interstitial subhedral plates. Accessory minerals include K-feldspar microlites and tiny interstitial grains of sphene. Based on modal mineral content, this rock is classified as an augite-olivine basalt. The presence of abundant olivine and biotite suggests an alkaline affinity. Some of the aphanitic mafic dikes are classified as shonkinite on the basis of abundant potassium-bearing mafic minerals as phenocrysts.

Field relations: In the lower half of Section 13 (T 14N, R8W), northwest and northeast-striking aphanitic mafic dikes intrude dolomite of the Helena Formation and porphyritic latite flows. Similar relations were observed in the northeast corner of Section 8 (T14N, R7W).

Porphyritic Rhyolite Intrusions (Tri)

Porphyritic rhyolite dikes form resistant free-standing ribs which occur near the southwestern and northeastern margins of the ash-flow tuff. This unit is texturally and compositionally similar to rhyolite ash-flow tuff, but both

quartz and sanidine phenocrysts are larger and less broken than those in the ash-flow sheet. The light gray porphyritic rhyolite weathers pale yellow and broken surfaces are studded with centimeter-size euhedral sanidine phenocrysts and smokey quartz crystals (Figure 41). Fragments of green glass and accidental lithic fragments are common. Intrusive rhyolite dikes cut rocks of the Belt Supergroup and the lower volcanic series and may represent fissure-type vents for rhyolite ash-flow tuff.

Field Relations: Northeast-striking porphyritic rhyolite dikes cut outcrops of argillite of the Spokane Formation and aphanitic trachyandesite flows west of Wizard Mountain (NE corner Section 12, T 14 N, R 7 W). A northeast-striking porphyritic rhyolite dike also intrudes aphanitic trachyandesite on the north fork of Humbug Creek (S. E. quarter Section 25 T 14 N, R 8 W). The dike forms a free-standing rib which can be followed south-southeast along strike for over 300 meters.

STRATIGRAPHY

For purposes of stratigraphic analysis, the study area is divided into three regions of reasonably continuous outcrop (Figure 42). These regions are separated by large covered areas or post-volcanic normal faults. The southeast region is separated from the southwest region by Seven-Up Pete Creek. The northern region lies north of the Blackfoot River.

Analysis of map patterns shows that most contacts between units of the Crater Mountain volcanic complex are not horizontal and many are discontinuous and exhibit more than 100 meters of vertical relief. This is due to the lobate nature of siliceous lava flows, the extensive periods of erosion between successive eruptions, and the irregular nature of the eroded substrate over which the lavas flowed.

Figure 43 is a fence diagram illustrating the stratigraphic relationships among units of the Crater Mountain volcanic complex. Maximum exposed thicknesses are used for the rock units in the three stratigraphic columns. Correlations between columns are based on similarities in lithologic character and stratigraphic relationships described in the Unit Description chapter above.

GEOCHEMISTRY

Thirty-one samples were analyzed for major and trace element content to aid in classification of units and to help understand the petrologic character of the Crater Mountain volcanic complex. Complete suites of most major map units were analyzed to test correlations based on phenocryst assemblages and field relations. Amygdaloidal andesite was not analyzed due to the ubiquitous presence of secondary minerals.

Collection and Preparation

Most of the units in the Crater Mountain complex exhibit some degree of deuteric alteration. Samples were selected from sites which showed minimal evidence of alteration or weathering. Collection sites are described in detail in Appendix I.

Petrographic examination shows significant alteration which was not evident in outcrop in five of the samples. Samples CM-153 (hornblende trachydacite) and CM-154

(porphyritic latite) show pervasive potassic alteration. Plagioclase laths are almost completely replaced by fine-grained, intergrown adularia, quartz, and carbonate, and locally, by clay minerals. Two samples of porphyritic latite (CM-105 and CM-126) contain secondary quartz and one rhyolite ash-flow tuff sample (CM-132) shows pervasive devitrification. These samples are not included in the analysis of geochemical results below.

With the exception of rhyolite ash-flow tuff samples, the samples are free of lithic fragments. All exposures of rhyolite ash-flow tuff contain lithic fragments, and collection of samples containing fragments from Belt Supergroup and lower volcanic series units was unavoidable. Macroscopic fragments were removed from crushed samples, but a small quantity of microscopic fragments remained.

Analyses of ash-flow tuff samples must be considered preliminary because the bulk chemical composition of a pyroclastic flow may vary considerably from that of the magma from which it was derived. Segregation and winnowing of particles in the gas-inflated eruptive column (elutriation) and during flowage may concentrate crystals and lithic fragments and deplete fine-grained vitric particles (Fisher and Schmincke, 1984).

Samples were crushed to chips approximately one centimeter in diameter with a chipmunk jaw crusher. Coarse grained and porphyritic samples were then pulverized to minus 80 mesh with a disc grinder and a one-quarter split of rock powder was prepared with a Jones splitter to minimize sample bias.

Analysis

Thirty samples were analyzed by the Geoanalytical Laboratory of Washington State University at Pullman, Washington. Major and trace element analysis was by by lithium tetraborate fusion and X-ray fluorescence (XRF) using a Rigaku Automatic X-ray Spectrometer. Major elements are reported as oxides in weight percent. Total iron is expressed as FeO*. Trace elements are reported in parts per million with detection limits of 1 to 30 ppm. The detection limits for Rb, Sr, Zr, Nb, and Y are 10.0 ppm. Results for Ni, Cr, Sc, V, and Ba can only be considered semi-quantitative for values below 30 ppm due to inherent nickel contamination of the Rh target.

One sample (CM-184) was part of a suite analyzed, by Chemical and Mineralogical Services, Salt Lake City, Utah for

The Seven-Up Pete Joint Venture. The sample was pulverized and subjected to four acid digestion and lithium meta-borate fusion. The sample was analyzed with an Inductively-Coupled Plasma Mass Spectrometer (ICP-MS) using a Nd:YAG laser sampler. Major elements are reported as weight percent oxides with detection limits ranging from 0.01 to 0.10 percent. Trace elements are given in parts per million with detection limits of 0.05 ppm to 0.10 ppm. Results for this unit must be considered preliminary because fragments from sedimentary units of the Belt Supergroup and from volcanic units of the lower volcanic series were not removed from the sample during preparation.

Results

Average whole rock geochemical analyses for map units of the Crater Mountain volcanic complex are given in Table 3. Individual analyses are listed in Appendix D. Units of the Crater Mountain complex range from 55 to 80 weight percent silica. Rocks of the lower volcanic series contain 55 to 65 percent whereas ash flow tuffs of the upper series contain 76 to 80 percent silica. These values are higher than the average silica content of 74 percent reported for rhyolite ash-flow tuffs (Hyndman, 1985, p. 273). Although

petrographic examination shows no evidence of secondary silica deposition, these rocks do contain abundant fragments of argillite. It is possible that the silica content of these samples is augmented by fine-grained siliceous lithic fragments in the matrix.

Harker diagrams indicate clear trends among most major oxides versus SiO_2 (Figure 44). This relationship cannot be due solely to magmatic differentiation because radiometric age data and field relations indicate a 10 million-year age difference between trachyandesite and trachydacite lavas and rhyolite ash-flow tuffs. The pronounced "silica gap" between units of the lower and upper series also argues against a simple genetic relationship between the two suites. The complex eruptive sequence is not indicative of evolution of the two series by simple differentiation of a single parent magma. The eruptive sequence is: trachydacite-trachyandesite-trachydacite-trachyandesite--dacite-rhyolite.

Many of the rocks of the lower volcanic series were previously mapped as andesites (Melson, 1964, Whipple and others, 1987). However, the average potassium content of these rocks is higher than the average range for typical arc andesites (Hyndman, 1985, p. 256, Table 7-4). The units of the lower series contain from 2.91 to 5.00 percent potassium oxide.

Most of the rocks of the lower series exhibit some degree of alteration. Potassium metasomatism manifested as replacement of plagioclase by K-feldspar may increase the potassium content of volcanic rocks adjacent to hydrothermal systems and wide spread metasomatism of silicic ignimbrites and mafic lavas by alkaline saline brines has been reported in active basins (Chapin, 1992). Augmentation of potassium is always accompanied by strong depletion of calcium and sodium. Samples CM-153 and CM-154, which were collected near a prospect which exploited quartz-barite veins, were considered unsuitable for use in geochemical classification schemes because whole rock analyses of these samples show enrichment of potassium and severe depletion of sodium and calcium (Appendix B). All of the 17 samples from units of the lower series considered fresh enough for geochemical classification show calcium and sodium contents consistent with those of average trachyandesites and dacites (Hyndman, 1985, p. 256, Table 7-4). This suggests that the rocks have not undergone potassium metasomatism and that the chemical analyses reflect the inherent potassium content of these rocks.

Normative Minerals

Normative minerals were calculated using conventions of of the CIPW system (Kelsey, 1965) and the results are given in Table 4. Normative minerals were calculated by the percent cation equivalent method of Barth and Niggli (Chayes and Metais, 1964) for use with the Irvine and Baragar (1971) alkaline vs. subalkaline classification system for volcanic rocks.

X-ray fluorescence analyses report total iron as FeO*. For the calculation of normative minerals, the ratio of FeO to Fe_2O_3 was recalculated following the method of Le Maitre (1976).

Classification

Streckeisen and LeMaitre Classification

Streckeisen and LeMaitre (1979) proposed a classification scheme for volcanic rocks based on CIPW normative quartz, anorthite, albite and orthoclase. This system is considered less reliable for aphanitic volcanic rocks because the fields for volcanic rocks are extrapolated

from the fields determined according to the IUGS scheme from modal mineralogy of their plutonic counterparts. Figure 45 is a plot of Streckeisen and LeMaitre's normative classification of volcanic rocks for samples from the Crater Mountain complex.

This system does not clearly differentiate among members of the lower volcanic sequence. Porphyritic andesite of the Silver Bell stock and porphyritic latite of the lower volcanic series plot in the quartz trachyte field Samples of aphanitic trachyandesite, hornblende trachydacite and aphanitic dacite plot in both the quartz trachyte and quartz latite fields. Rhyolite ash flow tuff and biotite-bearing rhyolite are well discriminated and plot in the alkali feldspar rhyolite field.

Irvine and Baragar Classification

The Irvine and Baragar (1971) classification of volcanic rocks is based on statistical evaluation of suites of volcanic rocks from many different magmatic associations. The system defines fields of chemically similar volcanic rocks based on elements from four subsystems. Alkaline suites are distinguished from subalkaline suites using the

alkali-silica plot of MacDonald and Katsura (1961) and the quaternary system Cpx-Ol-Ne-Q of Yoder and Tilley (1962). The AFM ternary system is used to discriminate calc-alkaline and tholeiitic suites. Plots of normative color index versus normative An % distinguish volcanic rock types within the calc-alkaline series. Each of these subsystems is discussed below. Analyses for rocks of the Crater Mountain volcanic complex are presented in Figures 45-49 and classified according to the Irvine and Baragar classification scheme in Table 5.

MacDonald and Katsura Classification

The MacDonald and Katsura (1964) classification system plots weight percent SiO_2 vs. Na_2O + K_2O to discriminate between alkaline and subalkaline suites (Figure 46). Irvine and Baragar (1971) modified the line dividing the two fields to more accurately represent the composition of many well studied suites of volcanic rocks. The rocks of the lower volcanic series of Crater Mountain complex plot on the boundary between the alkaline and subalkaline fields whereas those of the upper series are distinctly subalkaline.

Ol'-Ne'-Q' Classification

Figure 47 is a plot of the rocks of the Crater Mountain complex in the Ol-Ne-Q ternary system. Suites of alkaline and subalkaline volcanic rocks may be distinguished using CIPW normative minerals Ol, Ne, and Q (Irvine and Baragar, 1971). The contents of the Cpx-Ol-Ne-Q tetrahedron defined by Yoder and Tilley (1962) are projected from Cpx onto the basal triangle Ol'-Ne'-Q' as suggested by Poldervaart (1964). All of the units of the Crater Mountain volcanic complex plot in the subalkaline field (Figure 48).

AFM Classification

The AFM classification of igneous rocks plots total iron (Feo*= FeO + Fe_2O_3 recalculated as FeO) vs. total alkalis (A = Na_2O + K_2O) vs. magnesium (M = MgO) to discriminate between tholeiitic and calc-alkaline suites (Irvine and Baragar, 1971). Rocks of the Crater Mountain complex follow the calc-alkaline trend (Figure 48).

The calc-alkaline nature of the rocks is supported by the ubiquitous presence of magnetite crystals in the groundmass of units of the lower volcanic series. Calc-

alkaline suites do not show the iron enrichment trend characteristic of tholeiitic suites because iron is removed continuously from the magma as magnetite throughout the differentiation process (Hyndman, 1985).

Normative Color Index

Irvine and Baragar's (1971) classification scheme plots normative color index (Ol + Di + Hy + Mt + Il + Hm) versus An % (100 AN/(An + Ab). Field boundaries separating basalt, andesite, dacite and rhyolite are based on modal analyses of many suites of porphyritic volcanic rocks (Figure 47).

This system separates rhyolite ash flow tuffs from the rocks of the lower volcanic sequence, but does not discriminate among the units of the lower volcanic sequence. Porphyritic latite and aphanitic dacite fall in the dacite field and porphyritic trachyandesite intrusions and andesite porphyry lie in the andesite field. However, samples of aphanitic trachyandesite and porphyritic hornblende trachydacite lie in both fields.

Le Bas and Others Classification

The total alkali-silica classification of volcanic rocks devised by LeBas and others (1986) on behalf of the IUGS Subcommission on the Systematics of Igneous rocks plots SiO_2 vs. $Na_2O + K_2O$. Seventeen compositional fields are recognized based on computerized data bases which include chemical analyses of 24,000 volcanic rocks. This system is preferred for classification of the units of the Crater Mountain complex because it discriminates the potassium-rich members from the andesite and dacite fields defined by Irvine and Baragar (1971).

Porphyritic latite hornblende trachydacite and aphanitic trachydacite plot in the trachydacite field (Figure 50). Aphanitic trachyandesite plots on the boundary between the trachyandesite and trachydacite fields. Rhyolite ash-flow tuff and biotite-bearing rhyolite tuff plot in the rhyolite field.

K_2O vs SiO_2 Plot

The potassium content of the rocks of the lower volcanic series is much higher than the range for average andesites

and dacites. Variation in abundance of potassium versus silica content can be used to classify volcanic rocks and to discriminate among magmatic series (Peccerillo and Taylor, 1976).

Figure 51 is a plot of weight percent K2O versus weight percent SiO2. Most of the samples from rocks of the lower volcanic series plot in the high-K calc-alkaline series. However, three of the samples plot in the shoshonite series. Although the data show considerable scatter, this plot illustrates the potassic nature of the rocks of the lower series. The andesites of the Garnet Range volcanic pile (Carter, 1982) and the early intermediate-composition phases of the Challis volcanics (Hackett and others, 1988) show similar potassic affinities.

Alkali-Lime Index

Figure 52 is an alkali-lime plot for rocks of the Crater Mountain complex. The alkali-lime index devised by Peacock (1931) is used to compare the alkalinity of entire suites of genetically related rocks. The suite of chemical analyses for rocks of the lower volcanic series gives an alkali-lime index of 55 which is within the alkali-calcic field. Samples

from the upper volcanic series do not show enough variation to allow determination of alkali-lime index.

Chemical and petrographic data suggest that the rocks of the lower series may be genetically related, but field relations and geochemical trends do not support a genetic relationship between the rocks of the lower and upper series. The presence of olivine and abundance of magmatic biotite in aphanitic trachyandesite and in aphanitic and porphyritic mafic dikes support an alkaline affinity for rocks of the lower volcanic series. The high silica content and higher ratio of alumina to total alkalis indicate a calc-alkaline affinity for the rocks of the upper series.

Trace Element Chemistry

Figure 53 is a "spider diagram" for analyses from the rocks of the Crater Mountain complex. Elements are normalized to chondrite abundances using the normalization factors of Thompson (1982).

Trace element analyses differentiate the rocks of the upper and lower series into two chemically distinct suites. All of the samples analyzed show enrichment in large-ion lithophile and light rare earth elements. However, trace

element compositions for the units of the lower series show high concentrations of Ba (2801-3840 ppm) and Sr (1147-1648 ppm) compared to plots of upper series rhyolitic rocks. Ba enrichment is commonly associated with alkalic suites. Plots for rocks of the upper series show distinct troughs at Sr, P, and Ti whereas those of the lower series show a comparatively flat pattern from La to Y.

The rocks of the lower volcanic series are enriched in most incompatible elements relative to normal midocean ridge basalt. They are also enriched in low field strength elements (Ba, Sr, Rb, and Th) and depleted in high field strength elements (P, Zr, and Y) compared to within-plate alkaline basalt.

High valence cations in rocks of the lower volcanic series show higher abundances than typical cal-alkaline series. Nb abundance for rocks of the lower volcanic series is considerably higher than average andesitic values (4.3 ppm) reported by Taylor (1969). Nb values, which range from 7.8 to 22.8 ppm, are more consistent with analyses of high-K andesites (Peccerillo and Taylor 1976). Th abundance (average 13 ppm) is also elevated compared to that of average andesite.

GEOCHRONOLOGY

Sample Collection and Preparation

Nine samples collected from six of the map units of the Crater Mountain volcanic complex were submitted to Geochron Laboratories Division of Krueger Enterprises, Inc., Cambridge Massachusetts for potassium-argon age determination. Sample locations and results are given in Table 6. Sample sites were selected that could yield the freshest samples. Outcrops were excavated to remove weathered material and fresh cores were broken from excavated blocks. Sample locations are described in detail in Appendix C.

Analysis and Results

Whole-rock samples were crushed to -80/+200 mesh and treated with dilute HF and HNO_3. Argon analyses are reported in parts per million and potassium analyses are reported in weight percent. Averaged results from at least two analyses

were used in radiometric age calculations. Detailed K-Ar analyses are given in Appendix E.

Age is determined by the formula:

$$AGE = \frac{1}{\lambda_\beta + (\lambda_\theta + \lambda_{\theta'})} \ln \left[\frac{\lambda_\beta + (\lambda_\theta + \lambda_{\theta'})}{(\lambda_\theta + \lambda_{\theta'})} \times \frac{^{40*}Ar}{^{40}K} + 1 \right]$$

Constants Used:

$\lambda_\beta = 4.962 \times 10^{-10}$ / year

$(\lambda_\theta + \lambda_{\theta'}) = 0.581 \times 10^{-10}$ / year

$^{40}K / K = 1.193 \times 10^{-4}$ g/g

Age relations among units and precision of K-Ar analyses are shown in Figure 54. A hornblende separate prepared from sample CM-162D yields an age of 48.3 +/- 2.0 M.Y. for porphyritic hornblende trachydacite (Tpt). Petrographic analysis shows that, with the exception of thin opaque oxide rims, brown hornblende phenocrysts are free of inclusions or alteration products.

Biotite concentrate from intrusive andesite porphyry (Tap) yields a similar age of 48.5 +/- 1.2 M. Y. Brown biotite books contain abundant apatite inclusions, but appear

unaltered under the microscope and show no evidence of strain.

Melson (1964) noted that dikes of similar composition which occur in the contact aureole of the Silver Bell stock lack chilled margins which suggests that they were intruded before the stock had cooled. McKee (1978) showed that rocks of the lower volcanic series were hydrothermally altered within the contact aureole of the Silver Bell stock and inferred that the stock was younger than the altered volcanic rocks. The excellent agreement between the age obtained for hornblende trachydacite and andesite porphyry and the 48.2 +/- 1.8 Ma age reported for granodiorite of the Silver Bell stock (Daniel and Berg, 1981) indicates that the flows and associated intrusions of the lower volcanic series may have been deposited before the Silver Bell stock had cooled.

Sanidine concentrates prepared from rhyolite ash-flow tuff (Trt) samples CM-159D and 163D give ages of 37.7 +/- 1.0 m. y. and 38.0 +/- 1.0 Ma, respectively. Sample 163D was collected from the excavation from which Chadwick (1980) obtained a sanidine age of 27.8 +/- 1.5 Ma. Chatoyant sanidine crystals from the dated samples show some evidence of resorption, but are fresh and free of inclusions. The Eocene date of 37.7 +/- 1.0 Ma is preferred over the Oligocene date obtained by Chadwick because it is consistent

with radiometric ages given for similar ash flow tuffs in the Avon and Helena volcanic fields (Chadwick, 1978, 1981). Chadwick's (1981) sanidine separate may have experienced argon loss.

A sanidine separate from sample CM-184 (biotite-bearing rhyolite ash-flow tuff) gives an age of 36.5 +/- 0.9 M. Y. whereas biotite concentrate from the same sample yields an older age of 39.0 +/- 1.0 Ma Sanidine ages are usually considered more reliable than biotite ages because sanidine locks in argon at a higher temperature and is less susceptible to argon leakage. Stratigraphic relations also show that biotite-bearing rhyolite is younger than rhyolite ash-flow tuff.

Whole rock samples of porphyritic latite (Tpl) (CM-120D and KC-1D) and aphanitic trachyandesite (Tat) (CM-122D, KC-2D, and TA-2D) were also analyzed. Samples CM-120D and KC-1D give ages for the porphyritic latite of 38.6 +/- 1.0 M. Y. and 38.1 +/- 1.0 M. Y., respectively. Whole rock ages for aphanitic trachyandesite range from 37.2 +/- 1.0 Ma to 42.2 +/- 1.4 M. Y.

Petrographic analysis shows evidence of deuteric alteration in each of these samples which could result in argon loss. Ages given for these samples do not agree with stratigraphic relations which indicate that porphyritic

latite and aphanitic trachyandesite are older than hornblende trachydacite. Therefore, radiometric dates for these rocks must be regarded as minimum ages.

Hornblende can acquire excess radiogenic argon, yielding an erroneously old age, whereas biotite is susceptible to argon loss due to heating, deuteric or hydrothermal alteration, or deformation, giving an apparent age that is too young (Hyndman, 1985). However, the age given for hornblende trachydacite is considered valid because it is in good agreement with the biotite age obtained for intrusive andesite porphyry and hornblende and biotite phenocrysts show no evidence of alteration.

Potassium-argon analyses show a minimum age difference of approximately eight million years between hornblende trachydacite (Tpt) and rhyolite ash-flow tuff (Trt) (Figure 54). This age difference is supported by field relations which indicate that rhyolite ash-flows were deposited onto an irregular surface incised into the rocks of the lower volcanic series.

STRUCTURAL GEOLOGY

Introduction

Rocks in the study area show evidence of at least four episodes of deformation Structural features may be grouped into: (1) Pre-Eocene folds and faults which are older than and overlain by the Crater Mountain volcanic rocks (48-37 Ma) and (2) Eocene to Recent normal faults which offset units of the Crater Mountain complex.

Pre-Eocene Deformation

In Middle Proterozoic time, sedimentary rocks of the Belt Supergroup experienced gentle tilting and low-grade metamorphism which formed broad, open north and northwest-trending folds. Left lateral shear along some fault segments between Middle Proterozoic and Middle Cambrian time tightened and reoriented many of the early-formed north-trending folds (Harrison and others, 1974). Deformation was followed by a

long period of erosion which produced regional low-angle unconformities.

From late Cretaceous (72 Ma) to Eocene (48 Ma) time, east-directed thrusting associated with the Laramide orogeny produced a series of northwest-trending, broad open folds accompanied by development of a pervasive fracture cleavage (Melson, 1964; Mudge and Earhart, 1980; Gries, 1983). Laramide crustal shortening was closely followed or accompanied by an episode of Late Cretaceous to Eocene normal faulting with right lateral slip occurring along some fault segments (Wallace and others, 1990). Deformation in the study area may be associated with the intrusion of several granitic stocks thought to be related to the Boulder batholith (Melson, 1964).

Major structural elements in the region include: (1) the northwest-trending Black Mountain syncline (Bierwagen, 1964); (2) the N10W-striking Scapegoat thrust fault, located on the eastern margin of the study area; (3) the east-striking Saint Marys-Helena Valley fault which lies to the south (Wallace and others, 1990); and (4) the Rochester Gulch and several other unnamed northwest-striking normal faults south of the Crater Mountain volcanic complex (Melson, 1964; Whipple and others, 1987).

In the study area, fracture cleavage is most visible in pelitic Belt rocks and shows consistent dips to the northwest, regardless of bedding attitudes. This relationship shows that the area lies entirely within the northeast limb of the southeast-plunging Black Mountain syncline (Melson, 1964).

The Scapegoat thrust fault defines the western edge of the Montana Disturbed Belt and separates the Scapegoat thrust plate from the underlying Hoadley thrust plate. Rhyolite ash-flow tuffs of the upper volcanic series (38 Ma) overlie and clearly postdate movement of the Scapegoat thrust fault.

The Saint Marys-Helena Valley fault is the northeastern extension of a zone of aligned fold axes and strike-slip faults referred to collectively as the Montana lineament (Weidman, 1965) or the Lewis and Clark line (Harrison and others, 1974). Offset fold axes along the western segment of this fault indicate that at least 13 Km of right lateral slip displacement occurred between Late Cretaceous and Eocene time (Wallace and others, 1990).

Many normal faults in the region are oriented parallel to the northwest trend of the Montana lineament or the northeast trend of the Montana disturbed belt (Plate 1). Northwest-striking normal faults along the southern boundary of the study area repeat the contact between the Empire and

Helena Formations three times. The contact between the Helena and Snowslip formations is also repeated by a northwest-striking fault southwest of Baldy Mountain (Whipple and others, 1987).

According to Melson (1964) the contact aureole of the Silver Bell stock (48 Ma) affects Belt rocks on either side of the north-south-striking Rochester Gulch fault. The fault and associated breccia zone cut and displace the central portion of the stock; therefore the fault must have been active before, during, and after emplacement of the stock (McKee, 1978).

Eocene to Recent Structures

Field Characteristics

Units of the Crater Mountain volcanic complex are offset by northeast, northwest, north, and east-striking normal faults. Fault traces are recognized in locations where contacts are unusually linear or are abruptly offset. Faults which lie entirely within a single rock unit would not be identified unless distinct marker horizons were present. Many of the faults are not exposed because the shattered and brecciated rock is easily weathered and eroded. Faults are

generally expressed as low, heavily vegetated topographic depressions which commonly lie parallel to, but not necessarily along the axis of, major stream valleys.

Description of Principal Faults

The Rochester Gulch fault displaces the Helena Formation down-to-the-west against the Empire Formation. However the contact between porphyritic latite and the underlying Belt rocks shifts a minimum of 120 meters to the north on the west side of the fault. North of Humbug Creek, two splays of the fault place porphyritic latite breccia against aphanitic trachyandesite flows. These relationships could result from: (1) dip-slip motion down-to-the east, (2) dextral strike-slip movement or (3) scissors motion about a pivot point somewhere near the ridge crest with normal displacement down-to-the west along the southern segment and down-to-the east along the northern segment of the fault. The exact mechanism cannot be resolved due to poor exposure. The contact between porphyritic latite flow and Helena dolomite is also displaced by the Fool Hen fault of Melson (1964) and another unnamed northwest-striking fault near the head of Poorman Creek.

The northwest-striking Tar Head Creek fault (Melson, 1964) lies parallel to the trace of the Scapegoat thrust fault. Porphyritic latite flows (Tpl) and rhyolite ash-flow

tuff (Trt) are truncated against argillite of the Spokane Formation (Ys) to the east. The abrupt linear contact between Tpl and Ys indicates that normal fault motion postdates deposition of latite flows. It is not clear if Trt is cut by the fault or if the ash-flows were buttressed against an upthrown block of Ys.

South of Black Diamond Creek, Whipple and others (1987) mapped a northwest-striking fault which places Helena dolomite down to the west against shale of the Empire Formation, but shows no displacement of units of the lower volcanic series. Map patterns from this study show that the southeastern segment of this fault offsets the contact between porphyritic latite flows and Empire shale. The sinuous nature of the contact and dense vegetative cover make it difficult to recognize fault displacement between aphanitic trachyandesite and porphyritic latite across the fault trace.

North of Black Diamond Creek, two north-striking faults define a horst block comprised of Spokane argillite intruded by Late Proterozoic-age diorite. The faults host quartz fissure veins; adjacent to the veins, porphyritic latite and aphanitic trachyandesite flows are brecciated and silicified. The southern extension of the westernmost of these faults places aphanitic andesite down-to-the-west against hornblende

trachydacite near Columbia flat and is intruded by a rhyolite dike south of the Last Chance Mine. West of Crater Mountain, a block of hornblende trachydacite is down-dropped against porphyritic latite flows by two east-striking faults. A southwest-striking splay of the southern fault is exploited by quartz fissure veins.

The Beaver Creek fault forms the northwestern boundary of the Crater Mountain volcanic complex. The fault displaces unconsolidated sand and gravel beds of the upper volcaniclastic sedimentary unit (Tvsu), and northeast of Keep Cool Lakes, several small basalt dikes appear to have been intruded along the trace of the fault (Whipple and others, 1987; W. H. Wilkinson, pers. comm., 1990). Tvsu sediments are also displaced by several other minor northeast and northwest-striking faults (W. H. Wilkinson, pers. comm., 1991). Contact relations observed in drill core from the McDonald Meadow area indicate regional tilting of approximately twenty degrees to the north along these late Tertiary faults.

Based on field relations, I postulate that a major northeast-striking normal fault with a minimum displacement of 360 meters lies along the axis of the Blackfoot River valley which is herein named the Blackfoot Valley fault (Plate 2). Presence of this fault is based on: (1) downward

displacement of the lower volcanic series on the northwest side of the Blackfoot valley; (2) the presence of sheared, shattered rock and perched lenses of volcaniclastic sediments along the steep southeast slopes of the valley walls; and (3) the linearity of the Blackfoot River valley. The Blackfoot Valley fault must either terminate abruptly to the east across Willow Creek or it must display differential scissors-type motion along its strike because Proterozoic diorite sills within the Spokane Formation show no apparent offset in this area.

Influence of Regional Structures

The location of many of the late Cretaceous to Eocene igneous centers in western Montana has been influenced by long-lived regional structures. The Garnet Range volcanic rocks (Carter, 1982; Callmeyer, 1984) and the Avon Volcanic complex (Trombetta, 1987) lie along the northwest trend of the Montana Lineament. The Elkhorn Mountain volcanic field and the coeval Boulder batholith and the Bearpaw Mountains volcanic field (Hearn, 1989a,b) are aligned along the northeast trend of the Idaho-Montana porphyry belt. The Silver Bell stock and the Crater Mountain volcanic complex show similar northeast elongation.

Many of the normal faults which were active in late Cretaceous time were apparently reactivated in Cenozoic time. Normal faults which have inherited their orientations from older fracture systems have been recognized throughout the Rocky Mountain thrust and fold belt and in many other areas where extensional deformation has been superimposed upon thrusted terrane (see for example Ruppel and others, 1981). The Beaver Creek fault, the Fool Hen fault and many other normal faults south of the study area are aligned along the trend of the Montana Lineament. The Tar Head Creek fault and many other down-to-the west normal faults in the region follow the north-northwest strike of the Scapegoat thrust fault. Joints and fractures in units of the lower volcanic series and the Belt Supergroup also reflect these regional structural patterns (Figure 55).

Deep-seated fracture systems controlled by these regional structures have influenced the geomorphic grain of the region. Many of the major streams in the study area follow one of these trends. Field relations show that flows of the lower volcanic series were deposited upon a deeply incised substrate. Thus, incision along these through-going fractures had begun by Eocene time. Porphyritic hornblende trachydacite flows were channeled along a paleovalley which followed the North Fork of Humbug Creek. Renewed erosion

following deposition of the ash-flow tuffs of the upper volcanic sequence exhumed many of these paleovalleys. Sediments of the upper volcaniclastic unit were deposited in basins controlled, in part by regional structural fabric.

GEOLOGIC HISTORY

From Middle Eocene through Early Miocene time, the Crater Mountain area experienced seven episodes of volcanic activity punctuated by at least four periods of quiescence characterized by significant erosion and soil development. The mode of emplacement and possible source areas for each volcanic unit are discussed in depositional sequence below. Stratigraphic relations are illustrated in Figure 43 and Plate 2.

1. Magmatic activity in the Blackfoot River valley commenced in Middle Eocene time with the eruption of porphyritic latite lava flows (Tpl). The flows were erupted onto a rugged landscape carved into folded and faulted rocks of the Belt Supergroup. Coeval block-and-ash and ash-flow tuff (Tplt) sequences were erupted from a small flow dome complex (Tpli) which is exposed as a resistant plug on the North Fork of Humbug Creek. This center is too small, however to account for the volume of porphyritic latite flows present in the Crater Mountain complex. Rocks of similar composition in the Challis volcanic pile are thought to have been erupted from numerous small composite volcanoes or dome complexes (McIntyre and others, 1982). Porphyritic latite

flows apparently were channeled along valleys with orientations similar to modern stream valleys.

2. Aphanitic trachyandesite flows (Tat) were erupted onto a substrate subdued by thick outpourings of porphyritic latite. The absence of paleosol horizons at the base of the flows suggests that the eruption of porphyritic latite was closely followed by aphanitic trachyandesite flows. The basal flows contain pick-up breccias which incorporate fragments of Belt rocks and porphyritic latite. Interflow sediments in the upper flows suggest that trachyandesite eruptions were punctuated by periods of erosion and soil development characterized by reworking of earlier lavas and deposition in streams and lakes. Thin airfall tuff layers represent the onset of successive eruptions.

Although no vent areas have been recognized, aphanitic trachyandesite may have erupted from a series of fissures represented by porphyritic trachyandesite and rare shonkinite dikes. Aphanitic high-K andesites and shoshonites of the Challis volcanic complex are also thought to have erupted from fissure vents based on the abundance of dikes of similar composition and confinement of the flows to synvolcanic grabens (Moye and others, 1988).

3. Hornblende trachydacite (Tpt) erupted 48.3 Ma as thick, viscous flows and flow breccias. The flows covered

thin soils developed on aphanitic trachyandesite and porphyritic latite and some of them were channeled along a paleovalley with a trend similar to that of the modern South Fork of Humbug Creek. Isolated outcrops of hornblende trachydacite suggest the flows may have been extensive.

No source areas for hornblende trachydacite flows or associated pyroclastic rocks have been identified. However, because silicic lavas usually form short steep-sided flows which erupt explosively from dome complexes, the source must be close. (Williams and McBirney, 1979; Cas and Wright, 1988). Carter (1982) suggested that texturally similar high-K hornblende andesite flows in the Garnet Range volcanic pile erupted from fissures on the basis of the paucity of pyroclastic rocks and the abundance of dikes of similar composition. Sill-like bodies of andesite porphyry of the Silver Bell stock are the same age as the hornblende trachyandesite flows and may have intruded into fissure-like vents.

4. Amygdaloidal andesite (Taa) was deposited directly onto hornblende trachydacite flows with little or no intervening period of erosion. On the west side of Columbia flat, amygdaloidal andesite flows baked the underlying hornblende trachydacite. To the south, weathered fragments of aphanitic trachyandesite occur near the basal contact.

The source vent is unknown, but the highly vesicular nature of this unit suggests that it represents a more explosive, volatile-rich phase of intermediate-composition magmatism. Vesicular lavas commonly erupt from small composite cones which may be covered by subsequent flows (Williams and McBirney, 1979; Cas and Wright, 1988).

5. Aphanitic dacite flows (Td) were deposited onto thick soils developed on trachydacite flows and flow breccias. This relationship suggests that eruption of hornblende trachydacite flows was followed by a significant hiatus in volcanic activity. The well developed trachytic texture indicates that aphanitic dacite erupted as lava. The abundant pipe-like vesicles and the absence of interflow sediments or soil horizons suggest that the flows formed a single simple cooling unit. Closely spaced hematitic flow bands may represent post-depositional rheomorphic flowage of the cooling lavas. Dacitic magmas form short, viscous flows which are commonly erupted from dome complexes (Williams and McBirney, 1979; Cas and Wright, 1988). Aphyric dacites with hematitic partings have been described in the Avon volcanic complex (Trombetta, 1987). Similar aphanitic dacites in the eastern Garnet Range have K-Ar dates of 44 Ma. (Callmeyer, 1984). Deposition of aphanitic dacite was followed by as much as seven million years of erosion and entrenchment.

6. Magmatic activity resumed at 38 Ma with voluminous outpourings of rhyolite ash-flow tuff. The first thin ash-flows were followed immediately by ground surge deposits associated with the thick main ash flow sequence. The presence of surge deposits at the base of the ash flow sequence, and lithic-rich channel lag conglomerates at the base of individual flows, suggests that the ash flows were channeled along several steep-walled paleovalleys cut into rocks of the lower volcanic series. Fragments of rocks from the lower volcanic series, and from Belt rocks, were torn from the substrate and incorporated in the ash-flow tuff along with charred limbs from trees incinerated by the advancing ash flows. The ash flows erupted in such rapid succession that they apparently formed only two extremely thick cooling units separated by laminated surge deposits and glassy block-and-ash flows.

The source of the ash flows is unknown. McKee (1978) proposed that the quartz porphyry phase of the Silver Bell stock represents the source of the rhyolite ash flows. However, radiometric age data from this study show that the ash flows post-date the emplacement of the andesite porphyry phase of the Silver Bell stock by ten million years and field relations suggest that the quartz monzonite phase is younger than the andesite porphyry phase.

Cessation of rhyolitic magmatism was accompanied or quickly followed by block faulting which placed the ash-flow sheet down-to-the-northwest across the Blackfoot valley fault and dissected the ash-flow into several small fault blocks. Uplifted portions of the ash flow tuff were quickly reworked and deposited in a variety of fluvial and lacustrine depositional settings. The lower volcaniclastic sedimentary unit represents the combined products of these contemporaneous depositional facies. Hot springs formed sinter terraces near active hydrothermal vents. Volcaniclastic sandstones and siltstones were deposited by sediment-laden streams flowing from the hot springs. Organic-rich varved siltstones and mudstones were deposited in distal lakes fed by the streams.

7. Silicic volcanism resumed 36.5 m.y.a with the eruption of biotite-bearing rhyolite ash-flow tuff. The ash flows picked up abundant fragments of Belt rocks and rocks from the lower volcanic series from the eroded substrate. The ash flows were apparently confined to an area north of the Blackfoot Valley fault. Biotite-bearing ash flow tuff is present as scattered erosional remnants and no source area has been identified.

A period of renewed uplift and erosion accompanied by gentle tilting to the north followed deposition of the

biotite-bearing rhyolite ash flows. Sedimentary features suggest that monolithologic conglomerates and sandstones of the upper volcaniclastic sedimentary unit were deposited as alluvial fans and debris flows shed from the uplifted ash-flow tuffs.

These sedimentary rocks may correlate with Hanneman and Wideman's (1991) "sequence two depositional unit" which occurs in intermontane basins throughout southwestern Montana. Sedimentary rocks of this sequence, which have previously been assigned to the Renova Formation, range in age from 42 to 30 Ma and are characterized by conglomerates and stratified sandstones interpreted as fluvial channel and debris flow deposits.

In Pliocene time, conglomerates and sandstones of the upper volcaniclastic unit were offset by normal fault movement on the Beaver Creek fault north of the Blackfoot River valley (Figure 42). Basalt dikes intruded along the fault trace represent the last stage of magmatic activity in the region.

During Pleistocene time, the Blackfoot Valley and many of its tributaries hosted small valley glaciers. The glaciers deposited thick outwash sheets on the valley floors and cut steep cirques at the heads of many of the intermontane valleys, exposing the thick ash-flow sheet.

Renewed entrenchment which followed the retreat of the valley glaciers produced the modern drainage pattern which, in many places, follows the regional structural grain. Large Quaternary landslides at the heads of many drainages probably reflect collapse of saturated slopes oversteepened by retreating ice sheets. Many of the landslides in the Hogum Creek and Crater Mountain areas occurred as block failures which slipped along clay-rich agglomeratic layers or weathered rhyolite vitrophyre. Debris flows and landslides along Landers Fork and south of Krohn Lake occurred within poorly consolidated sediments of the upper volcaniclastic sequence. The presence of arcuate ground fissures and sheared tree roots at the heads of many of these features indicates that mass wasting and, possibly, tectonic activity is still occurring in these areas.

Possible Vent Areas for Ash-Flows

Large ash flow tuff eruptions are commonly associated with the formation of calderas (Williams, 1941; Ross and Smith, 1961; Smith and Bailey, 1968; Smith, 1979). The great thickness of the ash-flow sheet suggests that it was confined within a basin. However, arcuate fault segments or radial

fracture patterns commonly associated with caldera margins have not been recognized in the study area.

Ash flows are also commonly associated with flow dome complexes. A number of rhyolite flow domes have been recognized in the Helena volcanic field. Of these, the Avon volcanic complex, located 56 kilometers to the southwest, is the nearest possible source area for the thick ash-flow tuff sequence. The field contains up to 430 meters of porphyritic rhyolite flows which are apparently preserved in a tectonic basin. However, flow direction measurements indicate that the flows originated from an eruptive center to the north and K-Ar data show an age of 39.8 Ma which is older than the ash-flow tuffs of the Crater Mountain complex (Trombetta,1987).

It is more likely that the ash flows erupted from an irregular volcano-tectonic depression or cauldron (terminology of Smith and Bailey, 1968) which was subsequently buried beneath the thick ash-flow tuff sheet. Rhyolite dikes which are aligned along regional structural trends may represent fissure-like vent areas (Plate 1). Clast populations also suggest a local provenance. A similar setting has been proposed for rhyodacitic ash-flow tuffs in the Lowland Creek volcanic pile (Smedes and Thomas, 1965; Foster, 1987) and in the Garnet Range volcanic pile (Carter, 1982).

TECTONICS

Regional Tectonic History

Late Cretaceous to Eocene folding and thrust faulting were accompanied and closely followed by episodes of intense intermediate (andesitic-dacitic) volcanism (Burchfiel and Davis, 1975). In western Montana, this magmatism was manifested as the Elkhorn Mountain volcanic field and comagmatic Boulder batholith, the Garnet Range volcanic pile, and alkaline complexes of the Adel, Highwood, and Bearpaw Mountains.

The exact tectonic setting for Cenozoic magmatism in western Montana is controversial. However most workers agree that magmatic composition and spatial and temporal relations support some sort of behind-the-arc setting.

The most commonly accepted model relates the initiation of Cenozoic magmatism to shallow, east-directed subduction and imbrication of the Farallon plate beneath the North American plate (Lipman and others, 1971, 1972; Coney and Reynolds, 1977; Dickinson and Snyder, 1978; Lipman, 1980)

According to this scenario, an accelerated rate of convergence between the Pacific and North American plates near the end of the Cretaceous is thought to have produced a shallow, anomalously wide magmatic arc as hotter, more buoyant oceanic lithosphere was being subducted beneath the continental margin (Lipman and others, 1971, 1972; Coney and Reynolds, 1977; Hamilton, 1988). Increased magmatic activity far inboard of the arc may be attributed to underplating of the imbricated Farallon plate beneath the craton (Dickinson and Snyder, 1978; Lipman, 1980) or tectonic erosion of the continental lithosphere from beneath by the buoyant subducting slab (Cross and Pilgar, 1988). Table 7 shows the inferred tectonic setting and relative age of major episodes of volcanism in eastern Idaho and southwestern Montana.

Volcanism peaked in Eocene time as oblique subduction of the Farallon oceanic ridge beneath the continental margin initiated Basin and Range extension (Atwater, 1970). By Early Oligocene time, Basin and Range deformation apparently extended northward into southwestern Montana. The change from compressional to extensional tectonic regimes was accompanied by a distinct change in eruptive style and magmatic affinity of the ensuing volcanic sequences.

Initial pulses of Middle Tertiary magmatism were silicic and intermediate in character between arc and extensional

tectonic settings (Molnar and Atwater, 1976) and eruptive products suggest a back-arc setting (Best, 1986). This change has been attributed to steepening of the subduction angle due to subduction of colder, less buoyant lithosphere (Dickinson and Snyder, 1978). In Late Tertiary time, less voluminous basalt and basalt-rhyolite (bimodal) assemblages characteristic of extensional regimes were erupted as foreland basins evolved into north-trending fault block valleys (Snyder and others, 1976; Molnar and Atwater, 1978; Hamilton, 1988). An alternative model attributes initiation of Cenozoic igneous activity to intracontinental rifting triggered by collision of the Pacific and North American plates (Ewing, 1980; Fox, 1983; Fox and Beck, 1985).

Tectonic Significance of the Crater Mountain Volcanic Complex

Volcanic rocks comprise a significant portion of the Cenozoic rock record in southwestern Montana. However, most volcanic fields preserve either early Tertiary intermediate-composition sequences associated with Laramide compression or mid-Tertiary bimodal assemblages associated with Basin and Range extension.

The rocks of the Crater Mountain volcanic complex represent the products of a long-lived eruptive center which

records the change from Laramide fold and thrust compressional tectonics to extensional tectonism associated with the development of Basin and Range block fault valleys. Radiometric age data indicate that extension-related silicic magmatic activity began in western Montana by 38 Ma. Similar relationships are preserved in the rocks in the Avon volcanic complex (Trombetta, 1987) and the Challis volcanic center (McIntyre and others, 1982; Leonard and Marvin, 1982; Moye and others, 1988).

DISCUSSION

Throughout the Cenozoic Era, western Montana and southern Idaho experienced episodes of intense volcanism. In Eocene time, volcanic activity in southwestern Montana peaked with vast outpourings of lavas and ash-flow tuffs that range in composition from basalt to rhyolite. Eocene-age volcanic centers include the Lowland Creek, Adel Mountains, Highwood Mountains, Bearpaw Mountains, and greater Helena volcanic fields in western Montana and the Challis volcanic pile in south-central Idaho.

Nature and Source of the Volcanic Rocks

The Helena and Garnet Range volcanic fields and the Avon and Crater Mountain complexes comprise the greater Helena volcanic field. Volcanic activity in the Crater Mountain complex commenced 48 Ma with the eruption of voluminous latite lava flows and ash flows of the lower volcanic series. The basal contact of the lower volcanic series exhibits as much as 200 meters of relief. This suggests that the flows erupted onto an irregular substrate with geomorphic features similar to those present today. Flows were distributed, in part, along deep, fault-controlled valleys incised into

underlying metasedimentary rocks of the Belt Supergroup.

Subsequent eruptions of trachyandesite, trachydacite, and dacite lava were punctuated by periods of erosional entrenchment accompanied by formation of deep-red lateritic soils. North of the Blackfoot Valley, fluvial and lacustrine sedimentary rocks occur at the base of the trachyandesite flows. In the Garnet Range, lacustrine and laharic sediments separate 47 Ma latite flows and rhyolite ash-flow tuffs from overlying andesite and basalt flows. These relations suggest that significant periods of erosion in a humid environment occurred between subsequent flows. The presence of fossil redwood trees in the Challis volcanic field confirms that the Eocene climate in Montana and Idaho was humid and mild (Leonard and Marvin, 1982).

Intermediate-composition magmatic activity culminated with the eruption of trachydacite and dacite flows followed by at least 8 million years of erosion and entrenchment. Thick lateritic soils were deposited on the rocks of the lower series prior to the ash-flow eruptions of the upper volcanic series.

Rhyolite ash-flow tuffs of the upper volcanic series were deposited 38 Ma in a basin developed in volcanic rocks of the lower series and metasedimentary Belt rocks. The ash flows formed two simple cooling units which reach a maximum

thickness of 393 meters near Crater Mountain. Arcuate structures and radial drainage patterns indicative of a caldera setting are absent and no flow-dome complexes or vent facies have been recognized. The ash flows probably erupted from fissures within a linear cauldron which were covered by successive ash-flow eruptions and by epiclastic sediments. Fissures which parallel the Scapegoat thrust fault were intruded by porphyritic rhyolite.

Relation to Other Volcanic Centers in the Trans-Challis Volcanic Terrane

The rocks of the lower volcanic series are much more potassic than average andesites and dacites. The suite is calc-alkaline, but is enriched in low field strength elements compared to within-plate alkaline basalt. The alkaline nature of the magmas is demonstrated by coexisting biotite and olivine phenocrysts in latite and trachyandesite flows and the presence of shonkinite dikes that intrude latite flows. Similar sequences of 50-46 Ma latite and andesite flows exposed in the Garnet Range and Avon volcanic fields suggest that intermediate-composition volcanic activity occurred concurrently from numerous igneous centers within the greater Helena volcanic field. Geochemical studies are

needed to determine if these lavas also show alkaline affinities.

The high-silica rhyolite ash-flow tuffs of the upper volcanic series are similar in age (40-36 Ma) and composition to rhyolite ash-flows and lava flows throughout the greater Helena volcanic field. This relation indicates that the Helena, Avon and Garnet Range rhyolitic centers are portions of one large volcanic field.

The rocks of the Crater Mountain volcanic complex have many features in common with those of the Challis volcanic field. The early intermediate rocks of the Challis volcanic pile include latite, shoshonite, high-K andesite and high-K basalt flows which range in age from 51-48 Ma. Voluminous outporings of high-silica rhyolite ash-flow tuff were deposited 49-45 Ma on epiclastic shales and sandstones derived from eroded latite and andesite flows.

Vent locations were controlled by northwest-trending structures and the flows dip uniformly to the northwest rather than radially away from a central source area. There are no central-vent lithofacies indicators suggestive of construction of steep-sided stratovolcanoes. Mafic and intermediate-composition dikes follow similar trends. Evidence suggests that flows which erupted from fissure vents formed sheet-like lava plateaus which were later tilted by

faulting (Moye,and others, 1988). A similar setting is proposed for flows of the lower volcanic series. The volcanic section has been tilted approximately 20 degrees to the north by post-volcanic faulting. Flow indicators show no evidence of steep-sided volcanic edifices, and flows of the lower series are associated with dikes which are aligned along regional structural trends.

The subalkaline nature of the rocks of the lower series and the early lava flows of the Challis volcanic field suggests that the Montana high-potassium province may extend much further southwest than previously thought. Throughout Paleocene and Eocene time, a broad magmatic arc apparently stretched from southern Idaho northeast to central Montana. The position of volcanic centers along this belt was controlled by regional structural elements associated with long-lived zones of crustal weakness which guided magma generated from a subduction zone at depth.

SUMMARY and CONCLUSIONS

This study has used geochemical and petrographic data and stratigraphic relationships to characterize the rocks and explain the volcanic history of the Crater Mountain volcanic complex. Regional geochemical studies and additional radiometric age dating are needed to recognize possible source areas for the volcanic rocks. Studies focusing on the source of the volcaniclastic units using flow direction indicators would also be beneficial.

Major findings of this study are:

1. The Crater Mountain volcanic complex consists of a stratigraphically lower intermediate-composition sequence of lava flows and flow breccias unconformably overlain by an upper series of rhyolite ash-flow tuffs and volcaniclastic rocks.

2. Rocks of the lower series can be divided into five major map units on the basis of modal and geochemical analysis. In stratigraphic sequence they are: porphyritic latite flows and ash-flow tuffs, aphanitic

trachyandesite flows, porphyritic hornblende trachydacite flows, amygdaloidal trachyandesite flows, and aphanitic dacite flows.

3. The upper series is a 450 meter thick sequence of welded rhyolite ash-flows and associated ground surge deposits, overlain by a variety of volcaniclastic sediments and biotite bearing-rhyolite ash flows. Miocene volcaniclastic conglomerate overlies the biotite-bearing ash-flow tuff.

4. Rocks of the lower volcanic sequence probably erupted from a series of small flow domes and fissures which are represented by porphyritic and aphanitic shonkinite, trachyandesite, and latite dikes. Rhyolite ash-flow tuffs were probably deposited in an irregular cauldron which was buried by subsequent ash flow eruptions.

5. Major and trace-element analyses show that the rocks of the upper and lower series comprise two distinct suites which cannot be related to a single parent magma. Rocks of the lower series lie along a calc-alkaline trend, but both elevated K_2O and Ba

contents and presence of shonkinite dikes suggest an alkaline affinity. The rocks of the upper volcanic series are distinctly calc-alkaline.

6. A hornblende concentrate from hornblende trachydacite yielded a K-Ar age of 48.3 +\- 1.2 M.Y. which is consistent with an age of 48.5 +/- 1.2 M. Y. obtained for andesite porphyry of the Silver Bell stock. Sanidine and biotite separates from rhyolite ash-flow tuff and biotite-bearing rhyolite gave K-Ar ages of 37.8 +/- 1.0 and 36.5 +/- 0.9 M. Y., respectively.

7. Distribution of volcanic and sedimentary rocks was controlled by Eocene to Pliocene-age normal faults which reflect major regional structural trends. Regional structural elements which influenced depositional settings and control modern drainage patterns include: the northeast-trending Idaho-Montana porphyry belt/Great Falls tectonic zone, the northwest trending Montana lineament, and the Rocky Mountain thrust and fold belt.

8. A previously unrecognized normal fault herein named the Blackfoot Valley fault displaces rocks of the lower

volcanic series a minimum of 360 meters down to the south across the Blackfoot River Valley.

9. Rocks of the Crater Mountain volcanic complex record the transition from intermediate-composition volcanism associated with compression driven by shallow subduction of the Farallon plate beneath the western margin of North America to bimodal basalt-rhyolite volcanism associated with Basin and Range extension.

10. The Crater Mountain volcanic complex is part of the greater Helena volcanic field. The Avon volcanic complex and the Garnet range volcanic center contain rocks of similar age and composition to those of the upper and lower volcanic series. The alkaline nature of the intermediate-composition rocks of the greater Helena volcanic field suggests that the Montana high-potassium province may extend much further to the southwest than originally thought.

APPENDICES

APPENDIX A

FIGURES

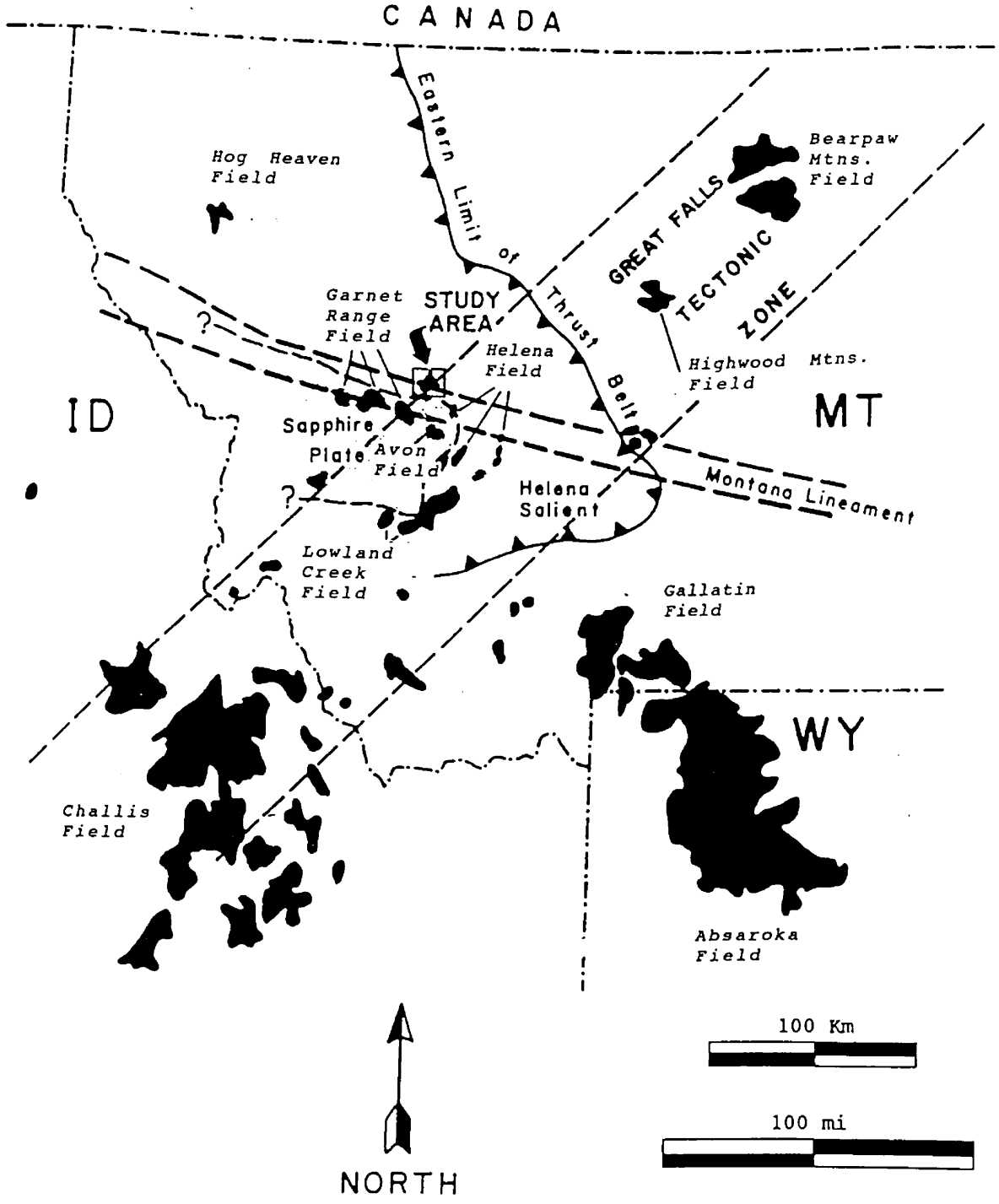

Figure 1. Map showing the location of the study area in relation to pertinent tectonic features in western Montana, northwestern Wyoming and eastern Idaho. Black pattern indicates Eocene to Oligocene volcanic fields. Modified from the works of Chadwick (1981), Callmeyer (1984), and Trombetta, (1987).

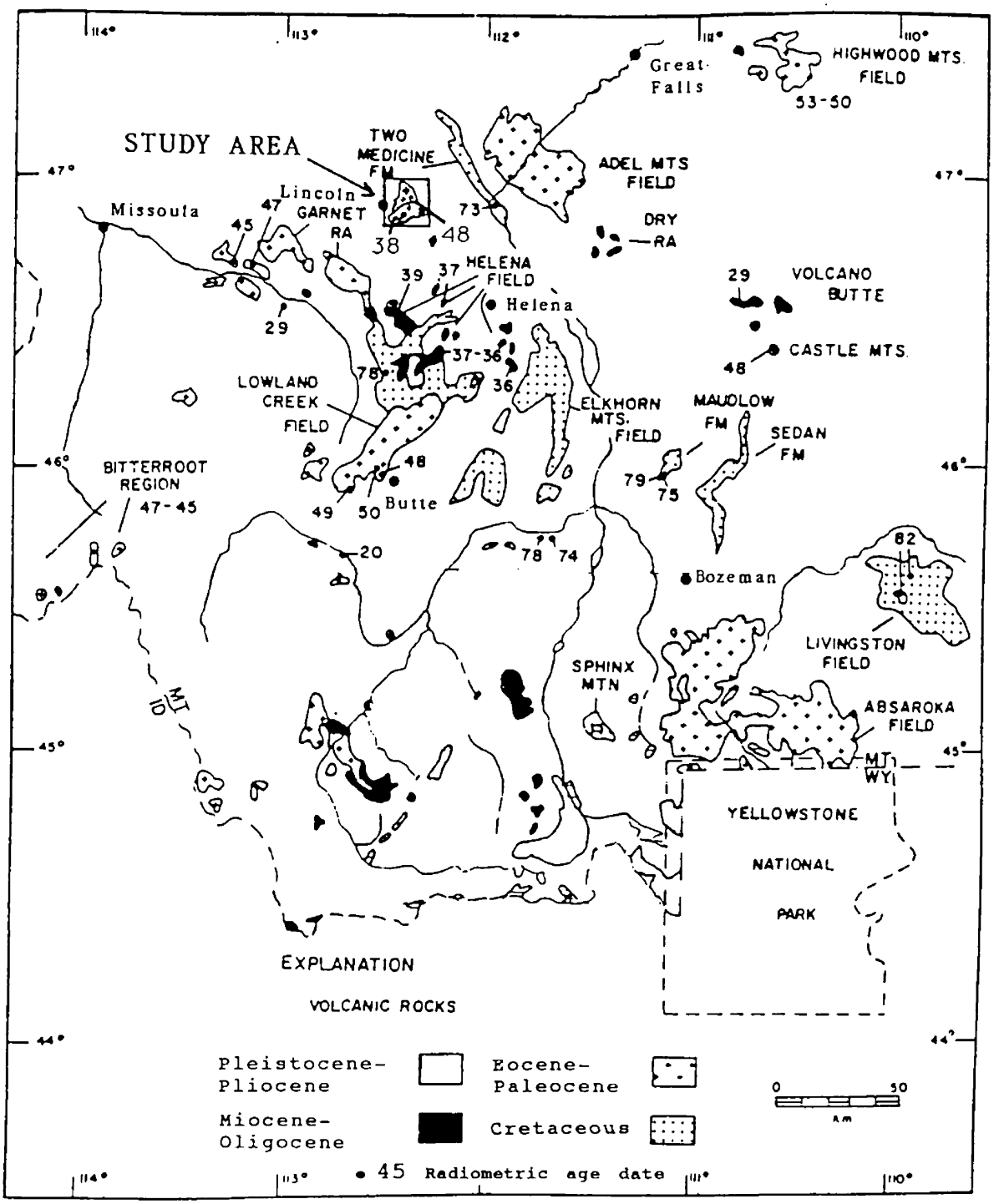

Figure 2. Map showing location of the study area in relation to Late Cretaceous and Cenozoic volcanic deposits in western Montana. Modified from Chadwick (1981).

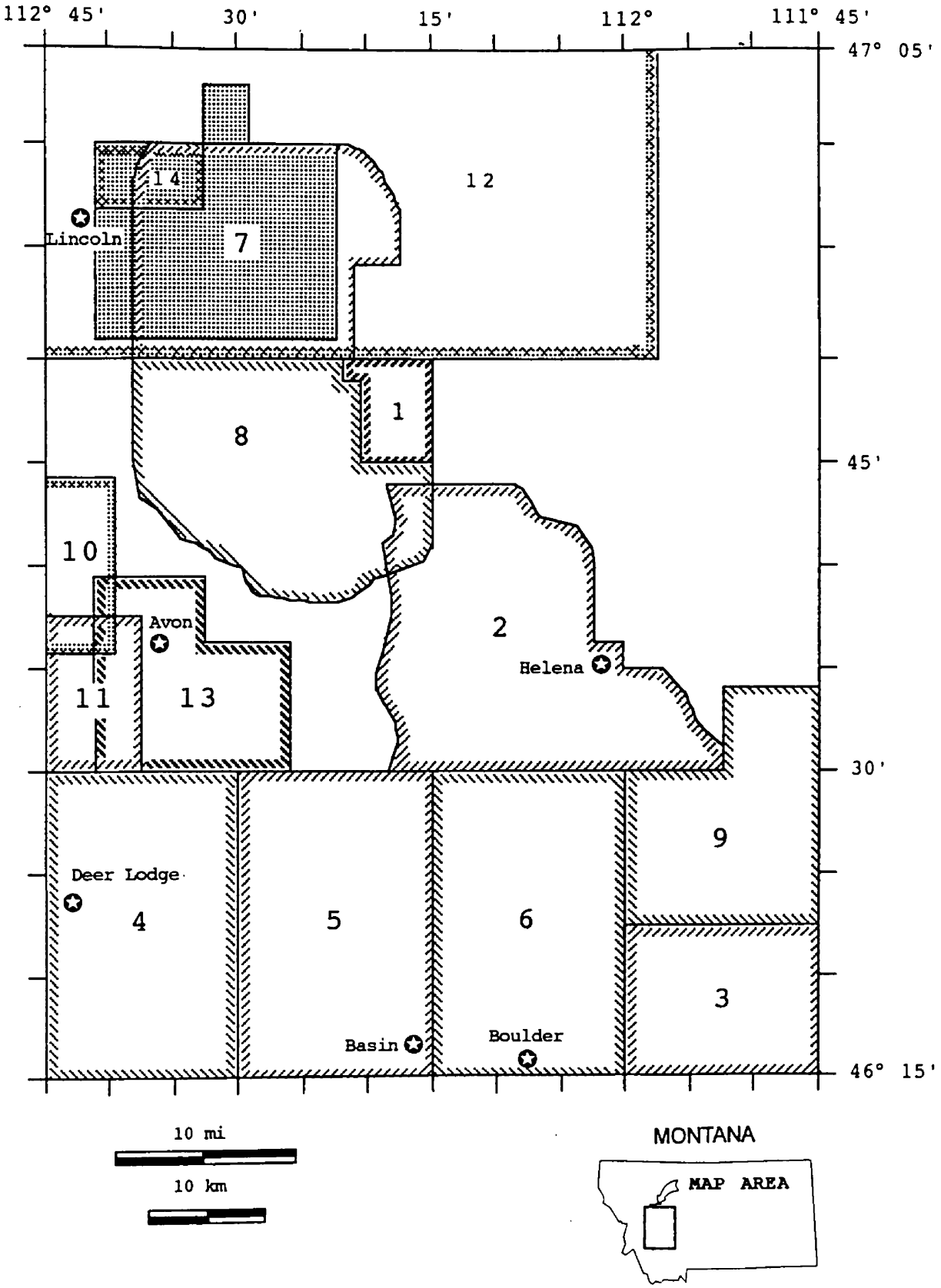

Figure 3. Map showing areas that have been mapped prior to this study which contain rocks of the Helena volcanic field. Shaded area denotes the Crater Mountain volcanic complex.

Key to map areas from previous workers shown in Figure 3.

1. Barrell (1907)
2. Knopf (1913)
3. Klepper and others (1957)
4. Ruppel (1961)
5. Ruppel (1963)
6. Becraft and others (1963)
7. Melson (1964)
8. Bierwagen (1964)
9. Smedes (1966)
10. Callmeyer (1984)
11. Peterson (1985)
12. Whipple and others (1987)
13. Trombetta (1987)
14. Wilkinson (1991)

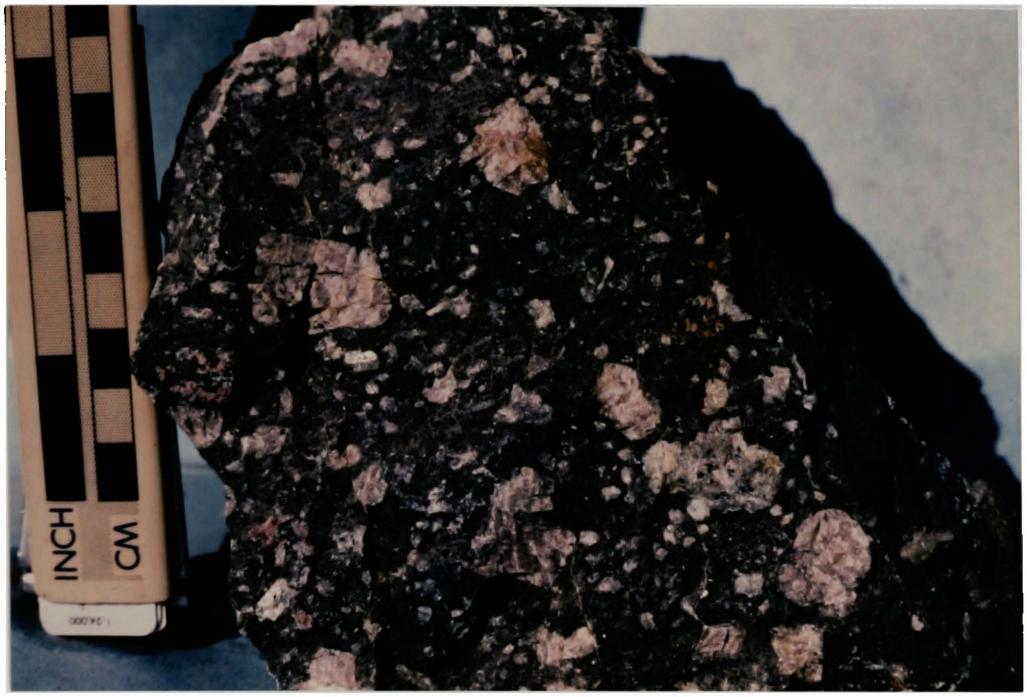

Figure 4. Photograph of hand specimen of andesite porphyry from the Silver Bell stock (Tap). Note large equant orthoclase phenocrysts. Sample CM-155. Biotite separate from this sample yielded a K-Ar age of 48.5 +/- 1.2 m.y.

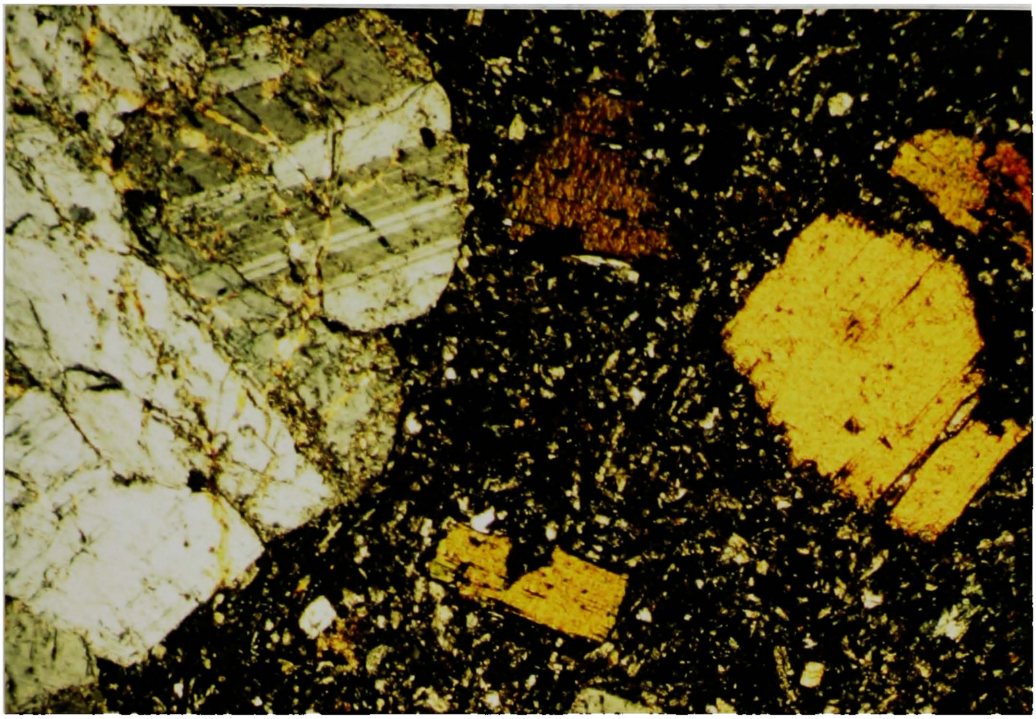

Figure 5. Photomicrograph of andesite porphyry of the Silver Bell stock (Tap). Note oscillatory zoning of large subhedral plagioclase glomerocryst and fresh brown biotite books. Sample CM-155D. Crossed polars. Field of view is approximately 5mm.

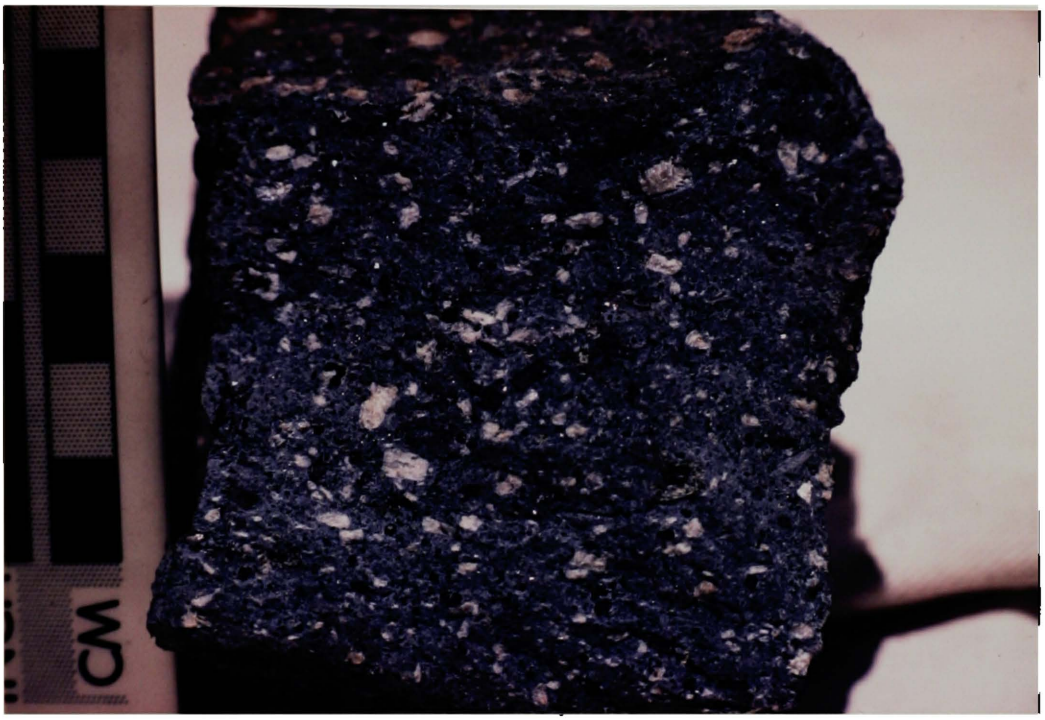

Figure 6. Hand specimen of porphyritic latite flow (Tpl). Note flow foliation defined by aligned plagioclase (white), augite (dark gray) and biotite (black) phenocrysts. Sample CM-76.

Figure 8. Porphyritic latite (Tpli) flow dome on north fork of Humbug Creek. SE 1/4 Sect. 26,T14N, R7W.

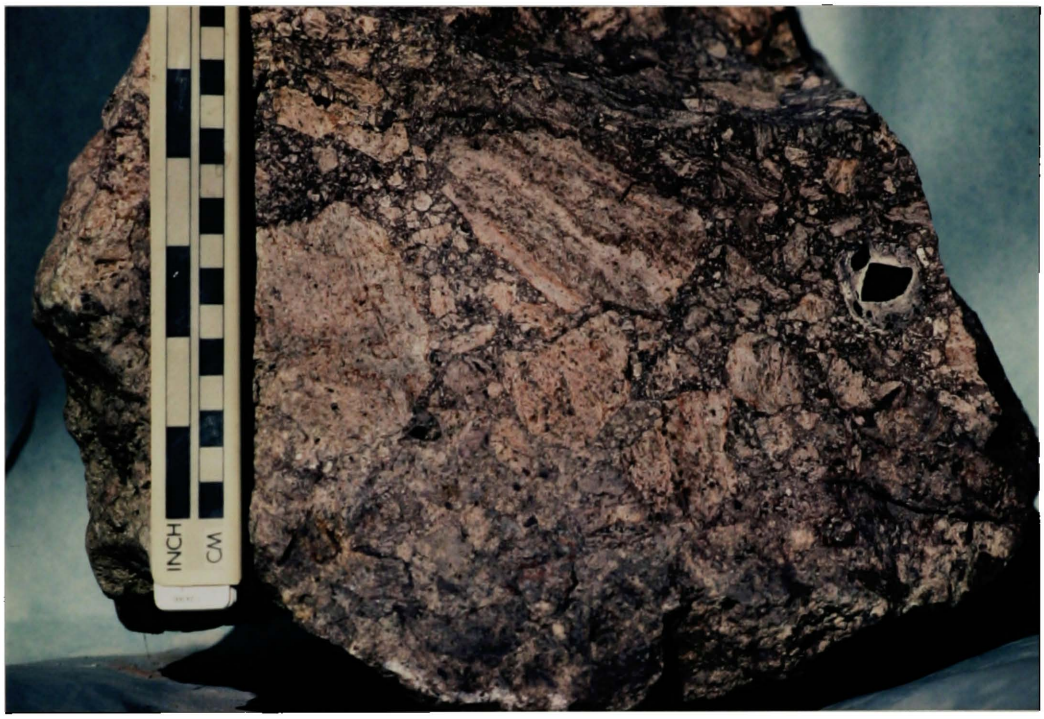

Figure 9. Hand specimen of porphyritic latite tuff (Tplt) flow breccia. Note draping of flow foliation around autoclasts and metasedimentary accidental lithic fragments (dark fragment on right side of sample) . Sample CM-9.

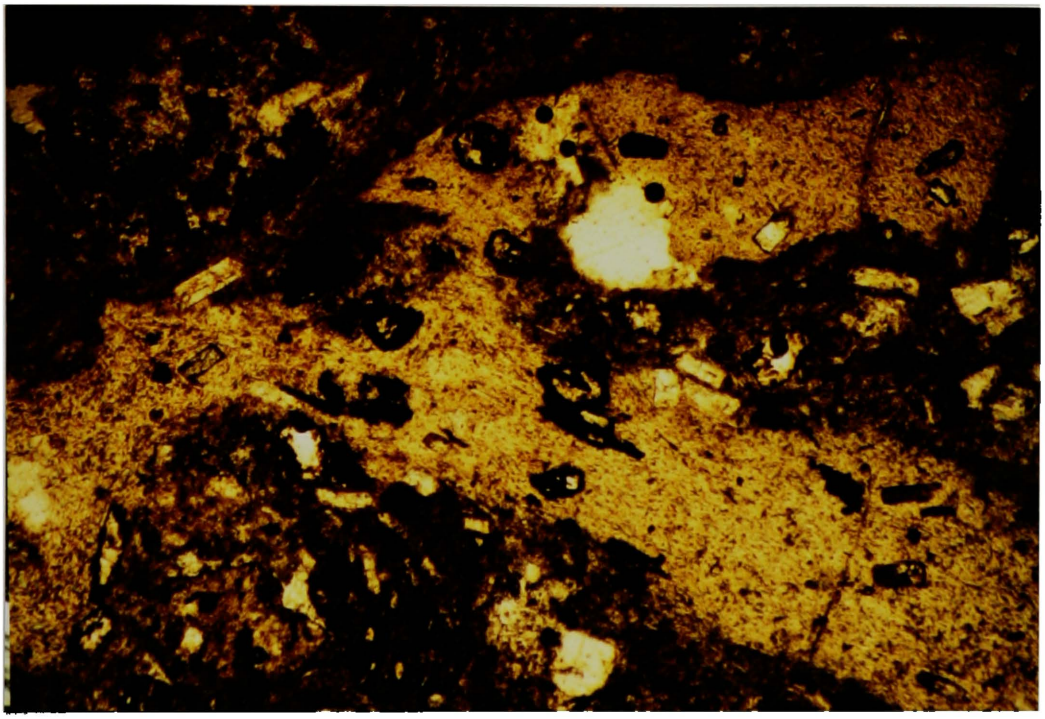

Figure 10. Photomicrograph of porphyritic latite tuff (Tplt). Note parallel arrangement of plagioclase laths and biotite books (upper left) and wrapping of flattened pumice lapilli around porphyritic lithic fragments. Sample CM-91. Field of view is approximately 5 mm.

Figure 11. Outcrop of aphanitic trachyandesite (Tat). Note platy fracture along flow foliation. Sample location CM-98.

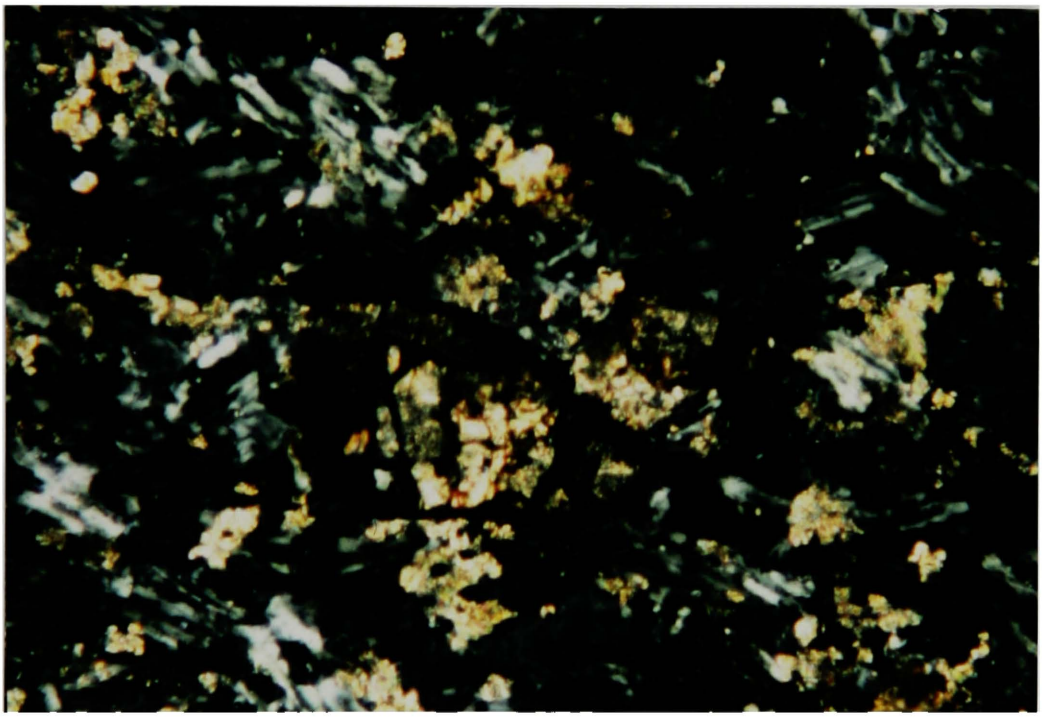

Figure 12. Photomicrograph of aphanitic trachyandesite (Tat). Note trachytic texture and altered olivine microcryst (center). Sample CM-122. Crossed polars. Field of view is approximately 0.2 mm.

Figure 13. Close-up of outcrop of porphyritic hornblende trachydacite (Tpt) showing strong parallel arrangement of hornblende phenocrysts. Location CM-11.

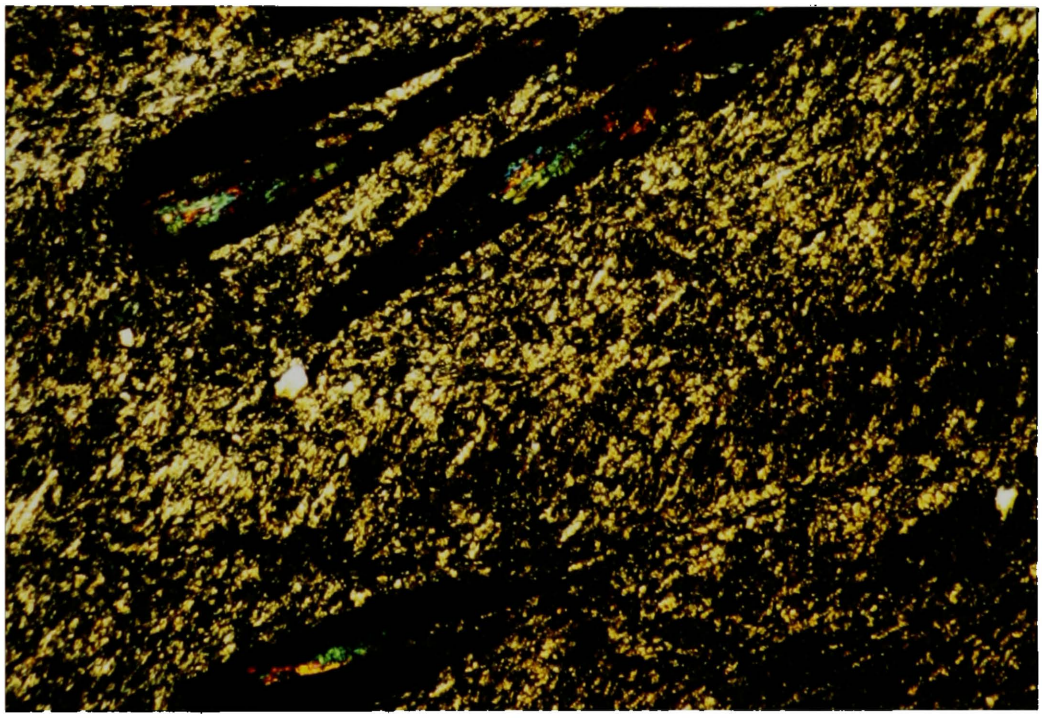

Figure 14. Photomicrograph of porphyritic hornblende trachydacite (Tpt). Note abundant fresh brown hornblende phenocrysts with black opaque oxide rims. Sample CM-162D. Hornblende separate prepared from this sample yielded a K-Ar age of 48.3 +/- 2.0 m.y. Crossed polars. Field of view is approximately 5mm.

Figure 15. Hand specimen of amygdaloidal andesite (Taa). Note uniform size of ovoid quartz-calcite amygdules. Sample CM-102.

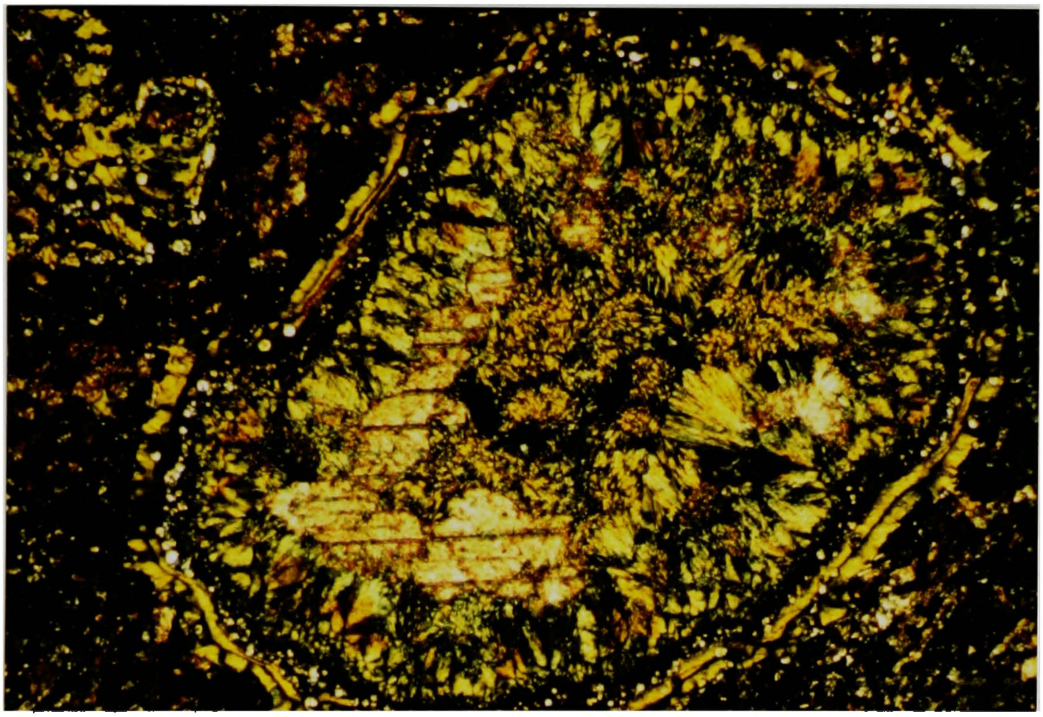

Figure 16. Photomicrograph of amygdaloidal andesite (Taa). Note open-space filling textures with calcite plates filling vesicles lined with chalcedonic or drusy quartz. Sample CM-108. Crossed polars. Field of view is approximately 5 mm.

Figure 17. Hand specimen of aphanitic dacite (Td). Note arborescent banding defined by pipe-like gas escape structures. Sample CM-118.

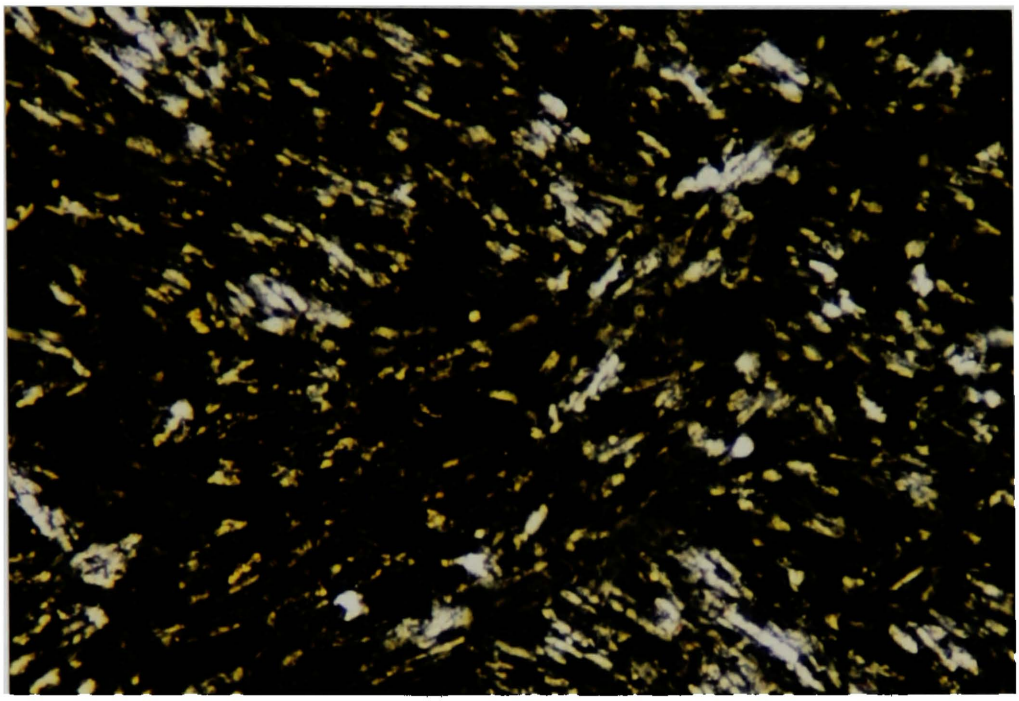

Figure 18. Photomicrograph of aphanitic dacite (Td). Note herringbone trachytic texture and entrainment of microlites within gas escape structure. Sample CM-69. Field of view is approximately 0.1 mm.

Figure 19. Outcrop of densely welded rhyolite ash-flow tuff showing extreme flattening of pumice fragments. Sample location CM-148.

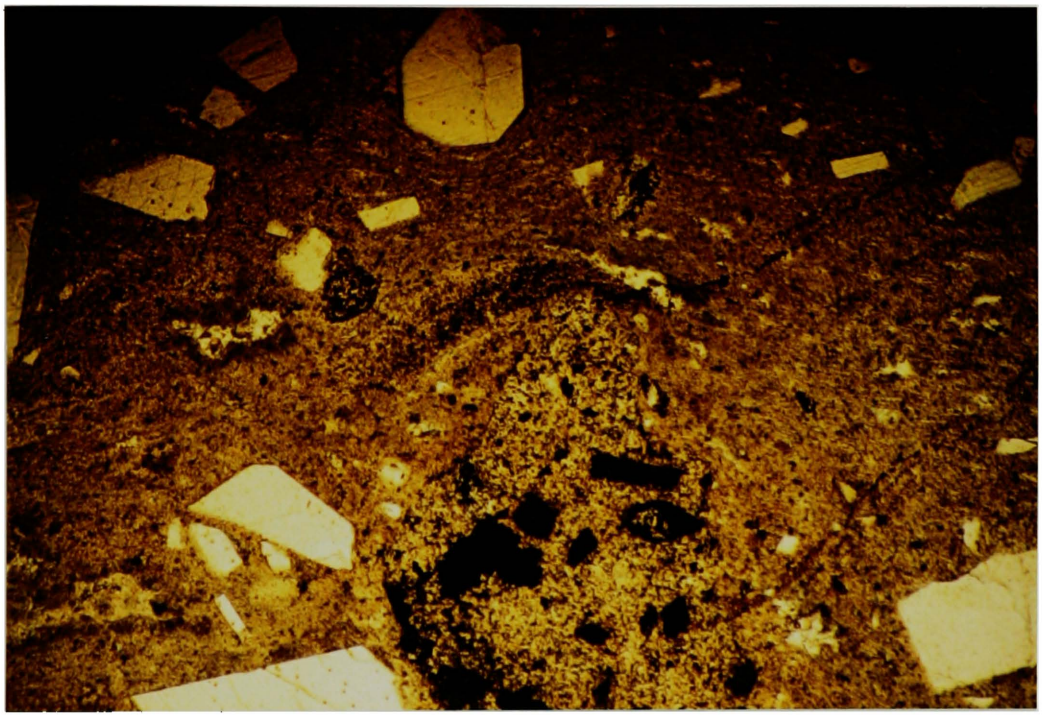

Figure 20. Photomicrograph of moderately welded rhyolite ash-flow tuff showing eutaxitic texture. Note draping of compacted pumice lapilli around sanidine and quartz crystals and large porphyritic trachydacite fragment (lower center). Sample CM-159. Sanidine separate from this sample yielded a K-Ar age of 38.0 +/- 1.0 m.y. Field of view is approximately 5mm.

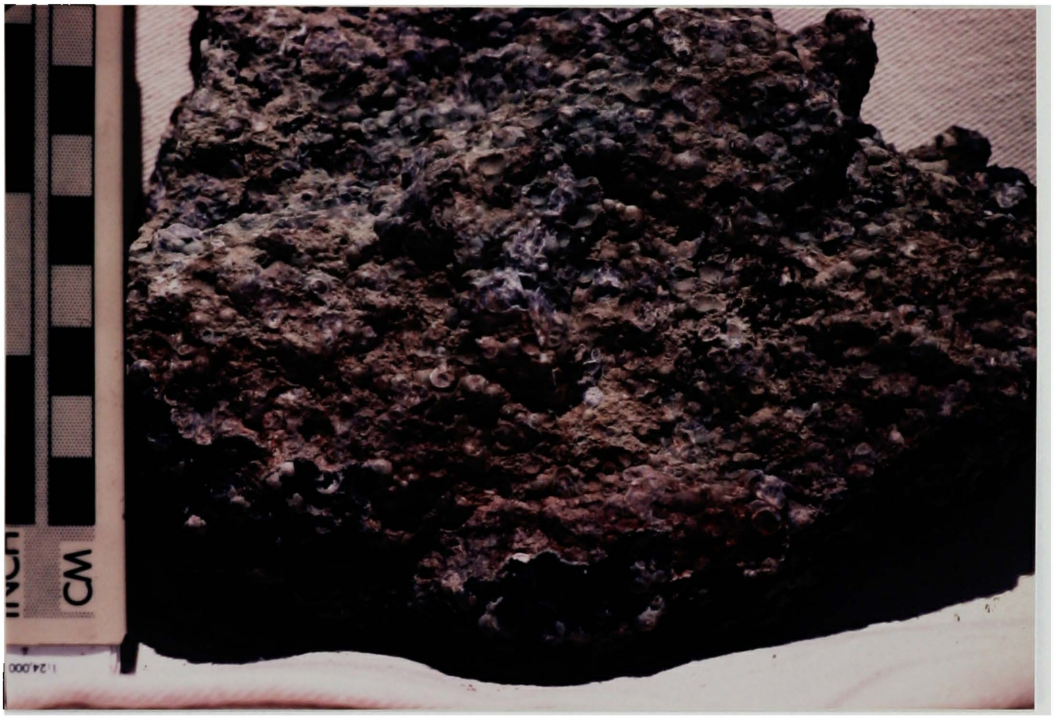

Figure 21. Hand specimen of spherulitic rhyolite ash-flow tuff from base of ash-flow sequence on east flank of Crater Mountain. Sample CM-157.

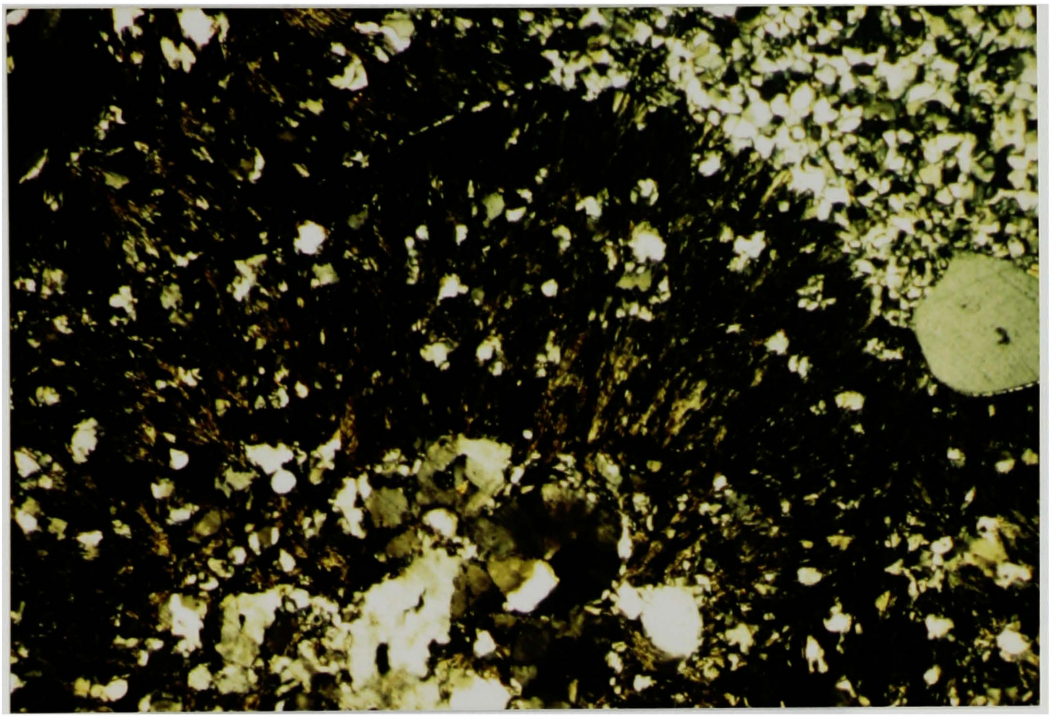

Figure 22. Photomicrograph of spherulitic rhyolite ash-flow tuff. Note orb texture defined by axiolitic cristobalite and feldspar fibers nucleated on sanidine crystals. Sample CM-70. Crossed polars. Field of view is approximately 3 mm.

Figure 23. Outcrop of surge deposit at base of ash-flow tuff sequence on west side of Crater Mountain (E 1/2 Sect 32,T14N, R7W). Note normal grading of low-angle cross beds (at lower right) and wavy laminated beds. Length of hammer is 40 cm.

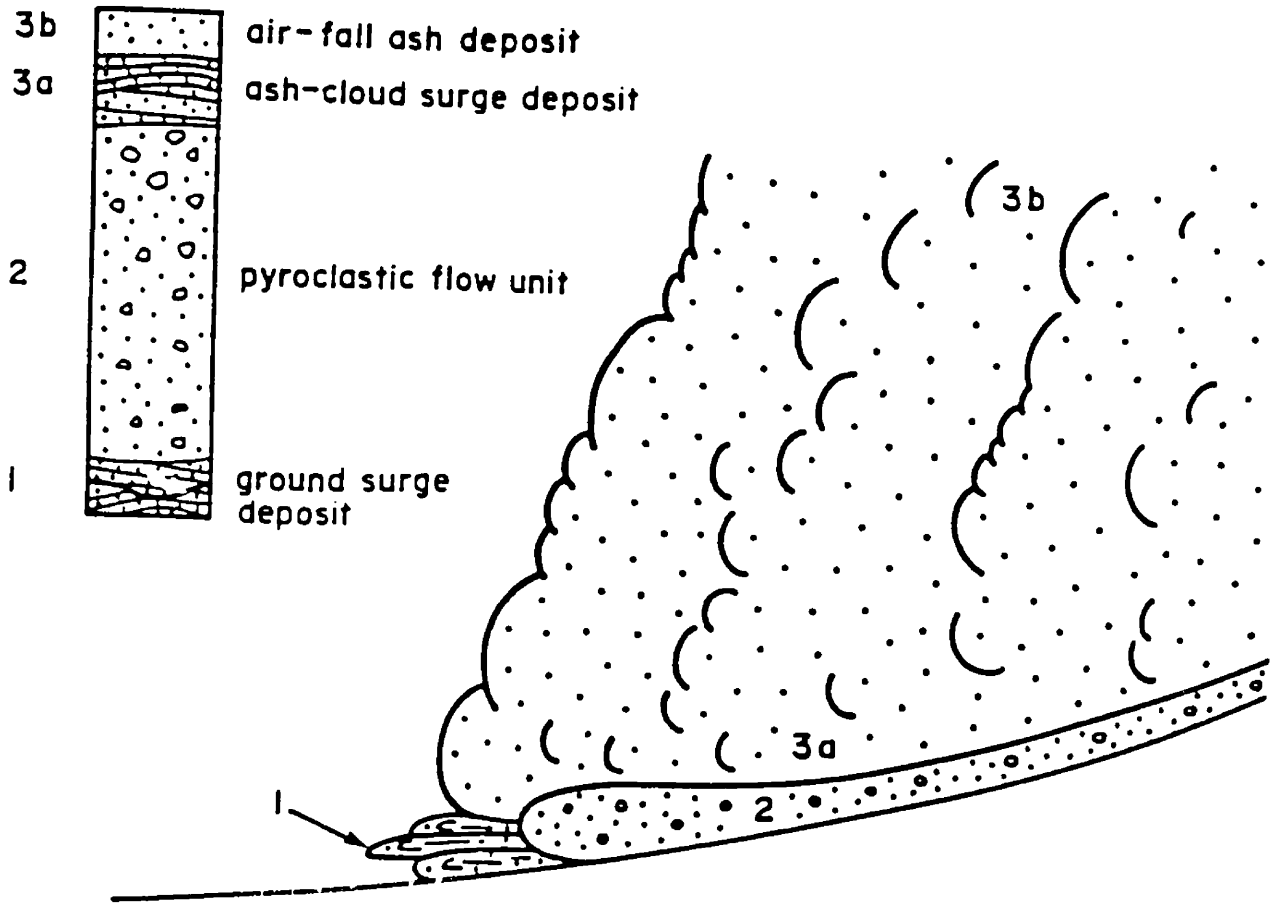

Figure 24. Diagram showing the structure and idealized deposits of a single pyroclastic flow. Modified form Sparks and others, (1973) and Cas and Wright (1988).

Figure 25. Outcrop of glassy block-and-ash flow breccia above surge deposit on west flank of Crater mountain Sample location CM-138. Length of scale is 18 cm.

Figure 26. View looking east at west side of Crater Mountain showing foliation in rhyolite ash-flow tuff (Trt) produced by slumping against wall of paleochannel cut into underlying aphanitic trachyandesite (Tat). Trees average 15 meters in height.

Figure 27. Charred limb in densely welded rhyolite ash-flow tuff near base of ash-flow sequence. Sample CM-150. Penny is shown for scale.

Figure 28. Hand specimen of glassy vitrophyre for base of rhyolite ash-flow tuff(Trt). Note abundant quartz and sanidine crystals.

Figure 29. View looking northeast toward unnamed plateau on east side of north fork of Humbug Creek (SW 1/4 sect 30, T14N, R7W) showing oxidized paleosol (reddish band near top of forested ridge in background) at contact between rhyolite ash-flow tuff (Trt) and aphanitic trachyandesite (Tat).

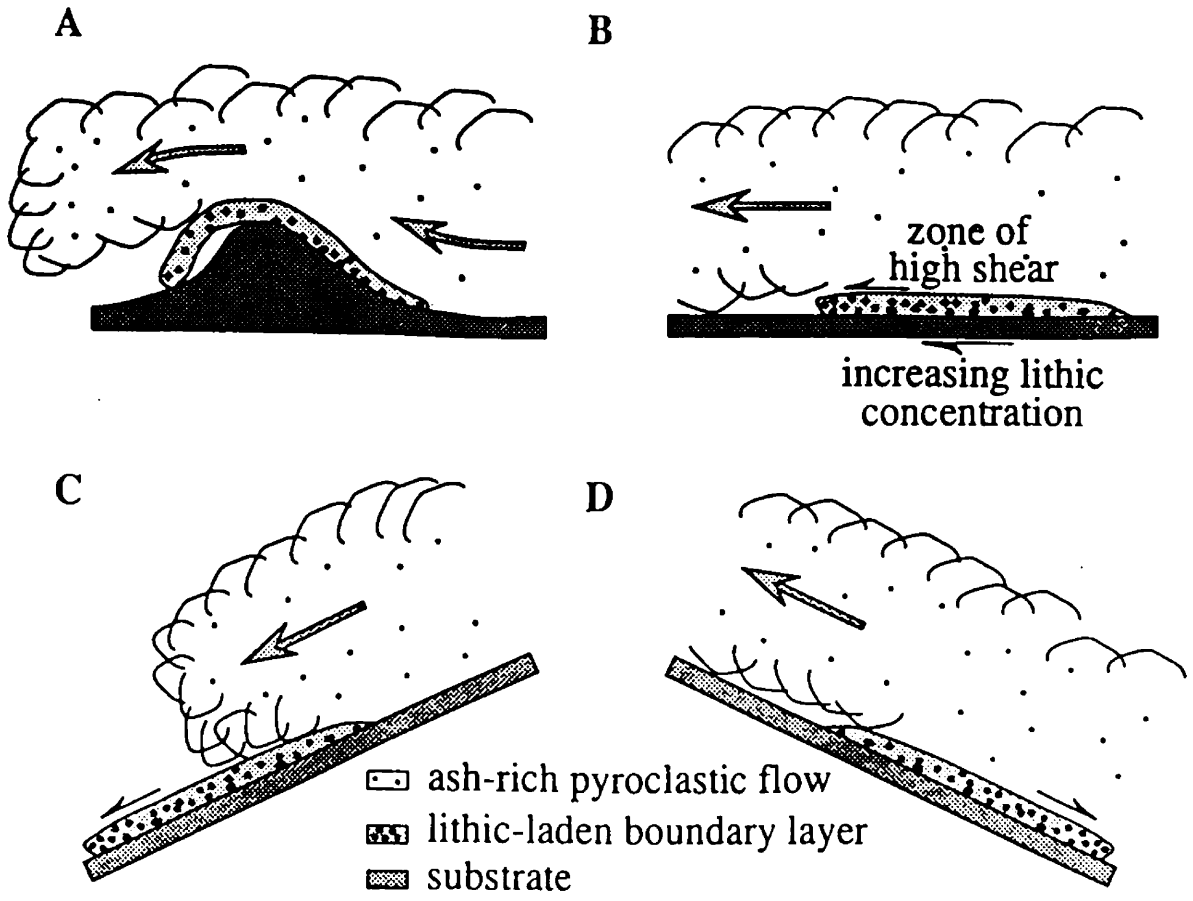

Figure 30. Models for formation of a lithic-rich pyroclastic flow by decoupling of a lithic-rich boundary layer from an ash-rich pyroclastic flow. (A) " Falling away" on lee side of topographic barrier due to density difference between two flows. (B) Basal breccia forms due to loss of momentum and shear developed at the top of the boundary layer. (C) Lithic-rich pyroclastic flow outruns the the ash-rich pyroclastic flow due to higher gravitational acceleration of the lithic-rich boundary layer. (D) Lithic-rich pyroclastic flow forms counter flow at the base of the ash-rich pyroclastic flow due to differences in gravitational acceleration between the ash-rich pyroclastic flow and the lithic-rich boundary layer. Modified from Buesch (1992).

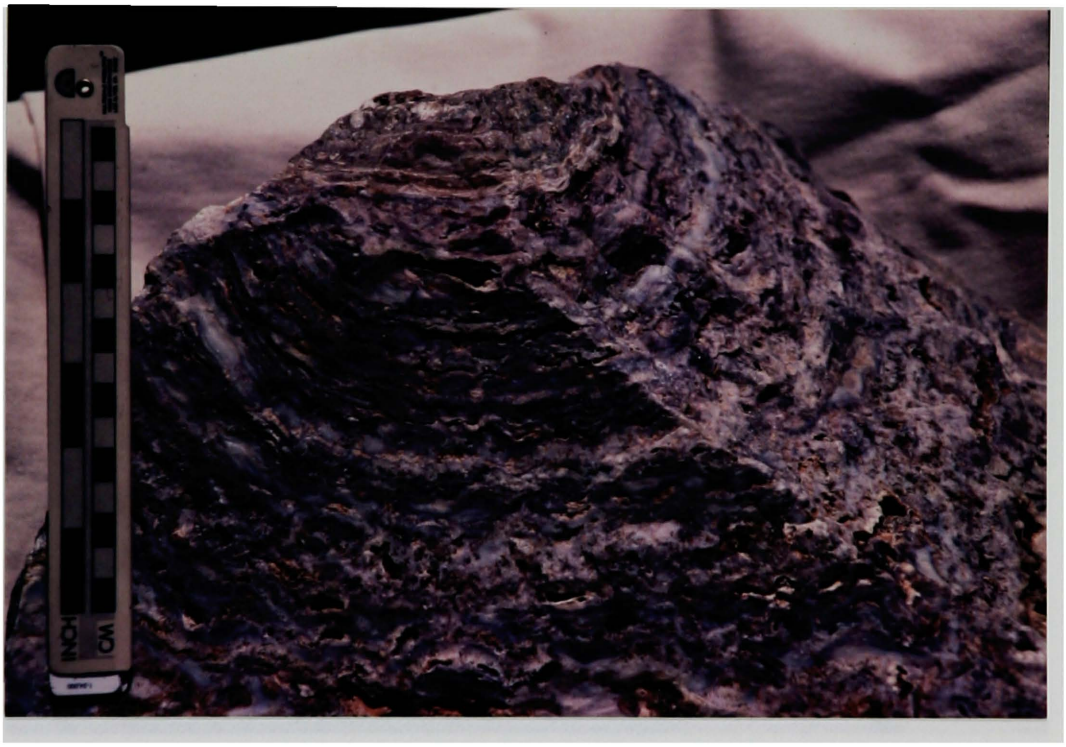

Figure 31. Hand specimen of laminated sinter of the lower volcaniclastic sedimentary unit (Tvsl). Sample MM-14.

Figure 32. Drill core specimen of varved mudstone and siltstone from the lower volcaniclastic sedimentary unit (Tvsl). Note wavy cross bedded volcaniclastic sandstone beds and dark carbonaceous laminae. Sample MM-18.

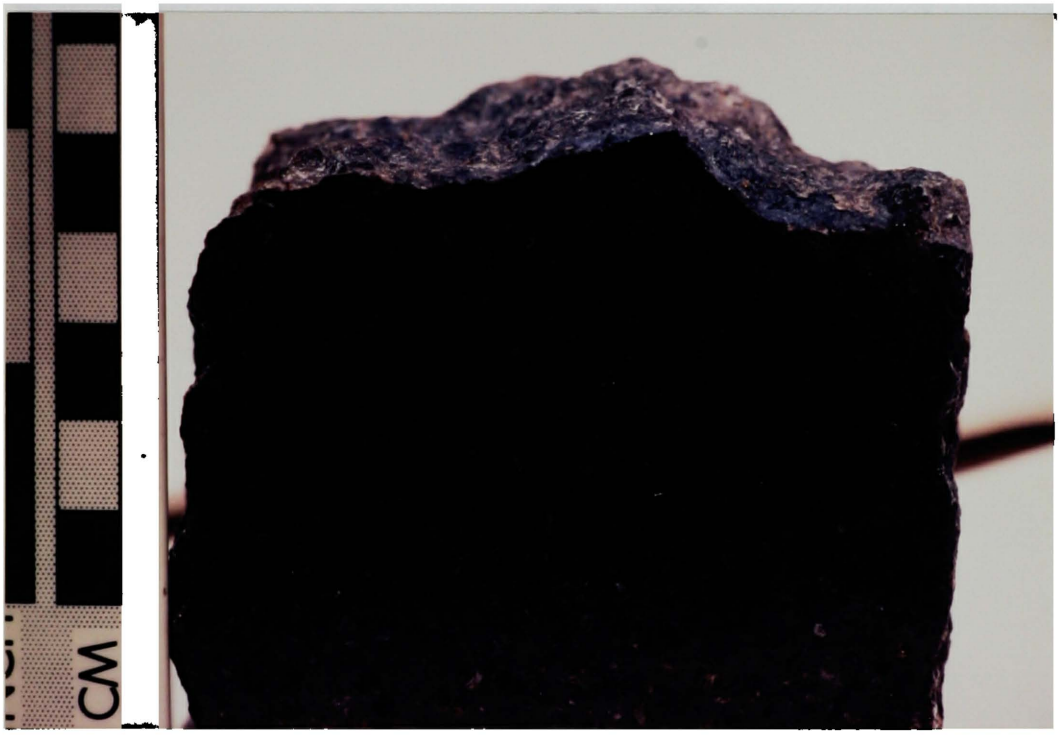

Figure 33. Hand specimen of biotite-bearing rhyolite ash-flow tuff (Trb). Note abundant angular lithic fragments, euhedral sanidine (white),quartz crystals (gray) and biotite books (black). Sample CM-184.

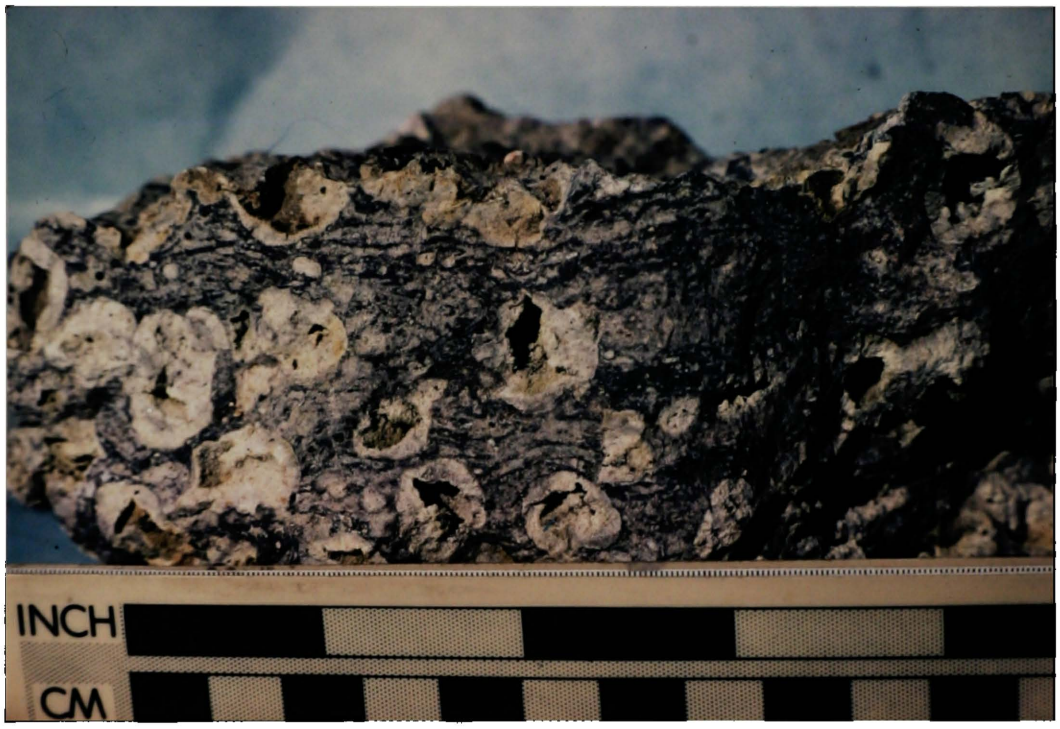

Figure 34. Hand sample of densely welded biotite-bearing rhyolite ash-flow tuff (Trb) showing eutaxitic texture and abundant lithophysae. Sample MM-6.

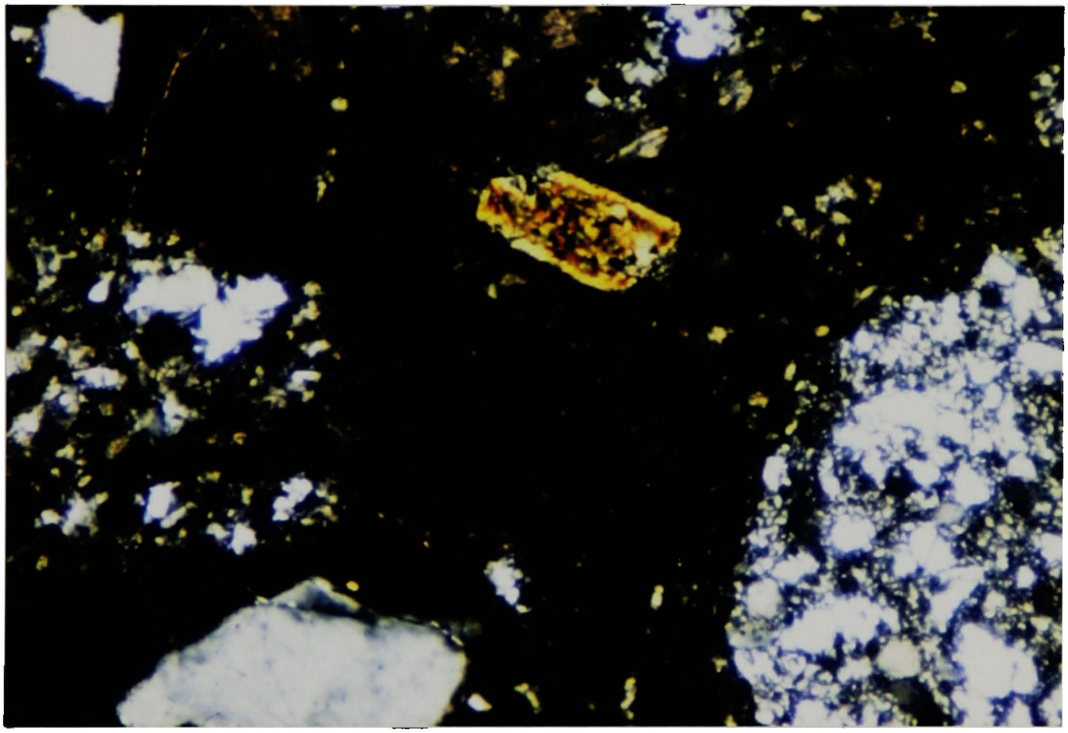

Figure 35. Photomicrograph of biotite-bearing rhyolite ash-flow tuff. Note biotite book (center), broken sanidine and bipyramidal quartz crystals (white) and fragments of and metasedimentary Belt rocks. Crossed polars Field of view is approximately 3mm. Sample CM-184.

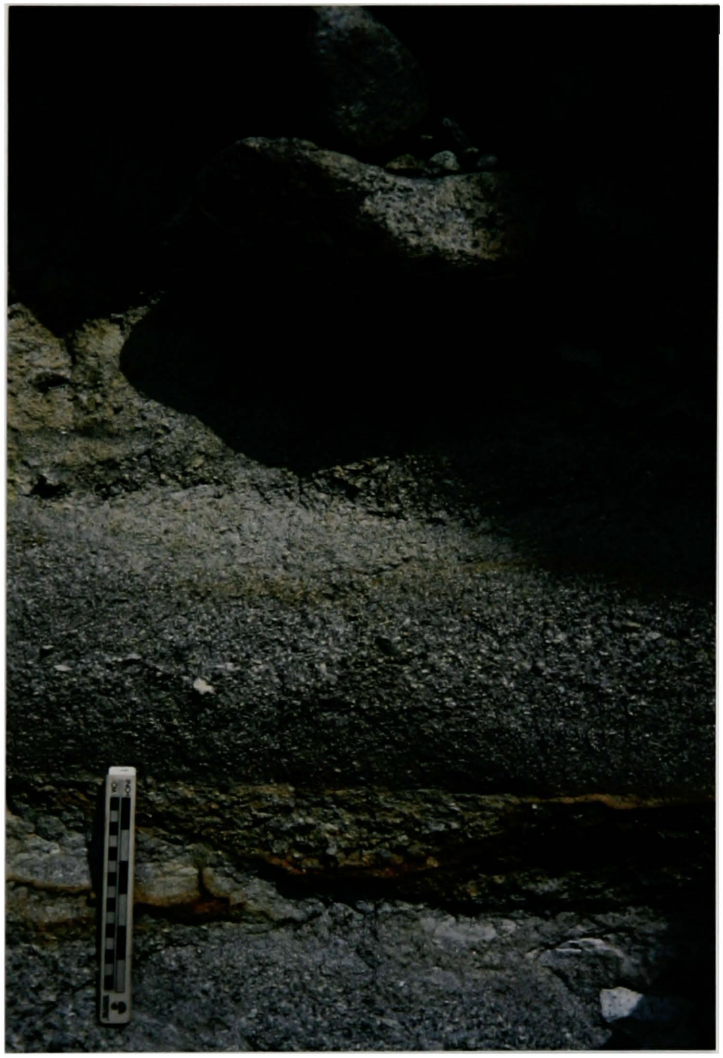

Figure 36. Outcrop of upper volcaniclastic unit (Tvsu). Note cut-and fill structure in coarse-grained sand beds beneath boulder conglomerate. West-facing slope east of Landers Fork (W edge of Sect. 30, T15N, R7W).

Figure 37. Outcrop of upper volcaniclastic sedimentary unit(Tvsu) showing reverse-graded pebbly sandstone interbeds in boulder conglomerate. Note predominance of oblate well rounded boulders. Sample location described in Figure 36.

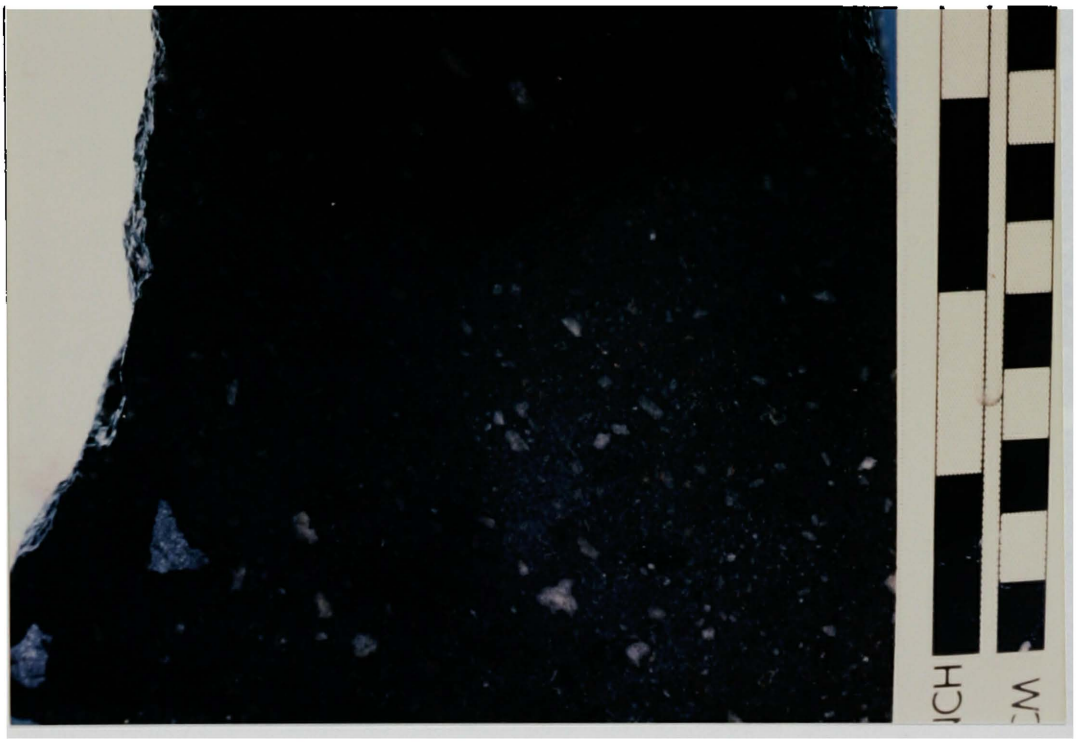

Figure 38. Hand specimen of porphyritic trachyandesite intrusion (Tpti). Note parallel alignment of plagioclase laths and iron oxide rims on mafic phenocrysts. Sample CM-75.

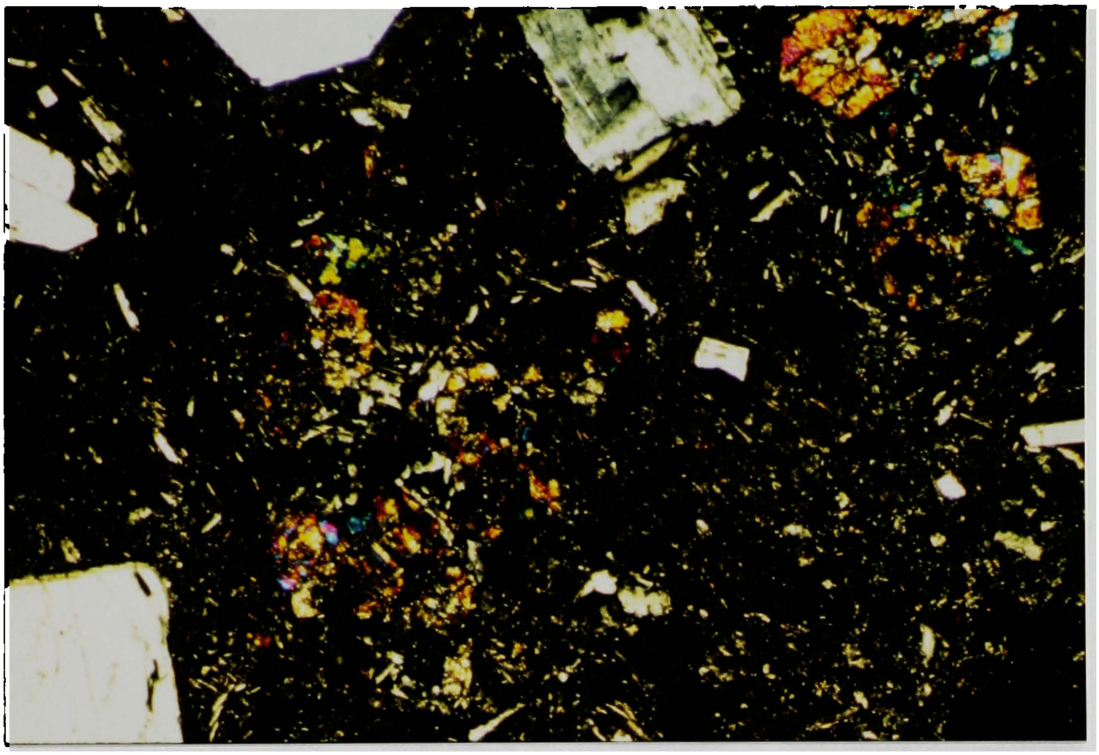

Figure 39. Photomicrograph of porphyritic trachyandesite intrusive. Note abundant augite phenocrysts (upper right) and altered olivine crystal (left center). Sample CM-146. Crossed polars. Field of view is approximately 3 mm.

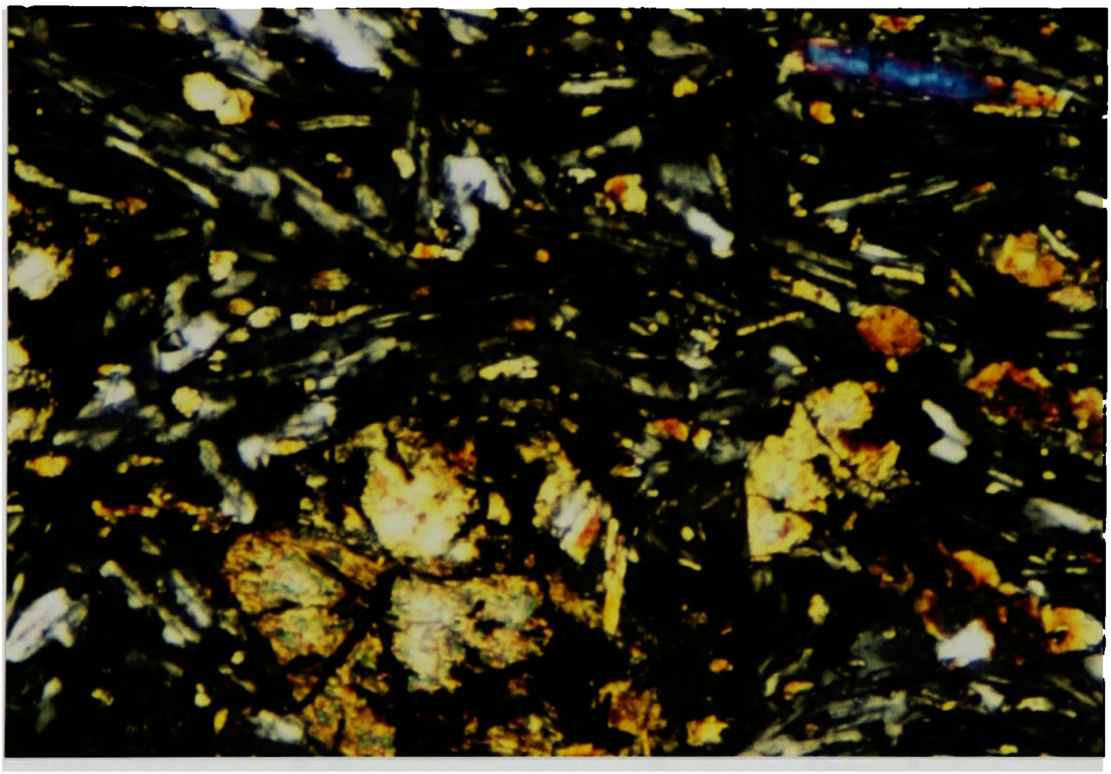

Figure 40. Photomicrograph of shonkinite intrusion (Tmi). Note intergranular texture defined by aligned plagioclase laths and interstitial augite and brown biotite crystals. Euhedral olivine crystals are pseudomorphed by brown 'iddingsite'. Sample CM-07. Crossed polars. Field of view is approximately 1.5 mm.

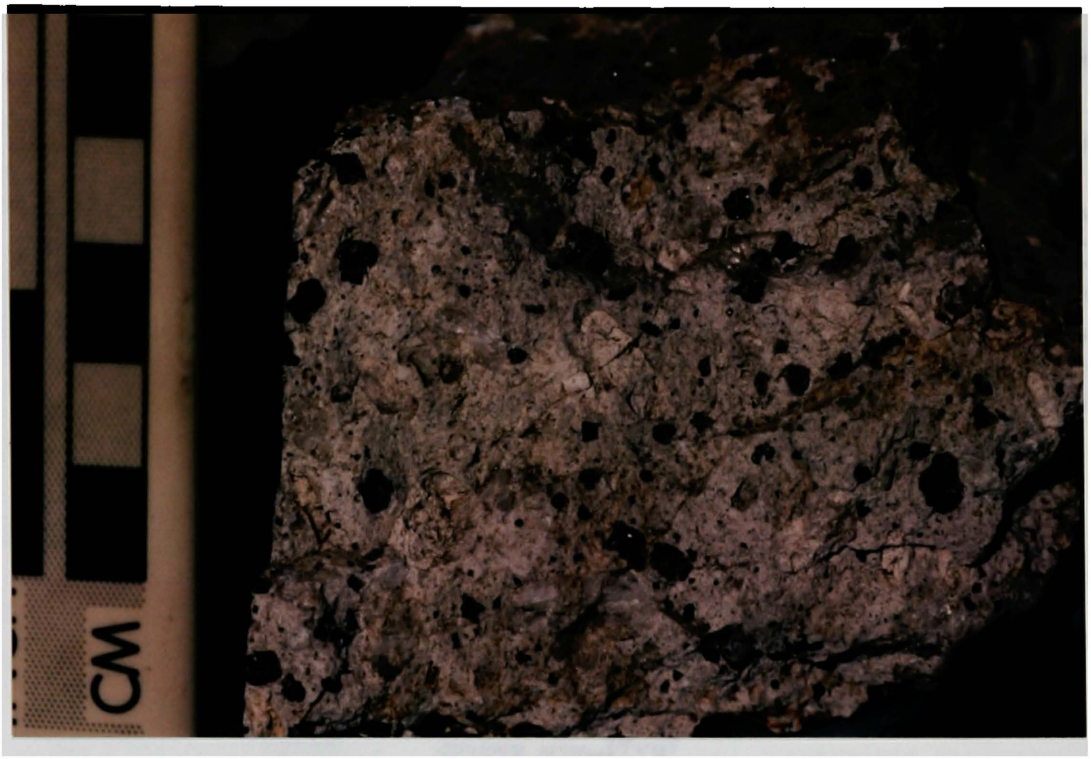

Figure 41. Hand specimen of porphyritic rhyolite intrusion (Tri). note abundant bipyramidal quartz crystals (black). Sample CM-58.

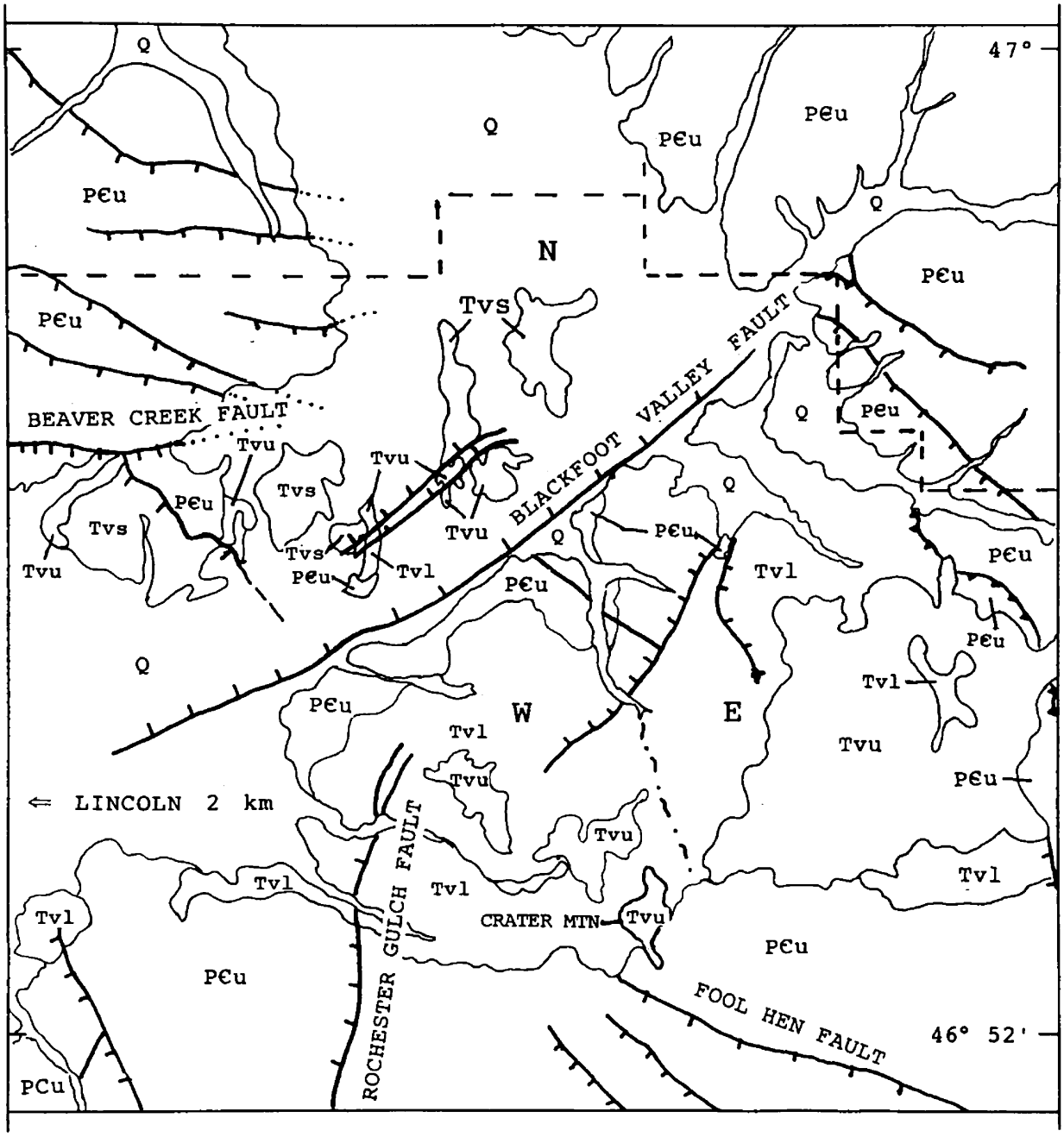

Figure 42. Generalized geologic map of the Crater Mountain volcanic complex showing three areas of semi-continuous outcrop selected for stratigraphic analysis. N = north, E = east, W = west.

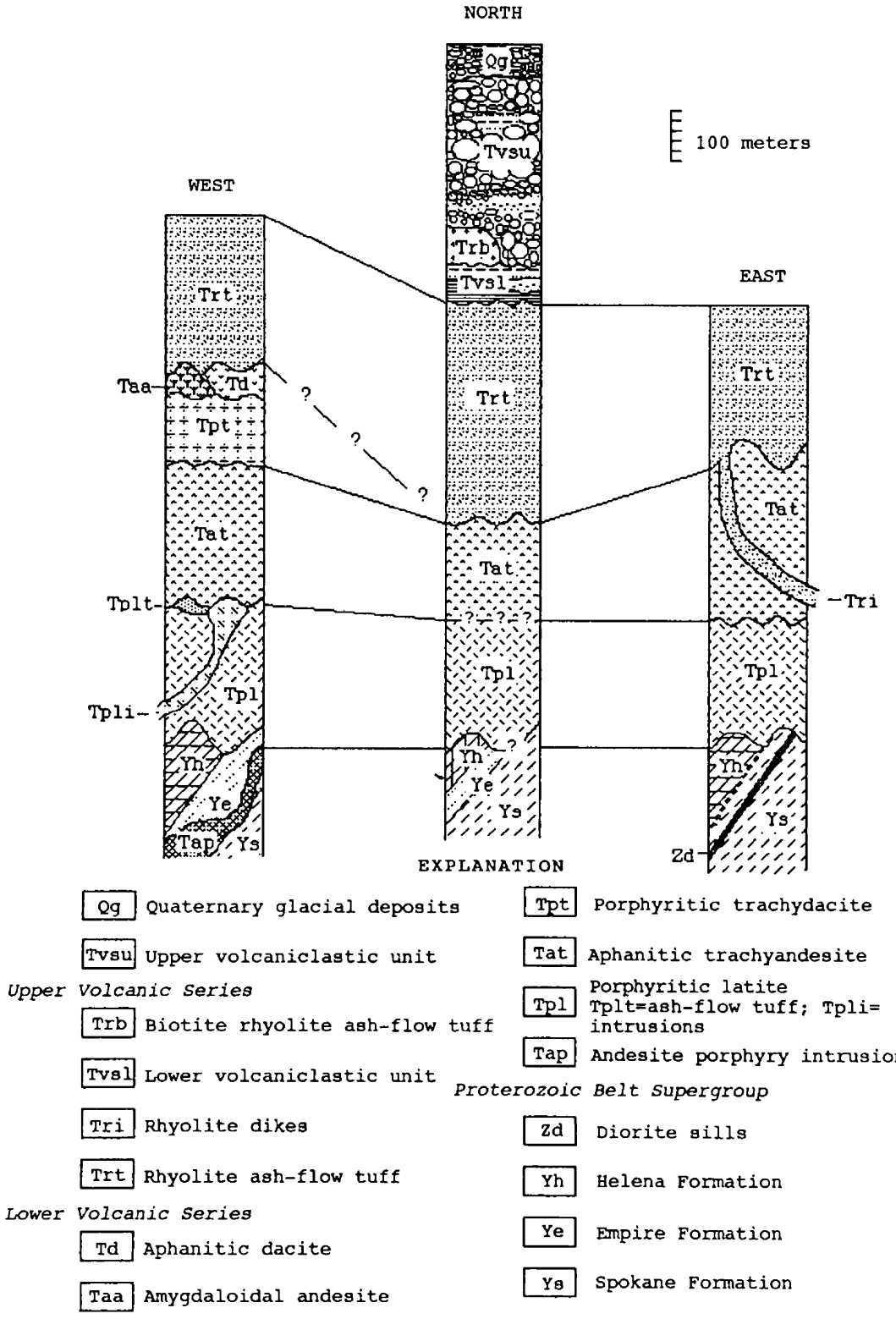

Figure 43. Idealized stratigraphic columns showing maximum exposed thicknesses of map units of the Crater Mountain volcanic complex. Locations are shown in Figure 42. Correlations between columns are shown as solid lines. Contacts which are not exposed are queried.

Explanation of symbols for figures 44 through 51:

LOWER VOLCANIC SERIES

□ = Porphyritic latite (Tpl)

△ = Aphanitic trachyandesite (Tat)

▲ = Porphyritic trachydacite (Tpd)

◇ = Aphanitic dacite (Td)

UPPER VOLCANIC SERIES

■ = Rhyolite ash-flow tuff (Trt)

✚ = Biotite-bearing rhyolite ash-flow tuff (Trb)

INTRUSIVE ROCKS

◆ = Andesite porphyry of the Silver Bell stock (Tap)

⬢ = Porphyritic trachyandesite dike (Tpi)

⬡ = Rhyolite dike (Tri)

Figure 44a-44c (following three pages). Plots of weight percent oxide versus weight percent silica for nine major oxides for 26 analyses from major rock units of the Crater Mountain volcanic complex. Total iron is expressed as FeO*. Note differences in scale for oxides. Dashed line defines field for rocks of the lower volcanic series. Field for rocks of the upper series is delineated by solid line.

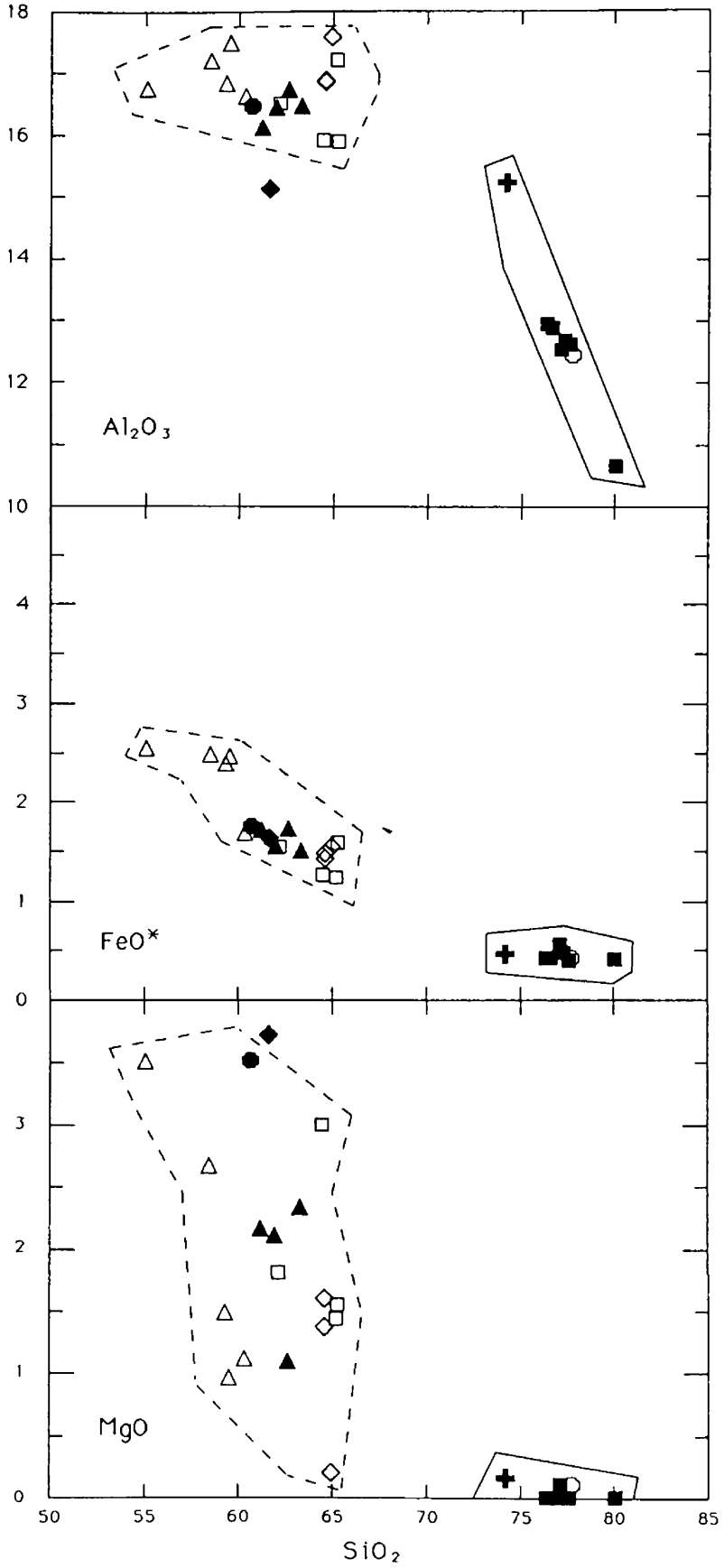
18
16
14
12
10
Al_2O_3
4
3
2
1
0
FeO*
3
2
1
0
MgO
50
55
60
65
70
75
80
85
SiO_2

Figure 44a.

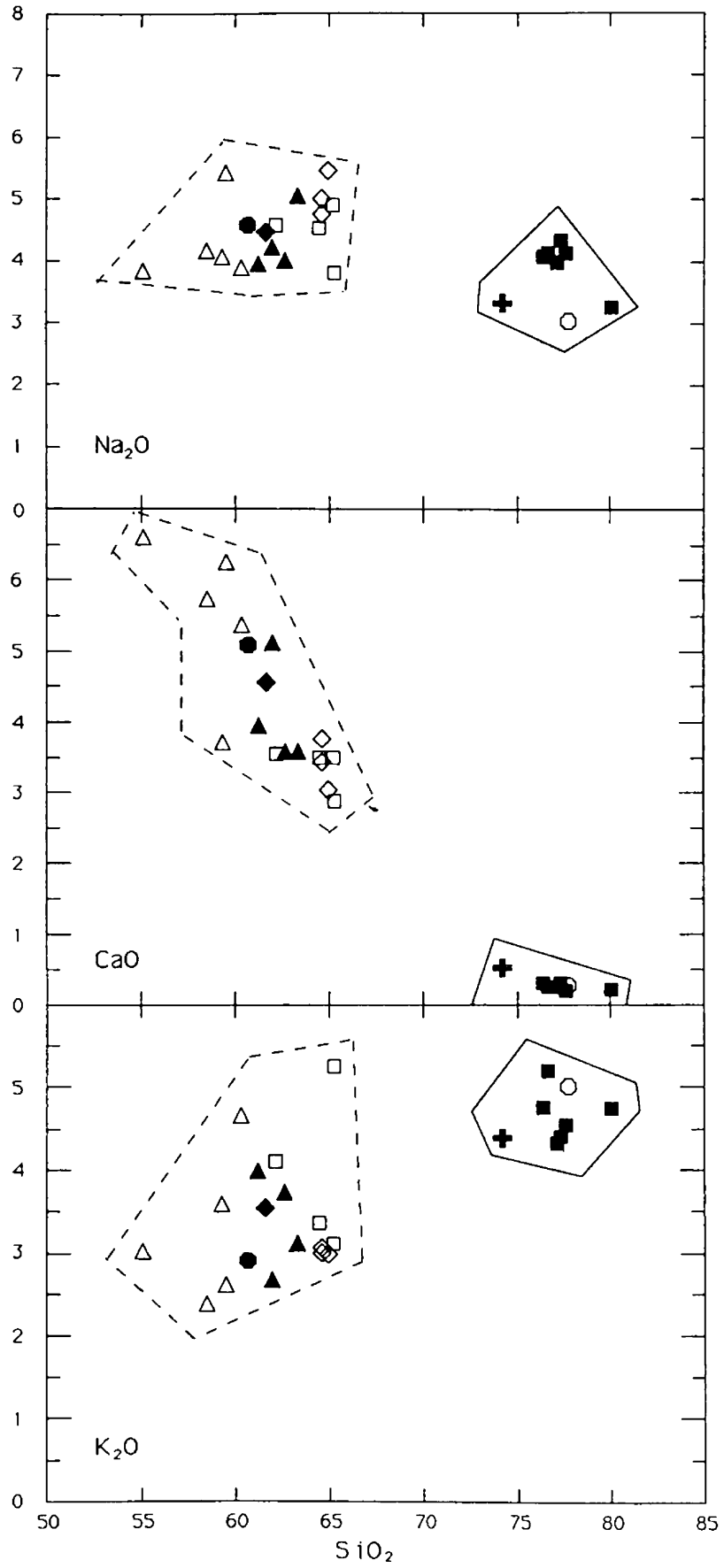

Figure 44b.

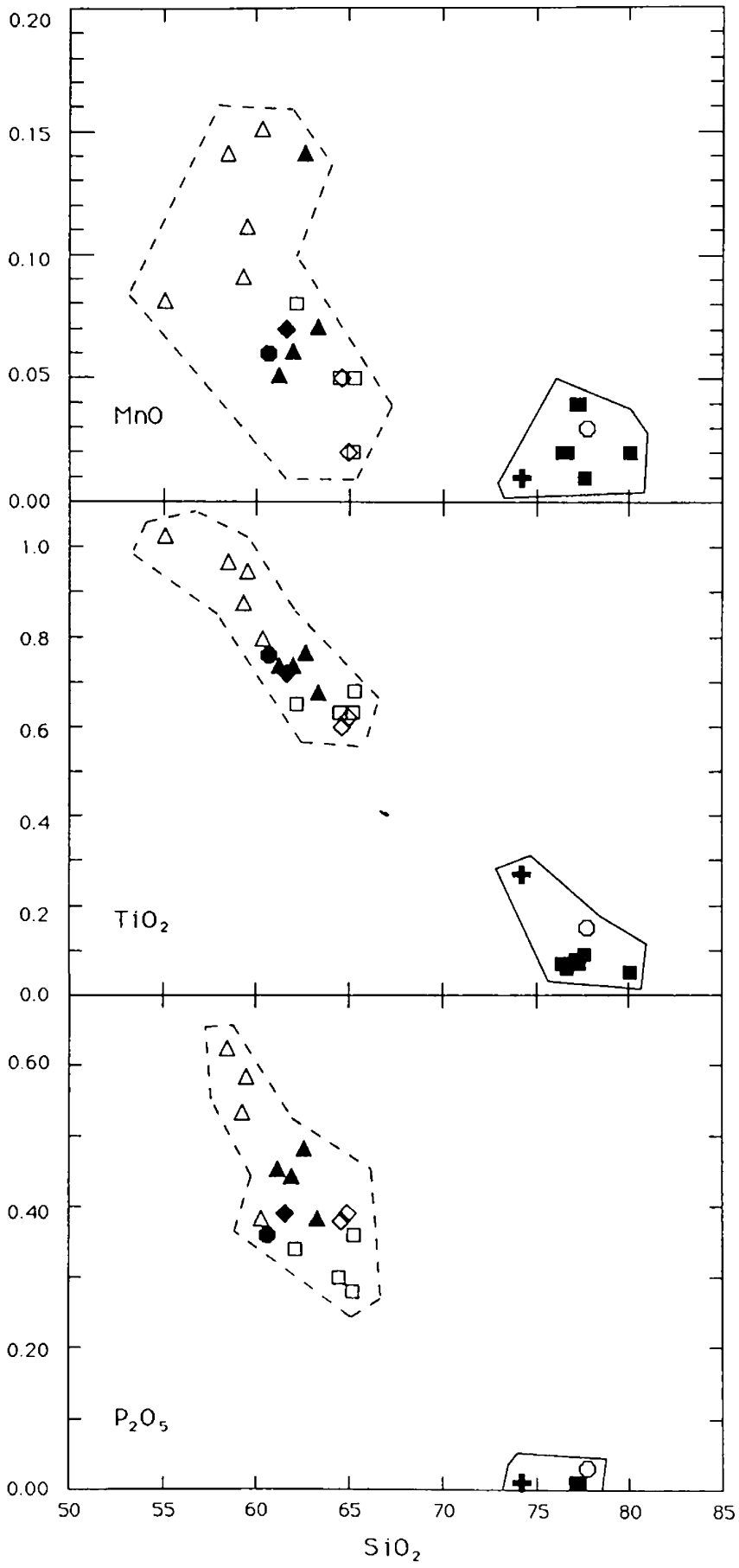
0.20
0.15
0.10
0.05
0.00
MnO
1.0
0.8
0.6
0.4
0.2
0.0
TiO2
0.60
0.40
0.20
0.00
P2O5
50
55
60
65
70
75
80
85
SiO2

Figure 44c.

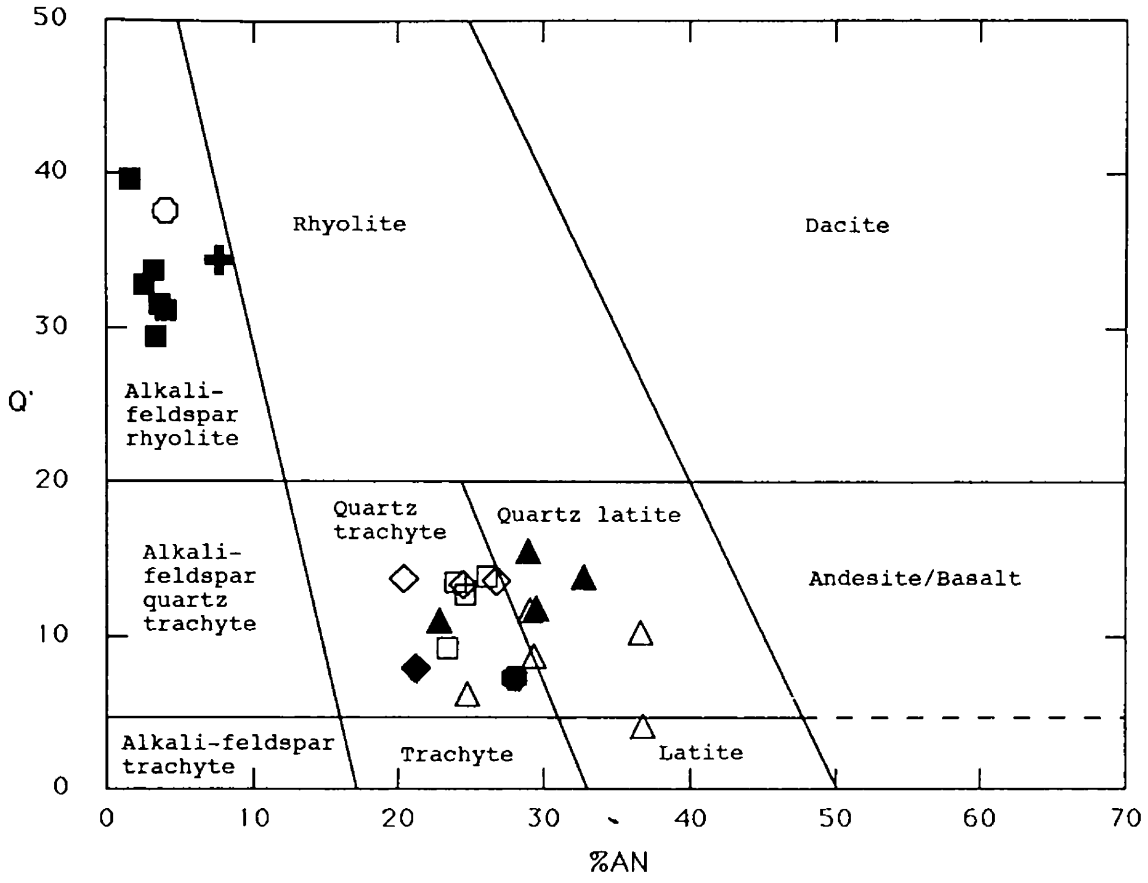

Figure 45. Normative classification of volcanic rocks for 26 analyses from the Crater Mountain volcanic complex. Modified from Streckeisen and LeMaitre (1979). Field boundaries are best fit lines which separate chemically analyzed suites of rocks classified according to the IUGS classification scheme. Normative minerals calculated by CIPW method. An % = 100 an / (an + ab). Q' = 100 q/ (q + or + an + ab). Symbols are same as those in Figure 44.

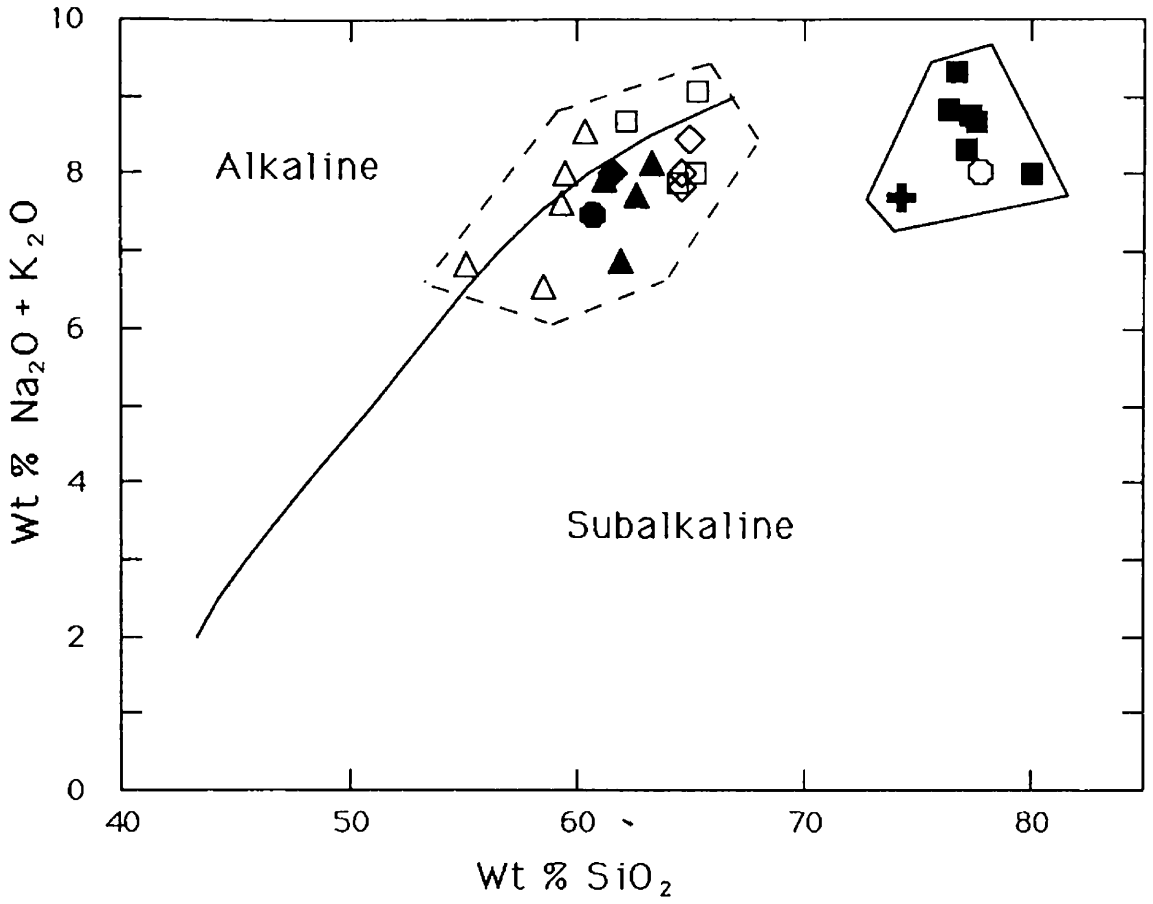

Figure 46. MacDonald and Katsura (1961) alkali-silica plot of twenty-six analyses from map units of the Crater Mountain volcanic complex. The line distinguishing alkaline from subalkaline compositions is from Irvine and Baragar (1971). Dashed line defines field for rocks of the lower volcanic series. Field for upper series delineated by solid line. Symbols as in Figure 44.

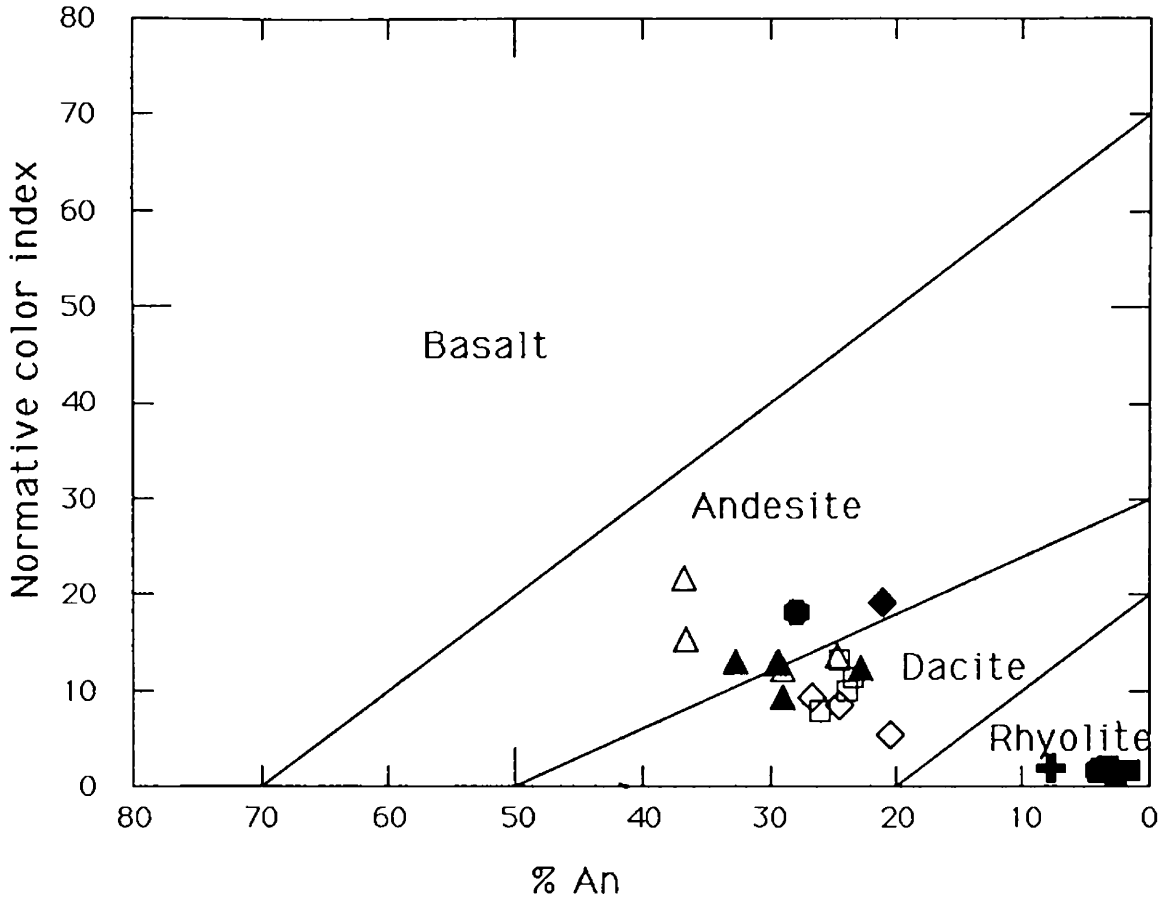

Figure 47. Plot of normative color index versus normative plagioclase composition for 26 analyses from map units of the Crater Mountain volcanic complex. Color index = Ol + Di + Hy + Mt + Il + Hm. An% = 100 An/(An + Ab). Normative minerals were calculated by the percent cation equivalent method. Fields for distinguishing basalts, andesites, dacites and rhyolites from Irvine and Baragar (1971). Symbols are the same as those in Figure 44.

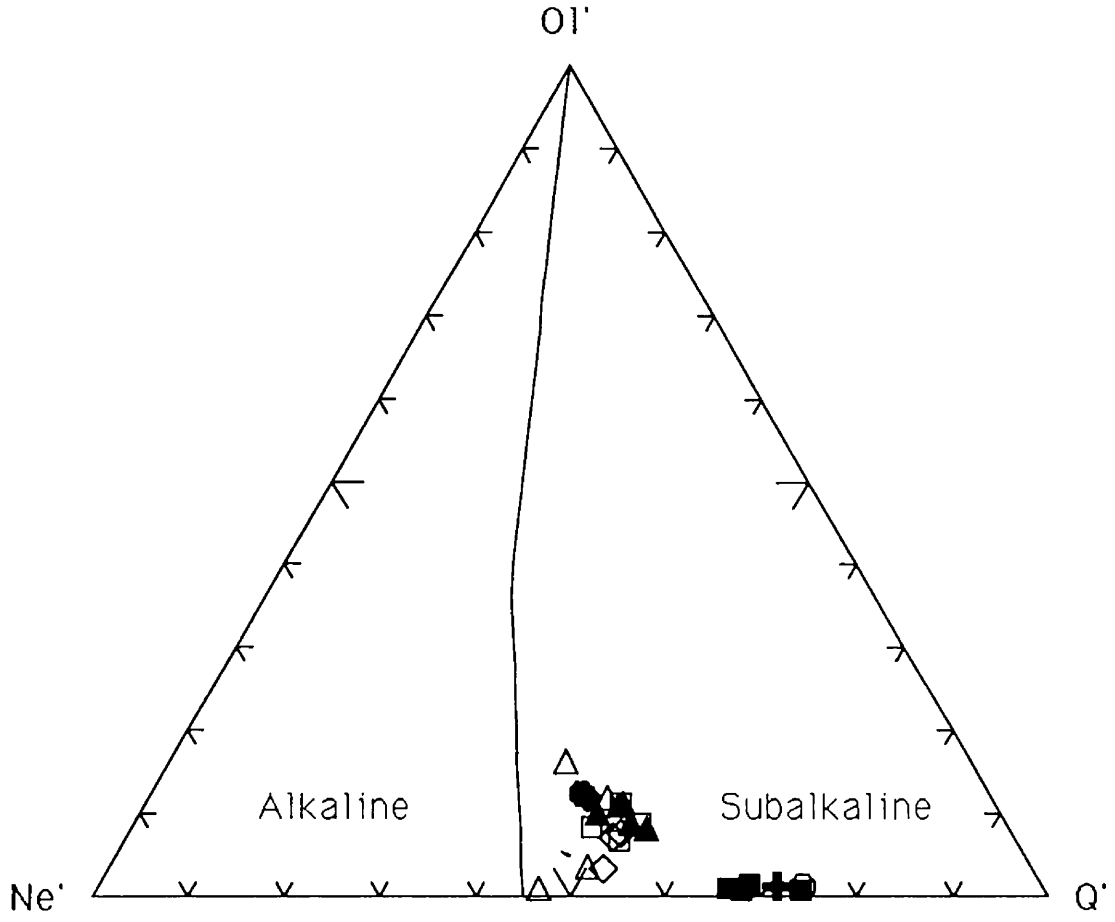

Figure 48. Plot of 26 analyses from the Crater Mountain volcanic complex in the ternary system Ol'-Ne'-Q'. Ol' = Ol + 3/4 Opx. Ne' = Ne + 3/5 Ab. Q' = Q + 2/5 Ab + 1/4 Opx. Plots are in percent cation equivalent based on the cation norm calculated acording to Chayes and Metais (1964). The curved line which separates alkaline from calc-alkaline compositions is modified from Irvine and Baragar's (1971) modification of Yoder and Tilley's (1962) critical path of silica saturation. Symbols are the same as those in Figure 44.

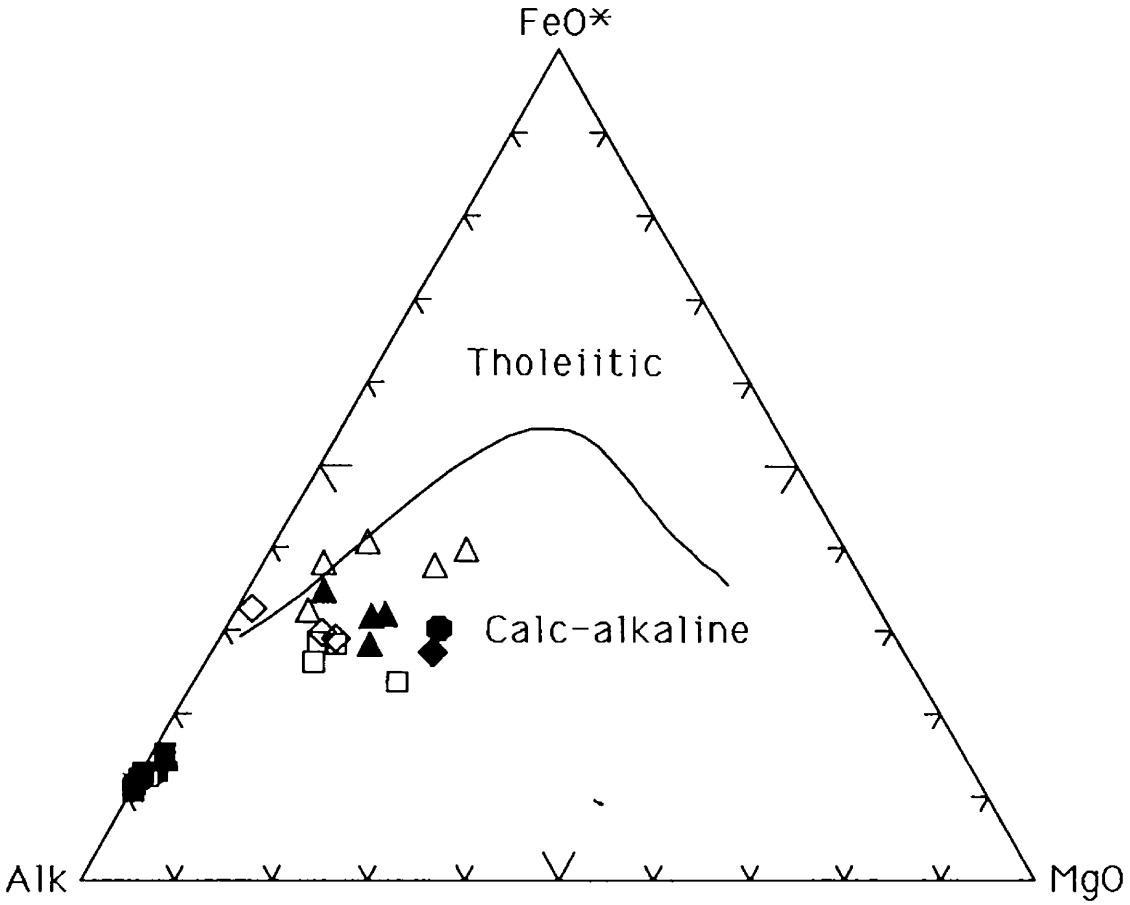

Figure 49. AFM diagram of 26 analyses from map units of the Crater Mountain volcanic complex. Alk = Na2O + K2O; FeO* = FeO + 0.8998 Fe2O3. The curved line separates calc-alkaline from tholeiitic compositions, based on the criteria of Irvine and Baragar (1971). Symbols are the same as those in Figure 44.

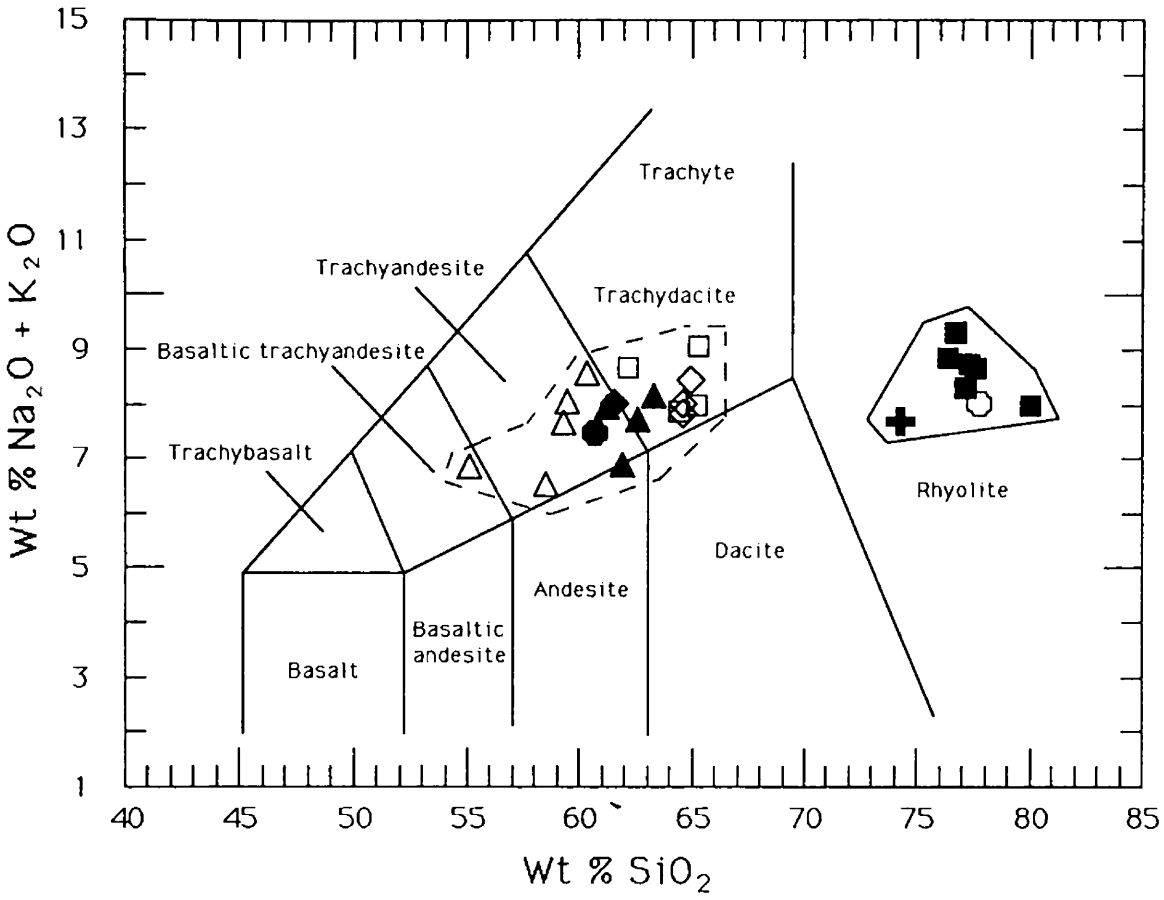

Figure 50. Total alkali-silica (TAS) diagram (modified from Le Bas and others, 1986) for 26 analyses from map units of the Crater Mountain volcanic complex. Symbols are same as those used in Figure 44. Dashed line defines field for rocks of the lower volcanic series. Field for rocks of the upper series is delineated by solid line.

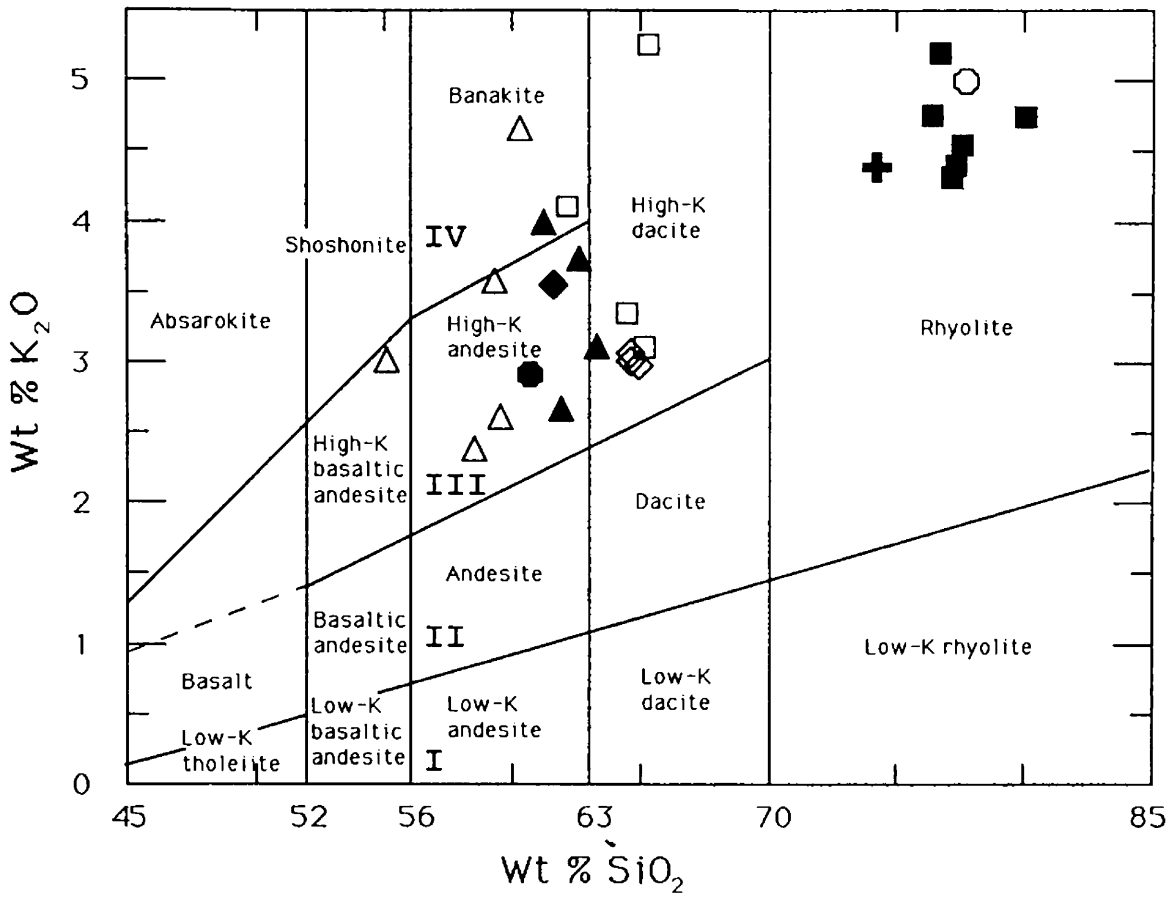

Figure 51. Plot of weight percent K2O versus weight percent SiO2 for 26 analyses from units of the Crater Mountain volcanic complex. Boundaries dividing arc tholeiite (I), calc-alkaline (II), high-K calc-alkaline (III), and shoshonite (IV) magmatic series are from Peccerillo and Taylor (1976). Symbols are the same as those in Figure 44.

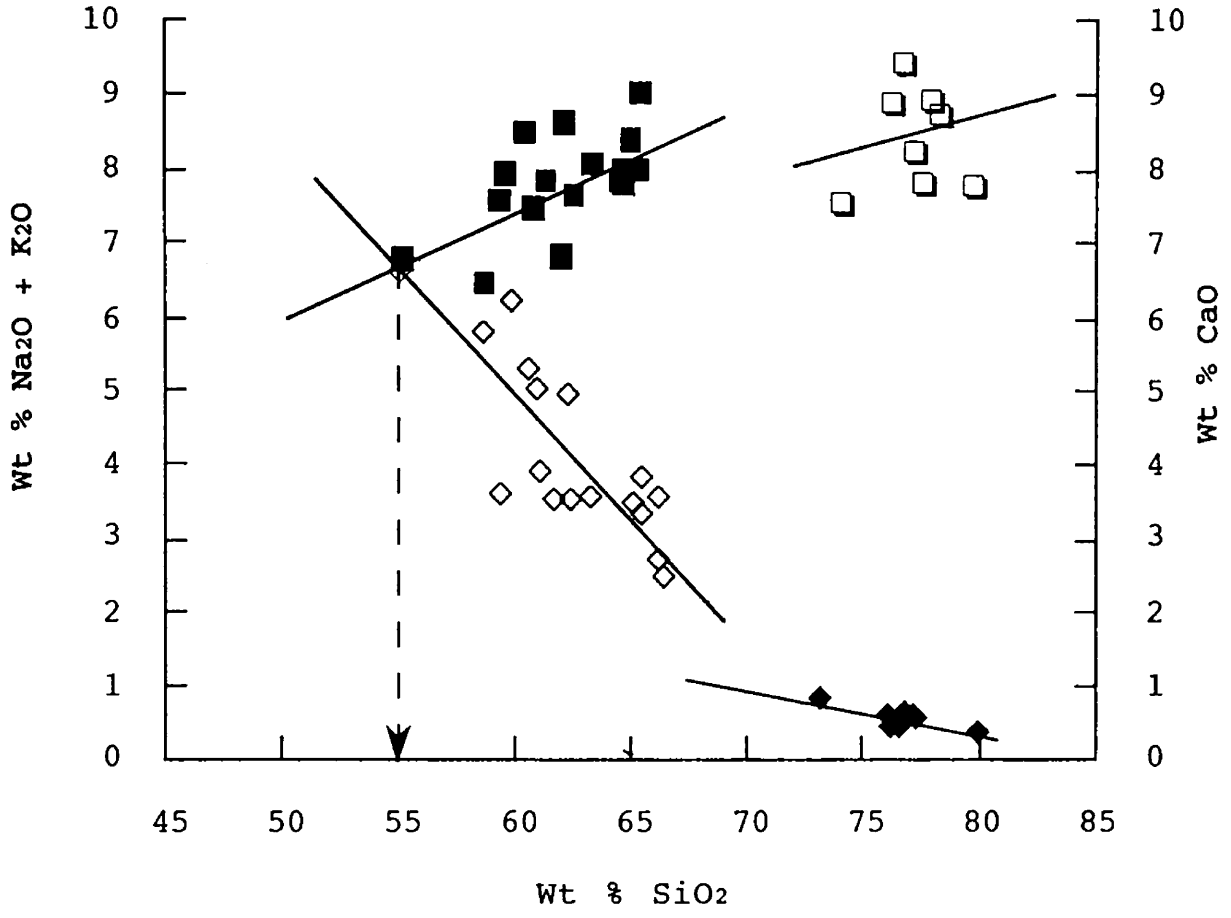

Figure 52. Alkali-lime diagram for rock units of the Crater Mountain volcanic complex (after Peacock, 1931). ◇ = CaO content, lower series; ◆ = CaO content, upper series; ■ = $Na_2O + K_2O$ content, lower series; ❑ = Na2O + K2O content, upper series. Alkali-lime index for lower series is approximately 55, which is within the alkali-calcic range of 51 to 56 weight percent SiO_2.

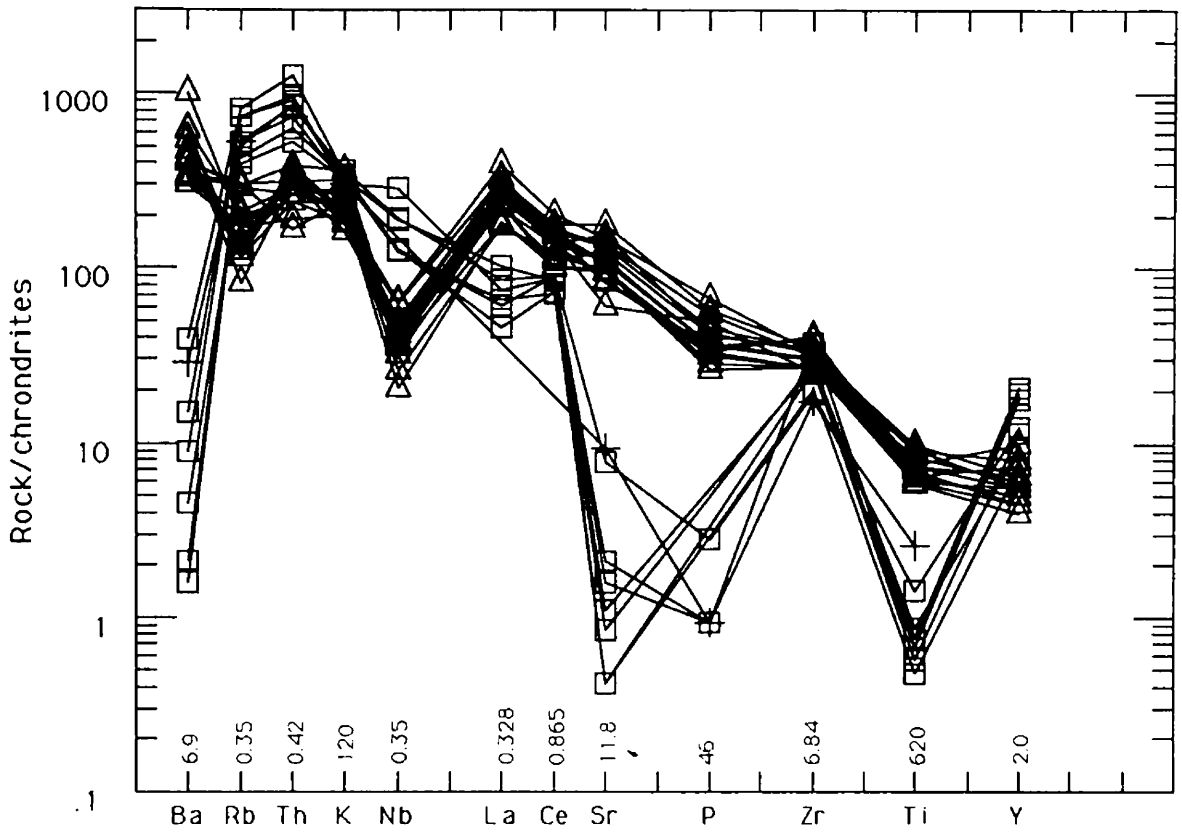

Figure 53. Spiderdiagram for 26 analyses from the Crater Mountain volcanc complex. Trace elements chondrite normalized according to the method of Thompson and others (1984). Normalization constants used are given at the base of the diagram. Δ = rocks of the lower volcanic series [porphyritic latite (Tpl), aphanitic trachyandesite (Tat), porphyritic hornblende trachydacite (Tpd), aphanitic dacite (Td), and porphyritic trachyandesite intrusive (Tpi)]; □ = rocks of the upper volcanic series [rhyolite ash-flow tuff (Trt) and rhyolite intrusive (Tri)]; + = biotite-bearing rhyolite ash-flow tuff of the upper volcanic series.

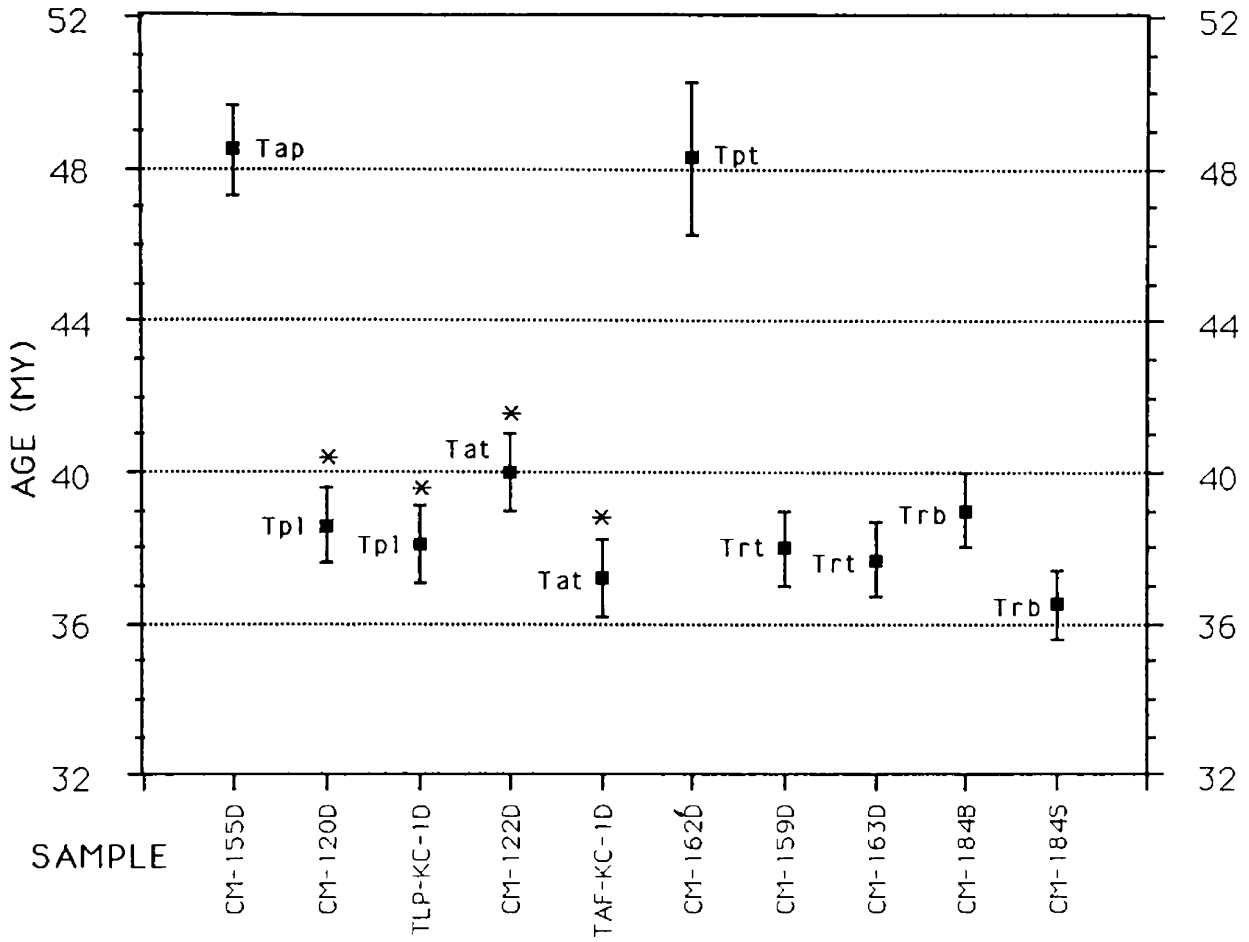

Figure 54. Scatter plot showing precision of K-Ar ages obtained for samples from major map units of the Crater Mountain volcanic complex. Symbols are the same as those in Figure 44. For sample 184: S = analysis for sanidine concentrate; B = analysis for biotite concentrate. Asterisk (*) indicates results which are considered minimum ages due to the presence of alteration of primary minerals.

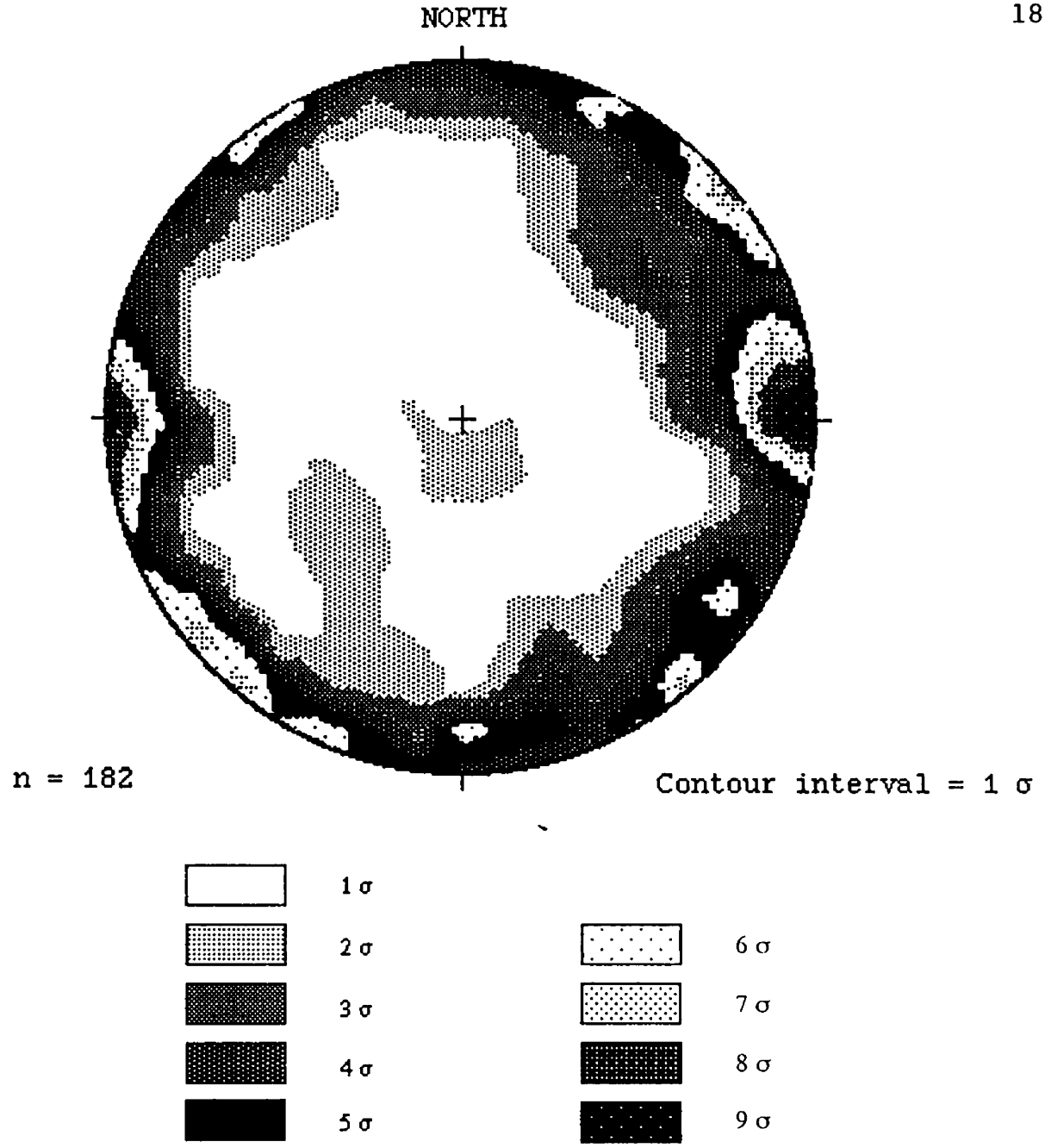

Figure 55. Equal area plot of poles to strike and dip for 182 measurements of joints, veins and fractures from the Crater Mountain volcanic complex. Data points are contoured using the point density method of Kamb (1959).

APPENDIX B

TABLES

Table 1. Major map units of the Crater Mountain volcanic complex.

RELATIVE AGE	MAP UNIT	CHEMICAL CLASSIFICATION (1)	MODE OF EMPLACEMENT	AERIAL COVERAGE (Km^2)
Youngest				
	Volcaniclastic Sediments (Tvsu)	No Data	Alluvial Fan	8.5
	Biotite Rhyolite Tuff (Trb)	Rhyolite	Ash-flow	0.1
	Volcaniclastic Sediments (Tvsl)	No Data	Stream/ Lake bed	.5
	Rhyolite Tuff (Trt)	Rhyolite	Ash-Flow	53.7
	Aphanitic Dacite (Td)	Dacite	Lava Flow	0.33
	Amygdaloidal Andesite (Taa)	Trachy-andesite (2)	Lava Flow	0.1
	Hornblende Trachydacite (Tpt)	Trachy-dacite	Lava Flow	2.2
	Aphanitic Trachy-andesite (Tat)	Trachy-andesite	Lava Flow	33.1
	Porphyritic Latite (Tpl)	Trachy-dacite	Lava Flow/ Block-and-Ash Flow	23.5
Oldest				

(1) Based on chemical classification of volcanic rocks of LeBas et al. (1986).

(2) Based on IUGS classification by modal percentages of crystals for porphyritic and aphanitic rocks.

Table 2. Modal composition of igneous map units of the Crater Mountain volcanic complex based on visual estimates from thin sections. Dashed lines indicate component not present.

Map unit	Tpl	Tat	Tpt	Td	Trt/ Tri	Tap	Taa	Tpti	Trb
Component %									
Groundmass	60-75	97-99	80-90	100	25-85	35-55	97-99	60-75	30-75
Phenocrysts	25-40	tr-3	10-20	---	15-35	45-65	tr-3	25-40	15-40
Pumice	0-10	---	---	---	7-25	---	---	---	5-75
Lithics	0-5	---	---	---	5-65	---	0-2	tr-2	5-20
Phenocryst Minerals									
Quartz	tr	---	---	---	45-60	---	---	---	35-60
Plagioclase	70-85	---	tr	---	tr-3	45-65	---	60-80	2-10
Orthoclase	---	---	---	---	---	15-30	---	---	tr
Sanidine	---	---	---	---	40-55	---	---	tr-2	25-40
Biotite	5-10	tr	1-3	---	tr	3-7	tr	2-10	2-5
Hornblende	---	---	7-20	---	---	tr-3	tr	0-2	---
Olivine	tr-2	tr	tr-3	---	---	tr-1	tr	2-10	---
Augite	2-5	tr	---	---	---	tr-1	tr	tr-5	---
Accessory Minerals									
Apatite	tr-2	tr	tr-1	---	tr	2-5	tr	tr-3	tr-2
Sphene	tr	tr	tr	1-2	---	tr-1	tr-1	tr-1	---
Magnetite	tr-2	tr-1	1-3	2-5	---	1-2	1-5	1-5	---
Zircon	tr	---	tr-1	1-2	tr	tr-1	tr	tr	tr
Rutile	---	---	tr	---	---	---	---	---	---
Groundmass Minerals									
Plagioclase	65-80	60-80	75-90	45-65	---	50-65	60-80	60-80	---
Quartz	0-3	---	---	1-3	25-35	tr	---	---	15-30
K-feldspar	tr-5	---	tr-3	20-30	10-15	tr-2	tr-5	tr-3	5-15
Augite	5-15	15-30	tr-5	10-15	---	20-30	20-30	20-30	---
Olivine	---	3-15	---	---	---	---	---	2-10	---
Opaques	2-10	5-15	3-7	3-7	tr-2	2-7	2-7	2-7	tr-1
Glass	---	---	---	---	35-55	---	---	---	40-60

Table 3. Average whole-rock chemical analyses for igneous map units in the Crater Mountain volcanic complex.

Map Unit	Tpl	Tat	Tpt	Td	Trt	Tap	Tpti	Tri	Trb
				Major elements (weight percent)					
SiO_2	64.25	58.53	62.24	64.70	77.54	61.58	60.65	77.74	74.23
TiO_2	0.65	0.92	0.72	0.61	0.07	0.62	0.76	0.15	0.27
Al_2O_3	16.38	16.95	16.40	17.11	12.39	15.13	16.47	12.46	15.23
FeO*	3.82	5.63	4.33	4.01	1.41	4.42	4.77	1.17	1.23
MnO	0.05	0.11	0.08	0.04	0.02	0.07	0.06	0.03	0.01
MgO	1.96	2.38	2.17	1.07	0.02	3.73	3.52	0.11	0.17
CaO	3.35	5.50	4.02	3.41	0.17	4.55	5.09	0.27	0.52
Na_2O	4.49	4.23	4.26	5.07	4.21	4.47	4.56	3.03	3.32
K_2O	3.96	3.23	3.35	3.02	4.66	3.55	2.91	5.00	4.39
P_2O_5	0.40	0.57	0.44	0.38	0.01	0.39	0.36	0.03	na
Total	99.31	98.05	98.01	99.72	100.5	98.51	99.15	99.99	99.37
				Trace elements (parts per million)					
Ni	55	74	50	15	15	88	123	12	4
Cr	89	111	71	17	3	144	178	5	68
Sc	8	11	8	6	2	11	12	0	49
V	69	95	77	55	3	97	111	9	10
Ba	2443	3169	4642	3105	39	2387	2101	275	2000
Rb	83	65	56	47	192	73	59	284	184
Sr	1111	1447	1541	1314	13	1134	1147	93	111
Zr	213	337	228	329	203	216	185	133	119
Y	11	14	10	8	29	13	13	25	na
Nb	10.2	17.8	13.6	16.2	70.2	15.5	12.3	45.0	na
Ga	18	19	19	19	24	15	20	16	39
Cu	22	19	19	14	4	25	27	7	22
Zn	71	95	94	92	74	72	75	28	41
Pb	21	20	23	22	33	23	18	26	22
La	67	106	87	96	23	52	59	20	na
Ce	100	149	123	128	75	124	101	79	na
Th	12	12	11	15	33	15	8	53	31

Total iron reported as FeO*; na = not analyzed

Table 4. Average CIPW normative minerals for map units of the Crater Mountain volcanic field. Normative minerals calculated according to the "percent cation equivalent" method of Barth and Niggli (Chayes and Metais, 1964). an% = 100 an/(an + ab).

Map unit	Tpl	Tat	Tpt	Td	Trt	Tap	Tpti	Tri	Trb
Q	12.26	7.41	12.74	13.52	32.73	7.81	7.28	37.56	34.30
or	22.13	20.85	20.22	17.86	27.73	21.03	17.15	30.01	26.35
ab	40.00	39.05	38.97	45.52	36.08	40.25	40.85	27.64	30.28
an	13.00	16.54	15.45	14.22	1.19	10.77	15.84	1.17	2.55
C	0.00	0.00	0.00	0.31	0.38	0.00	0.00	1.82	4.54
di	1.28	5.89	2.21	0.00	0.00	7.47	5.60	0.00	0.00
hy	6.92	5.11	7.12	7.29	0.90	9.14	9.62	1.06	1.08
mt	1.48	2.41	1.71	1.75	0.48	1.71	1.84	0.46	0.48
il	0.90	1.29	1.03	0.99	0.18	1.00	1.05	0.22	0.38
ap	0.66	1.18	0.94	0.81	0.00	0.81	0.75	6.16	0.02
an%	25	30	29	24	03	21	28	04	08

Table 5. Summary of the Irvine and Baragar (1971) chemical classification of the map units of the Crater Mountain volcanic complex.

Map unit	TAS Classification	Ol'-Ne'-Q'	AFM	An% vs color index
Andesite porphyry	Subalkaline		Calc-alkaline	Andesite
Porphyritic latite	Subalkaline		Calc-alkaline	Dacite
Aphanitic trachynadesite	Subalkaline		Calc-alkaline	Andesite/ dacite
Hornblende trachydacite	Subalkaline		Calc-alkaline	Andesite/ dacite
Aphanitic dacite	Subalkaline		Calc-alkaline	Dacite
Porphyritic trachyandesite intrusive	Subalkaline		Calc-alkaline	Andesite
Rhyolite ash-flow tuff	Subalkaline		Calc-alkaline	Rhyolite
Biotite-bearing rhyolite ash-flow tuff	Subalkaline		Calc-alkaline	Rhyolite
Rhyolite intrusive	Subalkaline		Calc-alkaline	Rhyolite

Table 6. Sample descriptions and results of Potassium-Argon age dating analysis of map units of the Crater Mountain volcanic complex. Asterisk (*) indicates results which are considered minimum ages due to the presence of alteration of primary minerals.

SAMPLE	LOCATION	MAP UNIT	MINERAL(S) ANALYZED	AGE (M.Y.)
CM-184S	NE 1/4 Sect. 36, T15N, R8W	Trb	Sanidine Concentrate	36.5 ± 0.9
Taf-KC-1D	NE 1/4 Sect. 11, T15N, R8W	Tat	Whole Rock	37.2 ± 1.0 *
CM-163D	SE 1/4 Sect. 32, T14N, R7W	Trt	Sanidine Concentrate	37.7 ± 1.0
CM-159D	NW 1/4 Sect. 35, T14N, R7W	Trt	Sanidine Concentrate	38.0 ± 1.0
Tlp-KC-1D	NW 1/4 Sect. 12, T15N, R8W	Tpl	Whole Rock	38.1 ± 1.0 *
CM-120D	SE 1/4.Sect. 20, T14N, R7W	Tpl	Whole Rock	38.6 ± 1.0
CM-184B	NE 1/4 Sect. 36, T15N, R8W	Trb	Biotite Concentrate	39.0 ± 1.0 *
CM-122D	NW 1/4 Sect. 21, T14N, R7W	Tat	Whole Rock	40.0 ± 1.0 *
CM-162D	SE 1/4 Sect. 21, T14N, R7W	Tpt	Hornblende Concentrate	48.3 ± 2.0
CM-155D	NE 1/4 Sect. 4, T13N, R7W	Tap	Biotite Concentrate	48.5 ± 1.2

Table 7. Tectonic style and magmatic evolution of associated erruptive products in western Montana and eastern Idaho. Modified from Lipman and others (1971, 1972) Dickinson and Snyder (1978), with data from Chadwick (1981); Hearn (1989); and Moye, and others (1988).

TECTONIC STYLE	AGE (MYBP)	ERUPTIVE PRODUCTS	EXAMPLES
Convergence-related compression	40-53	Andesite-trachyandesite, quartz latite, shonkinite flows	Absaroka-Gallatin, Elkhorn Mtn., Lowland Creek Adel Mtn., Garnet Range, Crater Mountain complex (lower series) Challis volcanic rocks (lower) Highwood and Bearpaw Mountains centers
Convergence-related intra-arc extension	±38-20	Basaltic andesite flows Rhyolitic flows Rhyolitic ash-flow tuffs [Bimodal]	Challis volcanic rocks (upper) Helena, Beaverhead Canyon City & Virginia City fields; Volcano Butte
Convergence related to back-arc extension	±20-10		Crater Mountain complex (upper series)
Aesthenospheric hot spot track	<10	Tholeiitic basalts	Snake River Plain, Yellowstone volcano

Appendix C : Sample Locations and Descriptions

[D denotes age-dated sample, G denotes whole-rock geochemical sample, T denotes microscopic petrography sample]

SAMPLE #	LITHOLOGY	DESCRIPTION SAMPLE LOCATION
CM-01(P)	Tat	brown aphanitic trachyandesite flow NE 1/4 SW 1/4 Section 20,T14N,R7W, drill road, 'Columbia flat'
CM-02	Tpl	green latite flow breccia NE cor NW 1/4 Section 20, T14N, R7W, roadcut, Hogum Creek Rd.
CM-03 (P)	Tpl	blue-gray porphyritic latite NE 1/4 SW 1/4 Section 17, T14N, R7W, roadcut, Hogum Creek Rd.
CM-04	Tat	black aphanitic trachyandesite flow SE 1/4 SW 1/4 Section 20, T14N, R7W, SW-facing drill road
CM-05(P)	Tat	black aphanitic trachyandesite flow SE 1/4 SW 1/4 Section 20, T14N, R7W, W-facing ridge
CM-06 (P)	Tat	brown flow-banded aphanitic trachyandesite SW cor SE 1/4 Section 20, T14N, R7W S-facing drill road
CM-07 (P)	Tmi	black aphanitic shonkinite dike SE 1/4 SW 1/4 Section 20,T14N, R7W, S-facing drill road
CM-08 (P)	Tat	green altered aphanitic trachyandesite NW 1/4 SE 1/4 Sect 20, T14N, R7W, 'Columbia flat'
CM-09	Tbr	gray silicified breccia dike NE cor NW 1/4 Section 29,14N, R7W, small prospect pit

CM-10 (P) Tbr green silicified pebble dike
NE cor NW 1/4 Section 20, T14N, R7W, S-facing drill road

CM-11 (P) Tpt gray amphibole-phyric trachydacite
NW 1/4 SE 1/4 Section 20, T14N, R7W, ridgecrest outcrop

CM-12 (P) Tpt gray amphibole-phyric trachydacite
SW 1/4 SE 1/4 Section 20, T14N, R7W, 'Columbia flat'

CM-13 (P) Tpt gray amphibole-phyric trachydacite
SW 1/4 NE 1/4 Section 29, T14N, R7W W-facing drill road

CM-14 Tvsu volcaniclastic mudflow
NE 1/4 SW 1/4 Section 6,T13N, R8W, streamcut, Poorman Creek

CM-15 Ysn dark red argillite
SW cor NW 1/4 Section 8, T13N, R8W, roadcut, Poorman Creek Rd.

CM-16 TKm altered monzonite porphyry
NW 1/4 SE 1/4 Section 8, T13N, R8W, roadcut, Poorman Creek Rd.

CM-17 Ye green argillite
SW 1/4 NW 1/4 Section 17, T13N, R8W, roadcut, Poorman Creek Rd.

CM-18 Ys purple argillite
NW cor SW 1/4 Section 16, T14N, R6W, Continental Divide Trail

CM-19 Trt light gray rhyolite crystal-lithic tuff
NE cor NE 1/4 Section 20, T14N, R6W, Continental Divide Trail

CM-20 Trt light brownish-gray silicified rhyolite tuff
NW 1/4 Ne 1/4 Section 20, T14N, R6W, Continental Divide Trail

CM-21 Trt light gray rhyolite crystal-lithic tuff
SW 1/4 SE 1/4 Section 17, T14N, R6W, NW-facing drainage

CM-22 Trt light gray rhyolite crystal-lithic tuff
NW 1/4 NE 1/4 Section 29, T14N, R6W, outcrop, low saddle

CM-23 Yh green calcareous mudstone
SE 1/4 NW 1/4 Section 17, T14N, R7W, roadcut, Hogum Creek Rd.

CM-24 Tpl red latite flow breccia near Yh contact
SE 1/4 NW 1/4 Section 17, T14N, R7W, E-facing ridge

CM-25 (P) Tpl grayish red-purple porphyritic latite
SE 1/4 NW 1/4 Section 17, T14N, R7W, NE-facing ridge

CM-26 Tpl pinkish-gray silicified porphyritic latite
NE 1/4 SW 1/4 Section 17, T14N, R7W, NE-facing ridge

CM-27(P) Tpl grayish-blue porphyritic latite
NE 1/4 NW 1/4, Section 20, T14N, R7W, outcrop, low saddle

CM-28 Tat dark gray aphanitic trachyandesite
SE 1/4 NW 1/4 Section 20, T14N, R7W, low subcrop, flat saddle

CM-29 Tpl yellowish brown silicified porphyritic latite
NW 1/4 SW 1/4 Section 17, T14N, R7W, low outcrop, ridgetop

CM-30 Yh green hornfels at Tpl contact
SE cor SW 1/4 Section 17, T14N, R7W, roadcut, Hogum Creek Rd.

CM-31 Tpl grayish-green latite breccia
NE 1/4 NE 1/4 Section 18, T14N, R7W, saddle, near Yh contact

CM-32 (P) Tpl light olive-gray porphyritic latite SW 1/4 NW 1/4 Section 18, T14N, R7W, small ridgetop knob

CM-33 Tpl yellowish-gray silicified porphyritic latite
SE 1/4 NE 1/4 Section 18, T14N, R7W, subcrop, NW-facing ridge

CM-34 Ye green siltstone
SW 1/4 SE 1/4 Section 7, T14N, R7WSW, NW-facing slope

CM-35 Yh gray calcareous siltstone
NW 1/4 SE 1/4 Section 7, T14N, R7W, N-facing slope

CM-36 Ye grayish-green siltstone
NE cor NW 1/4 Section 18, T14N, R7W, N-facing slope

CM-37 Tpl dark gray porphyritic latite
SW 1/4 NW 1/4 Section 18, T14N, R7W, W-trending saddle

CM-38 Yh gray calcareous siltstone
NW cor SW 1/4 Section 13, T14N, R7W, NW-trending saddle

CM-39 Yh gray calcareous siltstone W/ *Collenia*
NE cor SE 1/4 Section 13, T14N, R7W,outcrop, NW-facing slope

CM-40 Tat greenish-black aphanitic andesite dike
NE 1/4 SW 1/4 Section 13, T14N, R7W, low ridgetop hogback

CM-41 (P) Tpl olive gray porphyritic latite
SE cor NE 1/4 Section 8, T14N, R7W,SW-facing ridge

CM-42(P) Tat olive black aphanitic trachyandesite
NE cor NW 1/4 Section 9, T14N, R7W, outcrop, ridge top

CM-43 Tpl reddish-orange silicified porphyritic latite
SE 1/4 NE 1/4 Section 4, T14N, R7W, E-facing slope

CM-44 Tpl olive gray porphyritic latite
SW 1/4 NE 1/4 Section 4, T14N, R7W, NW-facing slope

CM-45 Tpl latite flow breccia
SW 1/4 SW 1/4 Section 34, T14N, R7W, NW-facing cliff

CM-46 Tpli purplish-gray porphyritic latite intrusion (?)
NW 1/4 SW 1/4 Section 3, T14N, R7W, small conical knob

CM-47 (P) Tpl dark purplish-brown porphyritic latite
NW 1/4 SW 1/4 Section 3, T14N, R7W, NE-facing slope

CM-48 Ys dusky red argillite
NE 1/4 NE 1/4 Section 8, T14N, R7W, float, ridge top

CM-49 Tpl grayish-purple latite porphyry
NE 1/4 NE 1/4 Section 8, T14N, R7W, outcrop, small saddle

CM-50 Tmi greenish-black aphanitic mafic dike
NW 1/4 NW 1/4 Section 8, T14N, R7W, outcrop, small saddle

CM-51(P) Tpli dark gray latite dike w/ K-spar megacrysts NW 1/4 NW 1/4 Section 8, T14N, R7W, subcrop, NW-trending swale

CM-52 (P) Tpl light gray porphyritic latite
SE cor NW 1/4 Section 4, T14N, R7W, cliff S of Blackfoot R.

CM-53 Tpl pinkish gray latite flow breccia
NE 1/4 NW 1/4 Section 4, T14N, R7W, knob, N of Blackfoot R.

CM-54 Tvbr pale orange volcaniclastic mudflow
SW 1/4 NE 1/4 Section 4, T14N, R7W, streamcut, Blackfoot R.

CM-55 Tpl light gray latite flow breccia
SE cor NW 1/4 Section 4, T14N, R7W

CM-56 Trt pinkish-gray argillic latite porphyry
SE 1/4 NW 1/4 Section 4, T14N, R7W, subcrop, small knob

CM-57 Tmi olive black aphanitic mafic dike
NE cor SW 1/4 Section 4, T14N, R7W, outcrop, NE-facing cliff

CM-58(P,G) Trd pale orange porphyritic rhyolite dike
SW cor NE 1/4 Section 12, T14N, R6W, roadcut, F. S. road

CM-59 Ys red-purple argillite w/ mudcracks
NE 1/4 NE 1/4 Section 12, T14N, R6W, roadcut, F. S. road

CM-61 (P) Trt light gray rhyolite crystal-lithic tuff
SW cor NE 1/4 Section 13, T14N, R7W, talus, ridgetop

CM-62 (P) Tat olive gray finely porphyritic trachyandesite
SE 1/4 SW 1/4 Section 34, T15N, R7W, outcrop, small knob

CM-63 (P) Tat dark greenish gray aphanitic trachyandesite
SW 1/4 SW 1/4 Section 34, T15N, R7W, float, W-trending saddle

CM-64 (P) Tpl red purple porphyritic latite
SW 1/4 SE 1/4 Section 34, T15N, R7W, outcrop, flat saddle

CM-65 Tpl grayish purple latite flow breccia
SW 1/4 SE 1/4 Section 34, T15N, R7W, outcrop, flat saddle

CM-66 Tpl grayish purple latite flow breccia
SW 1/4 SW 1/4 Section 34, T15N, R7W, talus, NW-facing slope

CM-67(P) Tplt greenish-gray volcaniclastic conglomerate
NE 1/4 SW 1/4 Section 34, T15N, R7W, roadcut, ranch road

CM-68 Tat dark gray aphanitic trachyandesite
NW 1/4 NW 1/4 Section 12, T14N, R7W, outcrop, top Wizard Mtn.

CM-69 (P) Td light olive gray banded trachyte ash flow
NW 1/4 SE 1/4 Section 29, T14N, R7W, roadcut, F. S. road

CM-70 (P) Trt light olive spherulitic rhyolite ash-flow
SW 1/ 4 SE 1/4 Section 29, T14N, R7W, W-facing ridge

CM-71 Trt grayish olive green rhyolite vitrophyre
NE cor SE 1/4 Section 29, T14N, R7W, NE-facing ridge

CM-72 Trt light gray densely welded rhyolite tuff
NW 1/4 SE 1/4 Section 29, T14N, R7W, subcrop, flat saddle

CM-73 Tpt black amphibole-phyric trachydacite
SE cor NW 1/4 Section 29, T14N, R7W, outcrop, small knob

CM-74 Yh black sucrosic limestone
SW 1/4 NE 1/4 Section 23, T14N, R8W, low outcrop, ridgetop

CM-75 (P) Tpti olive black porphyritic trachyandesite dike
NW 1/4 NE 1/4 Section 26, T14N, R8W, resistant rib, ridgetop

CM-76 Tpl pale purple porphyritic latite
SW cor NE 1/4 Section 26, T14N, R8W, roadcut, logging road

CM-77 Tplt grayish purple latite tuff(?)
NE 1/4 NW 1/4 Section 26, T14N, R8W, subcrop, SW-facing slope

CM-78 Tvbr dusky red volcaniclastic breccia
SE 1/4 NW 1/4 Section 26, T14N, R8W ,roadcut, logging road

CM-79 Tpli black intrusive latite porphyry dome
SE 1/4 SE 1/4 Section 26, T14N, R8W, outcrop, large knob

CM-80 Tvbr dusky red heterolithic volcaniclastic breccia
SE 1/4 NE 1/4 Section 26, T14N, R8W, outcrop, low knob

CM-81 Tat black flow-banded aphanitic trachyandesite
SW 1/4 NW 1/4 Section 26, T14N, R8W, S-facing slope

CM-82 Trd dark red perlitic rhyolite dike
NE cor SE 1/4 Section 25, T14N, R8W, steep NW-trending rib

CM-83 Trt light brownish-gray rhyolite crystal tuff
NE cor SW 1/4 Section 30, T14N, R7W, float, flat saddle

CM-84 Trd dark red rhyolite breccia dike
SW 1/4 NW 1/4 Section 30, T14N, R7W, NNE-trending rib

CM-85 Tplt dusky red (baked?) porphyritic latite tuff
NW cor SW 1/4 Section 24, T14N, R8W subcrop, small knob

CM-86 Tat red aphanitic flow breccia w/ scoria blocks
SW 1/4 SE 1/4 Section 24, T14N, R8W, outcrop, steep ribs

CM-87 Trt dark red densely welded rhyolite tuff
SW 1/4 SW 1/4 Section 19, T14N, R7W, float, NW-facing slope

CM-88 Tat dark purple flow-banded trachyandesite
SE 1/4 SW 1/4 Section 19, T14N, R7W, low E-trending rib

CM-89 Tpl dusky purple porphyritic latite flow breccia
SW 1/4 SW 1/4 Section 26, T14N, R8W, outcrop, NW-facing cliff

CM-90 Tplt grayish purple latite ash-flow breccia
NW 1/4 NE 1/4 Section 35, T14N, R8W, outcrop, flat knob

CM-91 Tvbr pale red purple densely welded l latite tuff
SE cor NE 1/4 Section 35, T14N, R8W

CM-92 Tlpt pale red densely welded latite tuff
SW cor NW 1/4 Section 36, T14N,R8W, outcrop, N-facing slope

CM-93 Tat brownish black aphanitic trachyandesite
NW 1/4 NE 1/4 Section 6, T14N, R7W, outcrop, ridgetop knob

CM-94 Tat dusky purple aphanitic trachyandesite
SW 1/4 NE 1/4 Section 6, T14N, R7W, outcrop, SW-facing slope

CM-95 Tplt grayish purple porphyritic latite tuff
NE 1/4 SE 1/4 Section 6, T14N, R7W, outcrop, flat saddle

CM-96(G) Tpt grayish purple amphibole-phyric trachydacite
NW 1/4 NW 1/4 Section 5, T14N, R7W, outcrop, N-facing slope

CM-97(G) Tpt grayish purple amphibole-phyric trachydacite
SE cor NW 1/4 Section 31, T14N, R7W, outcrop, E-facing slope

CM-98 Tat grayish blue porphyritic trachyandesite
NW cor SE 1/4 Section 31, T14N, R7W, NE fork Humbug Creek

CM-99 Tpti olive black porphyritic trachyandesite dike
SW 1/4 SE 1/4 Section 13, T14N, R8W, outcrop, low hogbacks

CM-100 Tpl grayish purple latite flow breccia
NE 1/4 NE 1/4 Section 24, T14N, R8W, subcrop, Seven-Up Pete Ck.

CM-101 Tat black, magnetic, aphanitic trachyandesite
NW 1/4 NW 1/4 Section 29, T14N, R7W, outcrop, Seven-Up Pete Ck.

CM-102 (P) Taa grayish red amygdaloidal andesite
NE 1/4 NW 1/4 Section 29, T14N, R7W, subcrop, NW-facing ridge

CM-103 Taa dusky red amygdaloidal aphanitic andesite
NE 1/4 SE 1/4 Section 30, T14N, R7W, subcrop, Seven-Up Pete Ck.

CM-104 Trt light gray spherulitic rhyolite tuff
NW 1/4 SE 1/4 Section 30, T14N, R7W, float, flat ridgetop

CM-105(P,G) Tpl grayish purple silicified porphyritic latite
SE 1/4 NW 1/4 Section 17, T14N, R7W, outcrop, F. S. road

CM-106 Tpl grayish purple latite flow breccia
NW 1/4 SE 1/4 Section 17, T14N, R7W, roadcut, F. S. road

CM-107 Yh greenish gray calcareous siltstone
NW cor SE 1/4 Section 17, T14N, R7W, roadcut, F. S. road

CM-108 (P) Taa grayish olive amygdaloidal andesite
SE 1/4 NW 1/4 Section 20, T14N, R7W, outcrop, N-facing facing slope

CM-109 Tmi olive black aphanitic mafic dike
T14N, R7WSE 1/4 NW 1/4 Section 20, T14N, R7W, rib, N-

CM-110(G) Tat purple aphanitic flow breccia
SW 1/4 NW 1/4 Section 20, T14N, R7W, outcrop, E-facing slope

CM-111 Tat black massive aphanitic trachyandesite
SW 1/4 NE 1/4 Section 29, T14N, R7W, roadcut, drill road

CM-112 Tpt dusky purple amphibole-phyric trachydacite
SW 1/4 NE 1/4 Section 29, T14N, R7W, outcrop, E-facing slope

CM-113 Tri grayish yellow green rhyolite dike
NE 1/4 SW 1/4 Section 29, T14N, R7W, roadcut, drill road

CM-114(G) Tpt dusky purple amphibole-phyric trachydacite
NE cor SW 1/4 Section 29, T14N, R7W, outcrop, small knob

CM-115 G) Td olive gray dacite flow
NW cor SE 1/4 Section 29, T14N, R7W, outcrop, W-facing slope

CM-116 Trt grayish pink rhyolite crystal-lithic tuff
NE 1/4 SW 1/4 Section 29, T14N, R7W, outcrop, Seven-Up Pete Ck.

CM-117 Tpt grayish purple amphibole-phyric flow breccia
NE 1/4 NE 1/4 Section 29, T14N, R7W, outcrop, SE-facing slope

CM-118(G) Td olive gray dacite flow
NE 1/4 NE 1/4 Section 29, T14N, R7W outcrop, flat ridgetop

CM-119 Tpt dusky purple amphibole-phyric trachydacite
NW 1/4 SE 1/4 Section 29, T14N, R7W, W-facing slope

CM-120(P,D,G) Tpl dusky blue porphyritic latite
NE cor NE 1/4 Section 20, T14N, R7W, roadcut, F. S. road

CM-121 Tat purple trachyandesite flow breccia
SW 1/4 NW 1/4 Section 21, T14N, R7W, outcrop, E-facing slope

CM-122(P,D,G) Tat greenish black aphanitic trachyandesite
NW 1/4 NW 1/4 Section 21, T14N, R7W, roadcut, F. S. road

CM-123 Tat gray finely porphyritic andesite
SW 1/4 NE 1/4 Section 21, T14N, R7W, streamcut, Hogum Ck.

CM-124 Tpl red latite flow breccia
NE 1/4 NE 1/4 Section 21, T14N, R7W, outcrop, N-facing cliff

CM-125 (P) Tpl light gray silicified porphyritic latite
NE 1/4 SE 1/4 Section 21, T14N, R7W, outcrop, small saddle

CM-126(P,G) Tpl pale red altered porphyritic latite
SW 1/4 SE 1/4 Section 21, T14N, R7W, subcrop, small drainage

CM-127 Trt pale green rhyolite lithic tuff
NW 1/4 NE 1/4 Section 28, T14N, R7W, streamcut, Hogum Ck.

CM-128 Trt grayish pink rhyolite crystal-lithic tuff
NE 1/4 NW 1/4 Section 28, T14N, R7W, outcrop, NW-facing ridge

CM-129 Trt grayish pink rhyolite crystal-lithic tuff
NE 1/4 NW 1/4 Section 28, T14N, R7W, outcrop, NW-facing ridge

CM-130 Tpl grayish purple porphyritic latite
NW 1/4 NE 1/4 Section 28, T14N, R7W, subcrop, W-facing slope

CM-131(P) Td grayish red dacite flow
SE 1/4 SW 1/4 Section 27, T14N, R7W, subcrop, flat saddle

CM-132(G) Trt light gray spherulitic rhyolite tuff
SE 1/4 NW 1/4 Section 28, T14N, R7W, outcrop, N-facing cliff

CM-133 Trt dusky green rhyolite tuff-breccia vitrophyre
SE 1/4 SW 1/4 Section 28, T14N, R7W, outcrop, flat ridgetop

CM-134 Tpl dusky purple porphyritic latite
SW 1/4 NE 1/4 Section 28, T14N, R7W, outcrop, small knob

CM-133 Trt olive green rhyolite breccia vitrophyre
SW 1/4 SE 1/4 Section 28, T14N, R7W, outcrop, E-facing slope

CM-136 (G) Td olive gray dacite flow
SE 1/4 SW 1/4 Section 29, T14N, R7W, outcrop, small knob

CM-137 (G) Trt pinkish gray spherulitic rhyolite tuff
NE 1/4 NW 1/4 Section 32, T14N, R7W, subcrop, small saddle

CM-138 (P) Trt grayish yellow green rhyolite flow breccia
SW 1/4 NE 1/4 Section 32, T14N, R7W, outcrop, top Crater Mt.

CM-139 (G) Trt blackish red perlitic rhyolite tuff
NW 1/4 SE 1/4 Section 32, T14N, R7W, outcrop, top Crater Mt.

CM-140 Tat pale red baked aphanitic trachyandesite
SW cor NE 1/4 Section 32, T14N, R7W, cliff, W slope Crater Mt.

CM-141(G) Trt dusky red perlitic rhyolite tuff
SW 1/4 NE 1/4 Section 32, T14N, R7W, outcrop top Crater Mt.

CM-142 Trt black perlitic rhyolite vitropyhre
SW 1/4 NE 1/4 Section 32, T14N, R7W, outcrop, top Crater Mt.

CM-143 Trt med. gray rhyolite crystal-lithic tuff
NE 1/4 SE 1/4 Section 32, T14N, R7W, outcrop, top Crater Mt.

CM-144 Tat greenish black porphyritic trachyandesite
SW 1/4 SE 1/4 Section 32, T14N, R7W, subcrop, W-facing slope

CM-145 Tpl grayish purple porphyritic latite
NW 1/4 NW 1/4 Section 4, T14N, R7W, outcrop,small saddle

CM-146(P,G) Tpti med. bluish gray porphyritic andesite dike
NW 1/4 NW 1/4 Section 4, T14N, R7W outcrop, steep rib

CM-147 Trt pale red rhyolite crystal-lithic tuff
NW 1/4 NW 1/4 Section 4, T14N, R7W, outcrop, S-slope Crater Mt.

CM-148 Trt light gray rhyolite lithic tuff
SW cor NE 1/4 Section 4, T14N, R7W, outcrop, S-facing slope

CM-149 Trt grayish pink rhyolite crystal-lithic tuff
SW cor NE 1/4 Section 4, T14N, R7W, outcrop, ridgetop

CM-15 Trt light gray rhyolite crystal-lithic tuff
SW 1/4 SE 1/4 Section 4, T14N, R7W, Continental Divide Trail

CM-151 (P) Tmi olive black porphyritic mafic dike
SW 1/4 SE 1/4 Section 4, T14N, R7W, Continental Divide Trail

CM-152 Ysn purple argillite w/ mudcracks
NW cor NE 1/4 Section 17, T13N, R8W, outcrop, Stemple Pass Rd.

CM-153(P,G) Tpt reddish brown amphibole-phyric trachydacite
SE 1/4 SE 1/4 Section 31, T14N, R8W, outcrop, W-facing slope

CM-154(P,G) Tpl grayish blue altered porphyritic latite
SE 1/4 NE 1/4 Section 5, T13N, R8W, subcrop, ridgetop

CM-155 (P,G,D) Tap greenish gray andesite porphyry stock
NE cor, NE 1/4 Section 9, T13N, R7W, roadcut, Page Gulch Rd.

CM-156 (P) Trt grayish green rhyolite tuff w/ root casts
NE cor SW 1/4 Section 34, T14N ,R7W, Continental Divide Trail

CM-157 Trt grayish pink rhyolite crystal-lithic tuff
SW 1/4 NE 1/4 Section 34, T14N, R7W, Continental Divide Trail

CM-158(G) Trt light gray rhyolite crystal-lithic tuff
NE 1/4 SE 1/4 Section 26,T14N, R7W, float, S-facing ridge

CM-159(P,G,D) Trt light gray rhyolite crystal-lithic tuff
SW 1/4 NW 1/4 Section 35, T14N, R7W, outcrop, S-facing cliff

CM-160 Tat brownish gray trachyandesite flow breccia
NW 1/4 NE 1/4 Section 14, T14N, R7W, subcrop, E-facing slope

CM-161 Trt pale orange coarse-grained rhyolite porphyry
SW 1/4 SW 1/4 Section 19, T14N, R6W, outcrop, ridgetop

CM-162(P,G,D) Tpt black amphibole-phyric trachydacite
NE 1/4 SW 1/4 Section 20, T14N, R7W, outcrop, small knob

CM-163(P,G,D) Trt grayish pink rhyolite crystal-lithic tuff
SE 1/4 SE 1/4 Section 32, T14N, R7W, small pit, Crater Mt.

CM-164(P,G) Tpl light brownish gray porphyritic latite
SE 1/4 SE 1/4 Section 31, T14N, R6W, outcrop, SW-facing cliff

CM-165 Trt greenish black rhyolite vitrophyre
SW cor SW 1/4 Section 30, T14N, R6W, subcrop, ridgetop

CM-166 Ys grayish red argillite w/ mudcracks
NW 1/4 NE 1/4 Section 15, T14N, R7W ,outcrop, Black Diamond Ck.

CM-167 Tpl dark red latite flow breccia
NW 1/4 NE 1/4 Section 15, T14N, R7W, outcrop, SE-facing slope

CM-168 Zd olive black diorite sill
SE cor SW 1/4 Section 10, T14N, R7W, outcrop, W-facing ridge

CM-169 Trt dusky red spherulitic rhyolite tuff
SW 1/4 NE 1/4 Section 32, T14N, R7W, outcrop, top Crater Mt.

CM-170 Trt light gray densely welded rhyolite tuff
SW 1/4 NE 1/4 Section 34, T14N, R7W, outcrop, SW-facing cliff

CM-171 Trt gray green rhyolite tuff w/ limb casts
NW 1/4 SE 1/4 Section 34, T14N, R7W, subcrop, SW-facing slope

CM-172 (P) Tri pale orange rhyolite porphyry
SW 1/4 SW 1/4 Section 30, T14N, R7W, outcrop, S-facing slope

CM-173 Tpl gray green latite flow breccia
SE 1/4 NE 1/4 Section 19, T14N, R8W, outcrop, NE-facing slope

CM-174 Tat grayish purple trachyandesite flow breccia
NE 1/4 NE 1/4 Section 11, T14N, R7W, streamcut, Horsefly Ck.

CM-175(P,G) Tat dark gray aphanitic trachyandesite
SW 1/4 SW 1/4 Section 1, T14N, R7W, outcrop, NW-facing slope

CM-176 Tvbr dusky pink volcaniclastic breccia
NE 1/4 SW 1/4 Section 27, T14N, R8W ,outcrop, low knobs

CM-177 Tpl grayish purple porphyritic latite
SW 1/4 SW 1/4 Section 27, T14N, R8W, roadcut, ranch road

CM-178(G) Tat brownish gray aphanitic trachyandesite
SW 1/4 SW 1/4 Section 35, T15N, R7W, streamcut, Blackfoot R.

CM-179(P,G) Tpl grayish blue porphyritic latite
SW 1/4 SW1/4 Section 26, T15N, R7W, outcrop, W-facing cliff

CM-180(G) Tat brownish black aphanitic trachyandesite
SW 1/4 SW 1/4 Section 33, T14N, R7W, low rib, W-facing ridge

CM-181 Trt olive black rhyolite vitrophyre
SW 1/4 SE 1/4 Section 36, T14N, R7W, float, flat saddle

CM-182 Yg med.gray laminated siltstone
NE 1/4 NE 1/4 Section 12, T14N, R6W, outcrop, N-facing slope

CM-183 Trt grayish orange rhyolite porphyry dike
SE 1/4 SW 1/4 Section 1, T14N, R6W, outcrop, low rib

CM-184 Tbr grayish brown crystal-lithic biotite tuff
NW 1/4 NW 1/4 Section 36, T15N, R7W, outcrop, W-facing cliff

Appendix D: Whole-rock Geochemical Analyses

[* denotes samples not included in evaluation of data due to alteration, CIPW normative minerals calculated according to the cation equivalent method of Barth and Niggli (Chayes and Metais, 1964)].

Sample	CM-58	CM-96	CM-97	CM-105*	CM-110	CM-114
SiO2	77.74	62.52	61.21	64.74	59.27	61.93
TiO2	0.15	0.76	0.73	0.80	0.87	0.73
Al2O3	12.46	16.69	16.07	16.40	16.80	16.41
FeO	1.17	4.60	4.56	4.23	6.13	4.10
MnO	0.03	0.14	0.05	0.02	0.09	0.06
MgO	0.11	1.09	2.15	0.78	1.48	2.10
CaO	0.27	3.55	3.91	0.80	3.67	5.08
Na2O	3.03	3.96	3.90	3.68	4.01	4.18
K2O	5.00	3.71	3.97	7.02	3.56	2.65
P2O5	0.03	0.48	0.45	0.43	0.53	0.44
Total	100.0	97.5	97.0	98.9	96.4	97.7
Ni	12	54	54	97	83	53
Cr	5	78	77	167	100	74
Sc	0	3	5	16	16	16
V	9	69	81	82	80	84
Ba	275	4390	6999	3586	2820	4300
Rb	284	73	62	145	106	40
Sr	93	1574	1482	818	731	1837
Zr	133	235	231	247	176	234
Y	25	11	9	19	12	9
Nb	45.0	14.4	14.5	17.1	14.4	12.4
Ga	16	17	20	17	20	20
Cu	7	20	18	8	16	17
Zn	28	92	96	67	113	99
Pb	26	24	20	22	16	23
La	20	96	74	65	81	85
Ce	79	141	97	112	126	120
Th	53	12	12	14	7	10
CIPW Normative Minerals						
Q	37.56	15.18	11.44	12.75	11.43	13.60
or	30.01	22.54	24.13	41.97	21.87	15.99
ab	27.64	36.56	36.02	33.44	37.44	38.32
an	1.17	14.90	15.04	1.19	15.34	18.36
C	1.82	0.96	0.00	2.56	1.07	0.00
di	0.00	0.00	1.50	0.00	0.00	3.37
hy	1.06	5.89	8.03	4.41	7.86	6.54
mt	0.46	1.83	1.81	1.66	2.58	1.62
il	0.22	1.09	1.05	1.13	1.26	1.04
ap	6.16	1.03	0.97	0.91	1.15	0.94
%An	4	29	29	3	29	33

Sample	CM-115	CM-118	CM-120	CM-122	CM-126*	CM-132*
SiO2	64.61	64.60	62.11	55.08	69.67	73.15
TiO2	0.60	0.60	0.65	1.02	0.42	0.21
Al2O3	16.86	16.89	16.52	16.71	14.88	14.35
FeO	3.87	3.99	4.19	6.65	2.62	1.63
MnO	0.05	0.05	0.08	0.08	0.04	0.01
MgO	1.61	1.39	1.82	3.49	0.47	0.19
CaO	3.76	3.43	3.54	6.56	1.84	0.17
Na2O	4.76	5.00	4.56	3.79	3.53	3.25
K2O	3.07	3.01	4.11	2.99	4.82	5.50
P2O5	0.38	0.38	0.34	0.72	0.21	0.04
Total	99.6	99.3	97.9	97.1	98.5	98.5
Ni	17	14	61	87	15	15
Cr	18	17	88	157	15	5
Sc	5	5	10	14	5	0
V	51	62	76	120	46	26
Ba	2976	3299	2852	3840	1869	1124
Rb	50	43	99	44	96	134
Sr	1333	1357	1117	1751	691	440
Zr	205	208	189	232	297	216
Y	8	8	10	13	12	11
Nb	15.7	15.5	11.2	22.8	16.8	18.7
Ga	19	18	20	16	15	17
Cu	14	12	22	9	7	7
Zn	88	96	89	91	51	31
Pb	20	23	22	18	26	33
La	89	93	77	128	77	81
Ce	118	127	88	175	121	149
Th	15	14	11	16	17	28
CIPW Normative Minerals						
Q	14.69	14.38	9.90	4.09	25.83	32.11
or	18.11	17.79	24.61	18.13	29.12	33.28
ab	42.69	44.91	41.50	34.93	32.41	29.83
an	15.56	14.55	12.64	20.28	7.91	0.62
C	0.00	8.30	0.00	0.00	1.14	3.16
di	0.50	0.00	2.35	6.62	0.00	0.00
hy	6.44	6.18	6.42	10.44	2.88	1.55
mt	1.50	1.54	1.64	2.70	1.04	0.65
il	0.83	0.83	0.92	1.45	0.60	0.30
ap	0.79	0.79	0.71	1.55	0.46	7.71
%An	28	24	23	37	20	2

Sample	CM-135	CM-136	CM-137	CM-139	CM-141	CM-146
SiO2	64.45	64.90	76.40	80.07	76.68	60.65
TiO2	0.63	0.62	0.07	0.05	0.06	0.76
Al2O3	15.91	17.59	12.96	10.67	12.89	16.47
FeO	3.44	4.18	1.15	1.12	1.13	4.77
MnO	0.05	0.02	0.02	0.02	0.02	0.06
MgO	3.01	0.21	0.00	0.00	0.00	3.52
CaO	3.50	3.04	0.31	0.22	0.26	5.09
Na2O	4.52	5.45	4.08	3.26	4.13	4.56
K2O	3.36	2.99	4.76	4.74	5.20	2.91
P2O5	0.30	0.39	0.00	0.00	0.00	0.36
Total	99.2	99.4	99.8	100.2	100.4	99.1
Ni	73	13	11	7	14	123
Cr	116	16	2	1	5	178
Sc	6	9	7	2	0	12
V	67	51	0	1	0	111
Ba	2286	3039	11	0	15	2101
Rb	69	47	174	147	183	59
Sr	1160	1273	13	5	5	1147
Zr	188	213	186	141	180	185
Y	11	9	36	15	23	13
Nb	9.0	17.4	66.0	44.0	67.0	12.3
Ga	17	21	25	17	24	20
Cu	24	16	6	2	6	27
Zn	64	93	62	50	70	75
Pb	18	24	38	33	42	18
La	57	105	34	22	28	59
Ce	102	139	75	62	78	101
Th	10	15	36	26	35	8
CIPW Normative Minerals						
Q	13.62	14.72	33.34	42.18	31.76	7.89
or	19.82	17.68	28.37	28.46	30.77	17.15
ab	40.53	48.97	36.96	29.75	37.14	40.84
an	13.18	12.56	1.55	0.49	1.28	15.84
C	0.00	0.86	0.59	0.00	0.00	0.00
di	1.79	0.00	0.00	0.50	0.01	5.60
hy	9.26	2.99	0.84	0.59	0.81	9.62
mt	1.33	1.62	0.45	0.44	0.44	1.84
il	0.87	0.86	9.56	0.08	0.09	1.05
ap	0.62	0.81	0.00	0.00	0.00	0.75
%An	25	20	4	2	3	28

Sample	CM-153*	CM-154*	CM-155	CM-158	CM-159	CM-162
SiO2	68.18	65.60	61.58	77.58	77.35	63.30
TiO2	0.50	0.56	0.72	0.09	0.07	0.67
Al2O3	16.43	16.39	15.13	12.62	12.69	16.43
FeO	2.89	3.59	4.42	1.08	1.30	4.04
MnO	0.02	0.02	0.07	0.01	0.04	0.07
MgO	0.16	0.66	3.73	0.00	0.00	2.33
CaO	0.56	1.86	4.55	0.20	0.31	3.55
Na2O	1.21	0.30	4.47	4.13	4.35	5.00
K2O	8.09	9.02	3.55	4.55	4.40	3.08
P2O5	0.20	0.28	0.39	0.00	0.01	0.38
Total	98.2	98.3	98.6	100.3	100.5	98.8
Ni	16	25	88	9	11	40
Cr	36	27	144	0	4	56
Sc	5	6	11	1	1	7
V	48	44	97	1	13	72
Ba	2542	2877	2387	32	62	2878
Rb	326	438	73	137	257	49
Sr	264	211	1134	10	19	1273
Zr	142	168	216	197	260	212
Y	13	16	13	19	39	10
Nb	6.8	10.1	15.5	45.0	100.0	13.2
Ga	19	19	15	23	29	20
Cu	8	7	25	3	4	20
Zn	48	82	72	72	85	90
Pb	24	23	23	18	27	24
La	41	60	52	15	25	91
Ce	69	89	124	64	76	135
Th	11	12	15	22	38	11
CIPW Normative Minerals						
Q	28.45	24.06	8.41	35.32	34.02	11.57
or	47.81	53.31	20.98	26.89	26.00	18.20
ab	10.24	2.54	37.82	34.95	36.81	42.31
an	1.49	7.39	10.74	0.99	1.54	13.29
C	5.14	3.43	0.00	0.54	0.21	0.00
di	0.00	0.00	7.46	0.00	0.00	1.48
hy	2.26	4.05	8.74	0.87	1.14	7.83
mt	1.55	1.93	2.37	0.58	0.70	2.17
il	0.95	1.06	1.36	0.17	0.14	1.27
ap	0.46	0.65	0.90	0.00	0.00	0.88
%AN	13	74	22	3	4	24

Sample	CM-163	CM-164	CM-175	CM-178	CM-179	CM-180
SiO2	77.15	65.28	58.49	60.31	65.17	59.48
TiO2	0.08	0.68	0.96	0.79	0.63	0.94
Al2O3	12.54	15.89	17.17	16.60	17.21	17.46
FeO	1.53	4.29	5.45	4.51	3.34	5.42
MnO	0.04	0.05	0.14	0.15	0.02	0.11
MgO	0.11	1.56	2.66	1.11	1.45	0.95
CaO	0.26	2.88	5.70	5.33	3.49	6.23
Na2O	4.00	3.81	4.12	3.85	4.89	5.38
K2O	4.32	5.26	2.36	4.64	3.11	2.59
P2O5	0.01	0.36	0.62	0.38	0.28	0.58
Total	100.0	100.1	97.7	97.7	99.6	99.1
Ni	15	36	85	50	51	66
Cr	7	63	113	99	89	84
Sc	1	9	9	6	5	10
V	0	75	101	85	58	91
Ba	105	2297	3762	2377	2340	3045
Rb	254	104	29	106	60	40
Sr	25	1015	2104	1000	1152	1648
Zr	256	287	242	270	188	217
Y	42	15	11	20	9	16
Nb	99.0	13.4	16.7	12.8	7.1	22.3
Ga	28	17	18	17	19	22
Cu	3	19	20	25	22	25
Zn	103	63	111	45	68	114
Pb	40	24	14	32	20	14
La	25	73	105	109	61	106
Ce	76	118	156	140	90	148
Th	40	16	13	13	12	14
CIPW Normative Minerals						
Q	36.01	14.44	10.50	8.81	15.02	6.41
or	25.53	31.09	13.95	27.42	18.38	15.31
ab	33.85	32.24	34.86	32.58	41.38	45.52
an	1.29	10.72	21.39	14.31	15.52	15.84
C	0.81	0.00	0.00	0.00	0.11	0.00
di	0.00	1.01	2.28	8.03	0.00	9.38
hy	1.62	6.29	8.11	1.89	5.67	0.25
mt	0.82	2.30	3.57	2.42	1.79	3.54
il	0.16	1.30	1.82	1.49	1.19	1.79
ap	0.00	0.83	1.44	0.88	0.64	1.33
%An	4	25	38	31	27	26

Sample	CM-184
SiO2	74.23
TiO2	0.27
Al2O3	15.23
FeO	1.23
MnO	0.01
MgO	0.17
CaO	0.52
Na2O	3.32
K2O	4.39
P2O5	0.01
Total	99.4
Ni	4
Cr	68
Sc	10
V	49
Ba	200
Rb	184
Sr	111
Zr	119
Y	NA
Nb	NA
Ga	39
Cu	8
Zn	41
Pb	22
La	NA
Ce	NA
Th	31
CIPW Normative Minerals	
Q	36.46
or	25.94
ab	28.09
an	2.51
C	4.10
di	0.00
hy	1.13
mt	0.66
il	0.52
ap	0.02
%An	8

Appendix E: Potassium-Argon Age Determination Data

[Analyses performed by Geocron Laboratories Division of Krueger Enterprises, Inc., Cambridge, MA; Sample localities are described in detail in Appendix I]

$$AGE = \frac{1}{\lambda_\beta + (\lambda_\theta + \lambda_{\theta'})} \ln \left[\frac{\lambda_\beta + (\lambda_\theta + \lambda_{\theta'})}{(\lambda_\theta + \lambda_{\theta'})} \times \frac{^{40*}Ar}{^{40}K} + 1 \right]$$

Constants Used:

$\lambda_\beta = 4.962 \times 10^{-10}$ / year

$(\lambda_\theta + \lambda_{\theta'}) = 0.581 \times 10^{-10}$/ year

$^{40}K/K = 1.193 \times 10^{-4}$ g/g

Sample: CM-120D

Description:
Dark gray porphyritic latite (Tpl) flow with 25% 7mm turbid plagioclase phenocrysts and 5% black 2mm euhedral augite and biotite crystals.

Material Analyzed:
Whole rock, -80/=200 mesh. Treated with dilute HF and HNO_3.

Argon Analyses:

^{40}Ar, ppm	$^{40*}Ar$/total ^{40}Ar	Ave $^{40*}Ar$, ppm
0.008013	0.873	0.008033
0.008053	0.852	

Potassium Analyses:

% K	Ave. % K	^{40}K, ppm
2.977	2.967	3.540
2.957		

$^{40*}Ar/^{40}K = .002269$

AGE = 38.6 +/- 1.0 M. Y.

Sample: CM-122D

Description:

Dark purplish gray aphanitic trachyandesite flow.

Material Analyzed:

Whole rock, -80/+200 mesh. Treated with dilute HF and HNO_3.

Argon Analyses:

^{40}Ar, ppm	$^{40*}Ar$/total ^{40}Ar	Ave $^{40*}Ar$, ppm
0.006520	0.836	0.006543
0.006565	0.862	

Potassium Analyses

% K	Ave. % K	^{40}K, ppm
2.328	2,332	2.781
2.335		

$^{40*}Ar/^{40}K = 0.002352$

AGE = 40.0 +/- 1.0 M. Y.

Sample: CM-155D

Description:

Andesite porphyry (Tap) with 25% 1 cm white plagioclase phenocrysts, 7% 2 cm pink orthoclase megacrysts and 10% biotite and augite crystals in a gray-green aphanitic groundmass composed mostly of plagioclase microlites.

Material Analyzed:
Biotite concentrate, -80/+200 mesh.

Argon Analyses:

^{40}Ar, ppm	$^{40*}Ar$/total ^{40}Ar	Ave $^{40*}Ar$, ppm
0.02536	0.778	0.0255
0.02573	0.795	

Potassium Analyses

% K	Ave. % K	^{40}K, ppm
7.484	7.499	8.946
7.514		

$^{40*}Ar/^{40}K$ = 002855

AGE = 48.5 +/- 1.2 M. Y.

Sample: CM-159D

Description:

Brownish gray crystal-lithic rhyolite ash-flow tuff (Trt) with 20% 2mm chatoyant sanidine crystals, 25% 3mm smokey gray bipyramidal smokey quartz crystals, and 7% accidental lithic fragments.

Material Analyzed:

Sanidine concentrate, -80/+200 mesh. Treated with dilute HF and HNO_3.

Argon Analyses:

^{40}Ar, ppm	$^{40*}Ar$/total ^{40}Ar	Ave $^{40*}Ar$, ppm
0.01478	0.838	0.01509
0.01540	0.815	

Potassium Analyses

% K	Ave. % K	^{40}K, ppm
5.679	5.622	6.755
5.645		

$^{40*}Ar/^{40}K = 0.02234$

AGE = 38.0 +/- 1.0 M. Y.

Sample: CM-162D

Description:

Medium gray porphyritic trachydacite flow with 20% 5mm black euhedral hornblende crystals which define a strong flow foliation.

Material Analyzed:

Hornblende concentrate, -80/+200 mesh. Treated with dilute HF and HNO_3.

Argon Analyses:

^{40}Ar, ppm	$^{40*}Ar$/total ^{40}Ar	Ave $^{40*}Ar$, ppm
0.001670	0.362	0.001691
0.001711	0.411	

Potassium Analyses

% K	Ave. % K	^{40}K, ppm
0.500	0.498	0.001691
0.496		

$^{40*}Ar/^{40}K = 0.002845$

AGE = 48.3 +/- 2.0 M. Y.

Sample: CM-163D

Description:

Pinkish brown crystal-lithic rhyolite ash-flow tuff with 25% euhedral 4mm sanidine crystals, 25% 3mm bipyramidal smokey quartz crystals, 1% biotite, and 10% angular lithic fragments.

Material Analyzed:
Sanidine concentrate, -80/+200 mesh. Treated with dilute HF and HNO_3.

Argon Analyses:

^{40}Ar,ppm	$^{40*}Ar$/total ^{40}Ar	Ave $^{40*}Ar$,ppm
0.01528	0.937	0.01517
0.01506	0.902	

Potassium Analyses

% K	Ave. % K	^{40}K, ppm
5.755	5.748	6.857
5.741		

$^{40*}Ar/^{40}K = 0.002212$

AGE = 37.7 +/- 1.0 M. Y.

Sample: CM-184

Description:

Dark reddish-brown welded rhyolite crystal-lithic rhyolite ash-flow tuff with 30% 5mm bipyramidal smokey quartz crystals, 15% 5mm euhedral chatoyant sanidine crystals, 2% 3mm biotite books and 15 percent lithic fragments and pumice lapilli.

Material Analyzed:

Sanidine concentrate, -80/+200 mesh. Treated with dilute HF and HNO_3.

Argon Analyses:

^{40}Ar,ppm	$^{40*}Ar$/total ^{40}Ar	Ave $^{40*}Ar$,ppm
0.02019	0.906	0.01977
0.01947	0.908	
0.01964	0.924	

Potassium Analyses

% K	Ave. % K	^{40}K, ppm
7.683	7.743	9.237
7.803		

$^{40*}Ar/^{40}K = 0.002140$

AGE = 36.5 +/- 0.9 M. Y.

Sample: CM-184

Description:

Dark reddish-brown welded rhyolite crystal-lithic rhyolite ash-flow tuff with 30% 5mm bipyramidal smokey quartz crystals, 15% 5mm euhedral chatoyant sanidine crystals, 2% 3mm biotite books and 15 percent lithic fragments and pumice lapilli.

Material Analyzed:

Biotite concentrate, -80/+200 mesh.

Argon Analyses:

^{40}Ar, ppm	$^{40*}Ar$/total ^{40}Ar	Ave $^{40*}Ar$, ppm
0.01964	0.780	0.01978
0.01992	0.762	

Potassium Analyses

% K	Ave. % K	^{40}K, ppm
7.263	7.246	8.644
7.229		

$^{40*}Ar/^{40}K = 0.002288$

AGE = 39.0 +/- 1.0 M. Y.

Sample: 2-TA

Description:

Dark greenish black aphanitic andesite with less than 1% 1mm augite phenocrysts.

Material Analyzed:

Whole rock, -80/+200 mesh. Treated with dilute HF and HNO_3.

Argon Analyses:

^{40}Ar,ppm	$^{40*}Ar$/total ^{40}Ar	Ave $^{40*}Ar$,ppm
0.002245	0.511	0.002241
0.002237	0.481	

Potassium Analyses

% K	Ave. % K	^{40}K, ppm
0.746	0.758	0.904
0.769		

$^{40*}Ar/^{40}K = 0.002480$

AGE = 42.2 +/- 1.4 M. Y.

Sample: TLP-KC-1D

Description:

Light bluish-gray porphyritic latite flow with 25% 5mm subhedral plagioclase phenocrysts and 5% 3mm biotite crystal in an aphanitic groundmass composed primarily of plagioclase microlites.

Material Analyzed:

Whole rock, -80/+200 mesh. Treated with dilute HF and HNO_3.

Argon Analyses:

^{40}Ar, ppm	$^{40*}Ar$/total ^{40}Ar	Ave $^{40*}Ar$, ppm
0.01033	0.886	0.01028
0.01022	0.892	

Potassium Analyses

% K	Ave. % K	^{40}K, ppm
3.842	3.853	4.596
3.863		

$^{40*}Ar/^{40}K = 0.002236$

AGE = 38.1 +/- 1.0 M. Y.

Sample: TAF-KC-1D

Description:

Dark brownish gray aphanitic andesite.

Material Analyzed:

Whole rock, -80/+200 mesh. Treated with dilute HF and HNO_3.

Argon Analyses:

^{40}Ar,ppm	$^{40*}Ar$/total 40Ar	Ave $^{40*}Ar$,ppm
0.007186	0.777	0.007180
0.007174	0.757	

Potassium Analyses

% K	Ave. % K	^{40}K, ppm
2.748	2.756	3.287
2.763		

$^{40*}Ar/^{40}K = 0.002184$

AGE = 37.2 +/- 1.0 M. Y.

REFERENCES CITED

Atwater, T., 1970, Implications of plate tectonics for the Cenozoic tectonic evolution of western North America: Geological Society of America Bulletin, v. 81, p. 3513-3536.

Barrell, J., 1907, Geology of the Marysville mining district, Montana: U. S. Geological Survey Professional Paper 57, 182 p.

Best, M. G., 1986, Some observations on Late Oligocene-Early Miocene volcanism in Nevada and Utah [abstract]: Geological Society of America Abstracts with Programs, v. 18, p. 86.

Bierwagen, E., 1964, Geology of the Black Mountain area, Lewis and Clark and Powell Counties, Montana [Ph.D. dissertation]: Princeton University, 120 p.

Bonnichsen, B, and Kauffman, D. E., 1987, Physical features of rhyolite lava flows in the Snake River Plain volcanic province, southwestern, Idaho *in* Fink, J. H. (ed.), The emplacement of silicic domes and lava flows: Geological Society of America Special Paper 212, P. 119-145.

Buesch, D. C., 1992, Incorporation and redistribution of locally derived lithic fragments within a pyroclastic flow, Geological Society of America Bulletin, v. 104, no 9, p. 1193-1207.

_____, and Fisher, R. V., 1988 Lithic breccia formed by density flow within an ignimbrite: [abstract] Geological Society of America Abstracts with programs, v. 20, p. 126.

Burchfiel B. C., and Davis, G. A., 1975, Nature and controls of Cordilleran orogenesis, western United States: extensions of an earlier synthesis: American Journal of Science, v. 275-A, p. 363-396.

Callmeyer, T. J., 1984, The structural, volcanic, and hydrothermal geology of the Warm Springs area, eastern Garnet Range, Powell County, Montana: [M. S. thesis], Bozeman, Montana, Montana State University, 84 p.

Carter, B., 1982, Geology of the Eocene volcanic sequence, Mt. Baldy-Union Peak area, central Garnet Range, Montana [M. S. thesis]: Missoula, Montana, University of Montana, 55 p.

Cas, R. A. F., and Wright, J. V., 1988, *Volcanic Successions Ancient and Modern*: Unwin Hyman, London, Boston, Sydney, Wellington, 528 p.

Chadwick, R. A.,1978, Geochronology of post-Eocene rhyolitic and basaltic volcanism in southwestern Montana: Isochron/West, no. 22, p. 25-28.

_____,1980, Radiometric ages of some Eocene volcanic rocks, southwestern Montana: Isochron/West, No. 24, p. 23-38.

_____ , 1981, Chronology and structural setting of volcanism in southwestern and central Montana *in* Tucker, T. E. (ed.), Guidebook to Southwestern Montana, Montana Geological Society 1981 Symposium and Field Conference, southwestern Montana p. 301-310.

_____, 1985, Overview of Cenozoic volcanism in the west-central United States, *in* Flores, R.M. and Kaplan, S.S., (eds.), Cenozoic paleogeography of the west-central United States: Society of Economic Paleontologists and Mineralogists, Rocky Mountain Symposium 3, p. 359-381.

Chapin, C. E., 1992, Mobility of elements during K-metasomatism of volcanic rocks by alkaline saline brines (abstract): Society of Economic Geologists Symposium, Mineralization Related to Continental Rifts, Abstracts with Programs Society of Economic Geologists 1992 Annual Meeting, Cincinatti, Ohio, p. A21.

_____ and Lowell, G. R., 1979, Primary and secondary flow structures in ash-flow tuffs of the Gribbles Run paleovalley, central Colorado *in* Chapin, C. E., and Elston, W. A. (eds.), Ash-flow tuffs, Geological Society of America Special Paper 180, p. 137-153.

Chayes, F., and Metais, D., 1964, On the reaction between suites of CIPW and Barth-Niggli norms: Carnegie Institute of Washington Year Book 63, p. 193-195.

Christiansen, R. L., 1979, Cooling units and composite sheets in relation to caldera structure *in* Chapin, C. E., and Elston, W. E. (eds.), Ash-flow tuffs: Geological Society of America Special Paper 180, p. 29-42.

_____, and Lipman, P. W., 1966, Emplacement and thermal history of a rhyolite lava flow near Fortymile Canyon, southern Nevada: Geological Society of America Bulletin, v. 77, p. 671-684.

Coney, P. J., and Reynolds, S. J., 1877, Cordilleran Benioff zones: Nature, v. 270, p. 403-406.

Cross, T. A., and Pilger, R. H., 1978, Constraints on absolute motion and plate interaction inferred from Cenozoic igneous activity in the western United States: American Journal of Science, v. 278, p. 865-902.

Daniel, F., and Berg, R. B., 1981, Radiometric dates of rocks in Montana: Montana Bureau of Mines and Geology Bulletin 114, 115 p.

Davis, R. A. Jr., 1983, *Depositional Systems: A Genetic Approach to Sedimentary Geology:* Prentice-Hall, Englewood Cliffs, New Jersey, 669 p.

Derkey, R, E., and Bartholemew, M. J., 1985, Geologic History of the Deerlodge-Elliston area with emphasis in the Elkhorn Mountains Volcanics and regional structures: Tobacco Root Geological Society, Guidebook 10th Annual Field Conference, p. 3.

_____, 1988, Geologic map of the Ramsay Quadrangle, Montana: Montana Bureau of Mines and Geology Map 47. Scale 1:24.000.

Dickenson, R. A., and Snyder, W. J., 1978, Plate tectonics of the Laramide orogeny: Geological Society of America Memoir 151 p. 355-366.

Ekren, E. B., 1982, Eocene cauldron-related events in the Challis Quadrangle *in* McIntyre, D. H., ed., Symposium on the geology and mineral deposits of the Challis 1° X 2° Quadrangle, Idaho: U. S. Geological Survey Bulletin 1658 A-S, p. 43-58.

Elston, W. E., 1984, Subduction of young oceanic lithosphere and extensional orogeny in southwestern North America during mid-Tertiary time: Tectonics, v. 3, no.2, p. 229-250.

Ewing, T. A., 1980, Paleogene tectonic evolution of the Pacific Northwest: Journal of Geology, V. 88, p. 619-638.

Fisher, R. V., 1961, Proposed classification of volcaniclastic sediments and rocks: Geological Society of America Bulletin, v. 72, no. 9, p. 1409-1414.

_____, 1966, Mechanism of deposition from pyroclastic flows: American Journal of Science, v. 264, no. 5, p. 350-363.

_____, 1966, Rocks composed of volcanic fragments and their classification: Earth-Science Reviews, v. 1, no. 1, p. 287-298.

_____, and Schmincke, H.-U., 1984, *Pyroclastic Rocks*: Springer-Verlag, Berlin, Heidelberg, New York, Tokyo, 472 p.

Foster, Fess, 1987, Epithermal precious-metal systems associated with an Eocene cauldron: Lowland Creek volcanic field, southwestern Montana, *in* 1987 guidebook to the Helena area: Montana Bureau of Mines and Geology Special Publication 95, p. 53-54.

Fox, K. F., Jr., 1983, Melanges and their bearing on Late Mesozoic and Tertiary subduction and interplate translation at the west edge of the North American plate: U. S. Geological Survey Professional Paper 1198, 40 p.

_____, and Beck, M. E., 1985, Paleomagnetic results for Eocene volcanic rocks from northeastern Washington and the Tertiary tectonics of the Pacific Northwest: Tectonics, v 4, no. 3, p. 323-341.

Gries, R., North-south compression of Rocky Mountain foreland basins and uplifts *in:* Lowell, J. D., and Gries, R., eds,, Rocky Mountain foreland basins and uplifts: Denver, Colorado, Rocky Mountain Association of Geologists, p. 9-32.

Gwinn, V. E., and Mutch, T. A., 1965, Intertongued Upper Cretaceous volcanic and nonvolcanic rocks, central western Montana: Geological Society of America Bulletin, v. 76, p. 1125-1144.

Hackett, W. R., Moye, F. J., and Mertzman, S. A., 1988, Petrology of mafic to intermediate rocks from the Eocene Challis volcanic field, central Idaho (abstract): Geological Society of America Abstracts with Programs, v. 20, no. 5.

Hamilton, W.,1978, Mesozoic tectonics of the western United States, *in* Howell, D. G., and McDougall, K. A., eds., Mesozoic paleogeography of the western United States: Pacific Section , Society of Economic Paleontologists and Mineralogists, Pacific Coast Paleogeography Symposium 2, p. 33-70.

_____, 1988, Tectonic setting and variations with depth of some Cretaceous and Cenozoic structural and magmatic systems of the western United States, *in* Ernst, W. G., ed., Metamorphism and Crustal Evolution of the Western United States, Rubey Volume VII, Prentice-Hall, Englewood Cliffs, New Jersey, p. 4-40.

_____, and Meyers, W. B., 1974, Nature of the Boulder batholith of Montana: Geological Society of America Bulletin, v. 85, p.365-378.

Hanneman, D. L., and Wideman, C. J., 1991, Sequence stratigraphy of Cenozoic continental rocks, southwestern Montana: Geological Society of America Bulletin, v. 103, p. 1335-1345.

Hardyman, R. F., 1989, Eocene magmatism , Challis volcanic field, central Idaho *in* Hyndman, D. W. (compiler), Cordilleran volcanism, plutonism, and magma generation at various crustal levels, Montana and Idaho: New Mexico Bureau of Mines and Mineral Resources Memoir 47, p. 276-285.

Harrison, J. E., Griggs, A. B., and Wells, J. D., 1974, Tectonic features of the Precambrian Belt basin and their influence on post-Belt structures; U. S. Geological Survey Professional Paper 866, 15 p.

Hearn, B. C., Jr., 1989, Introduction-T346 Montana high-potassium igneous province *in* Montana high-potassium igneous province, Field Trip Guidebook T346, B. C. Hearn, Jr.,(ed.), American Geophysical Union 28th International Congress, p. 1-5.

_____, 1989, Bearpaw Mountains, Montana *in*: Montana high-potassium igneous province, Field Trip Guidebook T346, B. C. Hearn, Jr. (ed.), American Geophysical Union 28th International Congress, p. 51-57.

Heiken, G., 1979, Pyroclastic flow deposits: American Scientist, v. 67, no. 5, p. 564-571.

Hyndman, D. W., 1985, *Petrology of Igneous and Metamorphic Rocks*: McGraw-Hill, New York, 786 p.

_____, Badley, R. and Rebal, D., 1977, Northeast-trending early Tertiary dike swarm in central Idaho and Western Montana: (abstract): Geological Society of America, Abstracts with Programs, Rocky Mountain Section Meeting, Missoula, Montana, p. 734.

Irvine, T. N., and Barager, W. R. A., 1971, A guide to the chemical classification of the common volcanic rocks: Canadian Journal of Earth Sciences, v. 8, p. 523-548.

Johnson, R. W., 1966, Mechanisms of cauldron subsidence: Nature, v. 210, no. 5033, p. 291-292.

Kamb, W. B. , 1959, Theory of preferred orientation developed by crystallization under stress: Journal of Geology, v. 76, p. 163-170.

Kelsey, C. H., 1965, Calculation of the CIPW norm; Mineralogy Magazine, v. 34, p. 276-282.

Klepper, M. R., Weeks, R. A., and Ruppel, E. T., 1957, Geology of the Southern Elkhorn Mountains, Jefferson and Broadwater Counties, Montana: U. S. Geological Survey Professional Paper 292, 82 p.

_____, Robinson, G. D., and Smedes, H. W., 1971, On the nature of the Boulder batholith: Geological Society of America bulletin, v. 82, p. 1563-1580.

Knopf, A., 1913, Ore deposits of the Helena mining region, Montana: U. S. Geological Survey Bulletin 527, 143 p.

_____,1950, Marysville granodiorite stock, Montana; American Mineralogist, v. 35, p. 832-844.

Lajoie, Jean, 1979, Facies model 15. Volcaniclastic rocks: Geoscience Canada, v. 6, no. 3, p. 129-139.

LeBas, M. J., LeMaitre, R. W., Streckeisen, A., and Zanettin, B., 1986, A chemical classification of volcanic rocks based on the total alkali-silica diagram: Journal of Petrology, v. 27, p. 745-750.

Leonard, B. F. and Marvin, R. F., 1982, Temporal Evolution of the Thunder Mountain caldera and related structures, central Idaho *in* Bonnichsen, W., and Breckenridge, R. M. (eds.), Cenozoic geology of Idaho: Idaho Bureau of Mines and Geology, Bulletin 26, p. 23-41.

Lipman, P. W., 1975, Evolution of the Platoro caldera complex and related volcanic rocks, southeastern San Juan Mountains, southwestern Colorado: U. S. Geological Survey Professional Paper 852, 128 p.

_____, 1980, Cenozoic volcanism in the western United States: implications for continental tectonics, *in* Continental tectonics: studies in geophysics: National Academy of Sciences, Washington, D. C., p.161-174.

_____, Protska, H. J., and Christiansen, R. L., 1971, Evolving subduction zones in the western United States, as interpreted from igneous rocks: Science, v. 174, p. 821-825.

_____, 1972, Cenozoic volcanism and plate-tectonic evolution of the western United States: early and middle Cenozoic: Philosophical Transactions of the Royal Society of London, v. 171, p. 217-248.

Maniar, P. D., and Piccoli, P. M. , 1989, Tectonic discrimination of granitoids: Geological Society of America Bulletin, v. 101, p. 635-643.

MacDonald, G. A., and Katsura, T., 1964, Chemical composition of Hawaiian lavas: Journal of Petrography, V. 5, P. 82-133.

McClernan, H. G., 1983, Metallic mineral deposits of Lewis and Clark County, Montana: Montana Bureau of Mines and Geology Memoir No. 52.

McIntyre, D. H., Ekren, E. B., and Hardyman, R. F., 1982, Stratigraphic and structural framework of the Challis Volcanics in the eastern half of the Challis 1° X 2° quadrangle, Idaho; *in* Bonnichsen, W., and Breckenridge, R. M. (eds.), Cenozoic geology of Idaho: Idaho Bureau of Mines and Geology Bulletin 26, p. 3-22.

McKee, J., 1978, Petrology, alteration and mineralization of the Poorman Creek-Silver Bell stock porphyry Cu-Mo deposit: [M. S. thesis], University of Montana, 97 p.

Melson, W. G., 1964, Geology of the Lincoln area, Montana and contact metamorphism of impure carbonate rocks [Ph.D. dissertation]: Princeton University, 153 p.

Molnar, P., and Atwater, T., 1878, Interarc spreading and Cordilleran tectonics as alternates related to the age of subducted oceanic lithosphere: Earth and Planetary Science Letters, v. 41, p. 330-340.

Moye, F. J., Hackett, W. R., Blakely, J. D., and Snyder, L. G., 1988, Regional geologic setting and volcanic stratigraphy of the Challis volcanic field, central Idaho, *in* Link, P. K., and Hackett, W. R., (eds.), Guidebook to the geology of central and southern Idaho: Idaho Geological Survey Bulletin 27, p. 87-97.

Mudge, M. R., 1982, A resume of the structural geology of the northern Disturbed Belt, northwestern Montana, *in* Geologic Studies of the Cordilleran Thrust Belt v.1: Rocky Mountain Association of Geologists, p. 91-122.

_____, and Earhart, R. L., 1980. The Lewis thrust fault and related structures in the disturbed belt, northwestern Montana: U. S. Geological Survey Professional Paper 1174, 18 p.

_____, Erickson, R. L., and Kleinkopf, M. D., 1968, Reconnaissance geology, geophysics, and geochemistry of the southern part of the Lewis and Clark Range, Montana: U. S. Geological Survey Bulletin 1252-E, 35 p.

O'Neill, J. M., and Lopez, D. A., 1985, Character and regional significance of the Great Falls tectonic zone, east-central Idaho and west-central Montana: American Association of Petroleum Geologists Bulletin, v. 69, no. 3, p. 437-447.

Pardee, F. T., 1950, Late Cenozoic block faulting in western Montana: Geological Society of America Bulletin, v. 61, p. 359-406.

_____, and Schrader, F. C., 1933, Metalliferous deposits of the greater Helena mining region, Montana: U. S. Geological Survey Bulletin 842, 311 p.

Peacock, M. A., 1931, Classification of igneous rocks: Journal of Geology, v. 39, p. 54-67.

Peccarillo, A., and Taylor, S. A. 1976, Geochemistry of Eocene calc-alkaline volcanic rocks from the Kastomonu area, northern Turkey: Contributions to Mineralogy and Petrology, v. 58, p. 63-81.

Peterson, D. W., 1979, Significance of flattening of pumice fragments in ash-flow tuffs *in* Chapin, C. E., and Elston, W. E. (eds), Ash-flow tuffs, Geological Society of America Special Paper 180, p. 195-203.

Peterson, M. P., 1985, The geology of the southwest quarter of the Avon 15 minute Quadrangle, Powell County, Montana [M. S. thesis]: Butte Montana, Montana College of Mineral Science and Technology, 39 p.

Phillips, W. M., and Griffen, D. T., 1981, *Optical Mineralogy: the Nonopaque Minerals*: W. H. Freeman Co., San Francisco, 677 p.

Poldervaart, A., 1964, Chemical definition of alkali basalts and tholeiites: Geological Society of America Bulletin, v. 75, p. 229-232.

Robinson, G. D., Klepper, M. R., and Obradovich, J. D., 1968, Overlapping plutonism, volcanism, and tectonism in the Boulder batholith region, western Montana *in* Coats, R. R., Hay, R. L., and Anderson, C. A. (eds.), Studies in volcanology: Geological Society of America Memoir 116, p. 557-576.

Rock Color Chart Committee, Geological Society of America, 1979, Rock color chart: Netherlands, Huyskes-Enschende, 11 p.

Roobol, M. J., Smith, A. L., and Wright, J. V., 1987, Lithic breccias in pyroclastic flow deposits on St. Kitts, West Indies: Bulletin of Volcanology, v. 49, no. 5, p. 694-707.

Ross, C. S.,and Smith, R. L. 1961, Ash-flow tuffs- their origin, geologic relations, and identification: U. S. Geological Survey Professional Paper 366, 81 p.

Ruppel, E. T., 1963, Geology of the Basin Quadrangle, Jefferson, Lewis and Clark and Powell Counties, Montana: U. S. Geological Survey Bulletin 1151, 121 p.

_____, Wallace, C. A., Schmidt, R. G., and Lopez, D. A., 1981. Preliminary interpretation of the Thrust Belt in southwest and west-central Montana and east-central Idaho: 1981 Montana Geological Society Field Conference and Symposium Guidebook, Southwest Montana, p. 139-159.

Rutland, C., Smedes, H. W., Tilling, R. I., and Greenwood, W. R., 1989, Volcanism and plutonism at shallow crustal levels: The Elkhorn Mountains Volcanics and the Boulder batholith, southwestern Montana *in* Hyndman, D. W. (compiler), Excursion 14B: Cordilleran volcanism, plutonism, and magma generation at various crustal levels, Montana and Idaho: New Mexico Bureau of Mines and Mineral Resources Memoir 47, p. 264-276.

Schmid, R., 1981, Descriptive nomenclature and classification of pyroclastic deposits and fragments: recommendations of the I.U G S subcommission on the systematics of igneous rocks: Geology, v. 9, no. 1, p. 41-43.

Schmidt, R. G., 1966, Source for Late Cretaceous breccia in west-central Montana *in* Geological Survey Research 1966: U. S. Geological Survey Professional Paper 550-A, p. A-76.

_____, 1972, Geologic map of the Wolf Creek Quadrangle, Lewis and Clark County, Montana: U. S. Geological Survey Map GQ-974. Scale 1:24,000.

Schmincke, H.-U., and Swanson, D. L., 1967, Laminar viscous flowage structures in ash-flow tuffs from Gran Canaria, Canary Islands: The Journal of Geology, v.75, no. 6, p 641-664.

Shand, S. J., 1951, *Eruptive Rocks*: Murby and Co.,London, 231 p.

Sheridan, M. F., 1979, Emplacement of pyroclastic flows: A review *in* Chapin, C. E. , and Elston, W. E. (eds.), Ash-flow tuffs: Geological Society of America Special Paper 180, p. 125-134.

Smedes, H. W., 1962, Lowland Creek volcanics, an upper Oligocene formation near Butte, Montana: Journal of Geology, v. 70, p. 255-266.

_____, and Thomas, H. H. 1965, Reassignment of the Lowland Creek volcanics to Eocene age: Journal of Geology, v. 73, p. 508-510.

_____, 1966, Geology and igneous petrology of the northern Elkhorn Mountains, Jefferson and Broadwater Counties, Montana: U. S. Geological Survey Professional Paper 510, 116 p.

Smith, G. A., 1986, Coarse-grained nonmarine volcaniclastic sediment: terminology and depositional process: Geological Society of America Bulletin, v. 97, p.1-10.

Smith, R. L., 1960a, Ash-flows, Geological Society of America Bulletin, v.71, p. 795-842.

_____1960b, Zones and zonal variations in welded ash flows: U. S. Geological Survey Professional Paper 354-F, p. 148-159.

Snyder, W. S, Dickinson, W. R., and Silberman, M. L., 1976, Tectonic implications of space-time patterns of Cenozoic magmatism in the western United States, Earth and Planetary Science Letters, v. 32, p. 91-106.

Sparks, R. S. J., 1976, Grain size variations in ignimbrites and implications for the transport of pyroclastic flows: Sedimentology, v. 23, p. 147-188.

_____,and Walker, G. P. L., 1973, The ground surge deposit: a third type of pyroclastic rock: Nature, v. 241, p. 62-64.

_____, Self, S., and Walker, G. P. L., 1973, Products of ignimbrite eruption: Geology, v.1, p. 115-118.

Streikeisen, A. L., 1976, To each plutonic rock its proper name: Earth Science Reviews, v. 12, p.1-33.

_____, and Le Matre, R. W., 1979, A chemical approximation to the modal QAPF classification of the Igneous rocks: *Neues Jahrbuch fur Mineralogie Abhandlungen*, v. 13, p. 169-206.

Thompson, R. N., 1982, Magmatism of the British Tertiary Volcanic Province: Scottish Journal of Geology, v. 18, p. 49-107.

_____, Morrison, M. A., Hendry, G. L., and Parry, S. J., An assessment of the relative roles of a crust and mantle in magma genesis: an elemental approach: Philosophical Transactions of the Royal Society of London, v. A310, p. 549-590.

Tilling, R. I., 1974, Composition and timing of plutonic and associated volcanic rocks, Boulder batholith region, Montana: Geological Society of America Bulletin, v. 85, p. 1925-1930.

Trombetta, M. J., 1987, Evolution of the Eocene Avon volcanic complex, Powell County, Montana [M. S. Thesis]: Bozeman, Montana Montana State University, 112 p.

Turek-Schwartz, K., and Hyndman, D. W., 1991, High-potassium igneous rocks of the Bearpaw Mountains, north-central Montana *in* Baker, D. W., and Berg, R. B., eds., Guidebook of the central Montana alkalic province, geology, ore deposits and origin, Montana Bureau of Mines and Geology Special Publication 100, p. 111-120.

Walker, G. P. L., and McBroom, L. A., 1983, Mount St. Helens 1980 and Mt Pele' 1902-flow or surge?: Geology, v. 11, p. 571-574.

Wallace, C. A., Lidke, D. J., and Schmidt, R. G., 1990, Faults of the central part of the Lewis and Clark line and fragmentation of the Late Cretaceous foreland basin in west-central Montana: Geological Society of America Bulletin, v. 102, p. 1021-1037.

Watson, S. M., 1986, The Boulder Batholith as a source for the Elkhorn Mountain Volcanics, southeast quarter of the Deerlodge 15' Quadrangle, southwestern Montana [Master's Thesis]: Missoula, Montana, University of Montana,100 p.

Weidman, R. M., 1965, The Montana lineament, *in:* Geology of the Flint Creek Range, Montana: Billings Geological Society 16th Annual Field Conference Guidebook, p. 137-143.

Whipple, J.A., Mudge, R. A., and Earhart, R. L., 1987, Geologic map of the Rogers Pass Area, U. S. Geological Survey Miscellaneous Investigation Series Map I-1642. scale 1:48,000.

Wilkinson, W. H., 1991, Geologic map of the Keep Cool Project, Lewis and Clark County, Montana: Unpublished map for Phelps Dodge Mining Company.

Williams, H., 1941, Calderas and their origin: Bulletin of the Department of Geological Sciences, University of California Publications, v. 25, no. 6, p. 239-346.

_____, 1942, The geology of Crater Lake National Park, Oregon: Carnegie Institute, Washington, Publication 540, 162 p.

_____, and McBirney, A. R., 1979, *Volcanology*: San Francisco, Freeman and Co., 397 p.

_____, Turner, F. J., and Gilbert, C. M., 1982, Petrography, an Introduction to the Study of Rocks in Thin Sections, San Francisco, Freeman and Co., 626 p.

Wilson, C. J. N., 1985, The Taupo eruption, New Zealand II. the Taupo ignimbrite: Philosophical Transactions of the Royal Society of London, v. A-314, p. 229-310.

Wolff, J. A., and Wright, J. V., 1981, Rheomorphism of welded tuffs: Journal of Volcanology and Geothermal Research, v. 10, p. 13-34.

Wright, J. V., and Walker, G. P. L., 1977, The ignimbrite source problem: Significance of a co-ignimbrite lag-fall deposit: Geology, v. 5, p. 729-732.

Yoder, H. S., and Tilley, C. E., 1962, Origin of basalt magmas: an experimental study of natural and synthetic rock systems: Journal of Petrology, v. 3, p. 342-352.